

**Physiological Chemistry and Physics
and Medical NMR
Volume 37, Number 2, 2005**

Addresses of Chief Editor and Editorial College

Chief Editor

Gilbert N. Ling
P.O. Box 1452
Melville, New York 11747

Editorial College

O. D. Bonner
Department of Chemistry
University of South Carolina
Columbia, South Carolina 29208

Harris Busch
Department of Pharmacology
Baylor College of Medicine
Houston, Texas 77030

Ivan L. Cameron
Department of Anatomy
University of Texas Health Science Center
San Antonio, Texas 78284

Doriano Cavallini
Institute of Biological Chemistry
University of Rome
00185 Rome, Italy

James S. Clegg
Bodega Marine Laboratory
University of California
Bodega Bay, California 94923

George H. Czerlinski
Leibnitz Foundation Institute
P.O. Box 28521
Bellingham, Washington 98228

W. Drost-Hansen
Laboratorium Drost
Williamsburg, Virginia 23188-9415

Ludwig Edelmann
Anatomie und Zellbiologie
Universitdt des Saarlandes
D-66421 Homburg (Saar), Germany

Carlton F. Hazlewood
Research Consultants International
P.O. Box 130282
The Woodlands, Texas 77393

Ferdinand Heinmets
Technology Incorporated
P.O. Box 790644
San Antonio, Texas 78279-0644

S.R. Kasturi
Tata Institute of Fundamental Research
Mumbai 400 005, India

Miklós Kellermayer
Department of Clinical Chemistry
University Medical School
Pécs, 7624 Hungary

Janos Ladik
Institute of Physics and Theoretical Chemistry
University of Erlangen-Nurnberg
D-8520 Erlangen
Germany

George M. Mrevlishvili
Department of Physics
Tbilisi State University
380028 Tbilisi
Republic of Georgia

Toshihiko Ubuka
Department of Clinical Nutrition
Kawasaki University of Medical Welfare
Kurashiki, Okayama, 701-0193, Japan

Denys Wheatley
Department of Cell Pathology
University of Aberdeen
Aberdeen AB24 4FA, Scotland
United Kingdom

Copyright © 2005 by Pacific Press, Inc., New York. All rights reserved. Scientific journals and listing services have permission to republish or reproduce, with credit, the titles, summaries and abstracts of original material contained herein. Printed in the U.S.A.

EDITORIAL AND BUSINESS OFFICE

Physiological Chemistry and Physics
and Medical NMR

P.O. Box 1452
Melville, New York 11747

Editor In Chief, Dr. Gilbert N. Ling
Managing Editor, Margaret M. Ochsenfeld

SCOPE: PCP provides a forum for the review and publication of reports of original research in a broad range of subjects in biophysics, biochemistry and cellular physiology. Reports of direct applications of basic knowledge to human studies are invited; examples would include the measurements of relaxation times as part of NMR imaging. Single experiments, conclusions based on inadequate statistics, purely speculative papers, and clinical case reports are not accepted.

POLICY: The pages of PCP are accessible to competing viewpoints, interpretations, theories and opinions. Debate is invited via Editorial Comments and Letters to the Editor. Criteria for evaluating submissions include soundness of the study and clarity of presentation, and papers are not rejected on the basis of interpretation or theory, however controversial. PCP believes that scientific issues should be settled by investigation and open debate, not by an appeal to anonymous authority.

PCP attempts to achieve a balance between freedom of expression and constructive peer review. All papers are refereed by reviewers who may remain anonymous, but the Chief Editors make all final decisions, and will handle appeals from authors who feel their papers are unfairly reviewed.

The Editors endeavor to make decisions regarding acceptance or rejection of manuscripts quickly, and have set self-imposed deadlines for doing so. Referees also are given deadlines.

TYPES OF PAPERS: *Regular papers* may be experimental or theoretical. *Short notes*, *Priority notes* and *Letters* in response to published papers are invited. *Reviews* are desired, but authors are urged to contact an Editor before sending a finished review manuscript. *Symposia* may be published as regular or supplemental issues.

SUBSCRIPTIONS: Price is US\$80.00 per volume in the United States and US\$87.00 outside the United States. *Physiological Chemistry and Physics and Medical NMR* is published biannually, 2 issues per year, the volume numbered yearly. New subscriptions will start with the first issue of the volume in progress, unless the subscriber directs otherwise. Most back issues are available

Contributions appearing herein do not necessarily reflect views of the publisher, staff or Editorial College.

Instructions to Authors

SUBMISSIONS: An original and two copies of all material are requested. The original must be typewritten on one side only. Papers should be sent to Dr. Gilbert N. Ling, Editor, P.O. Box 1452, Melville, New York 11747 U.S.A. Manuscripts should be submitted only to this journal and not have been published in part or whole in another publication, except as short preliminary notes, abstracts, or as unpublished work in reviews or symposia. Be sure to keep a copy of your manuscript.

NOTE: Referees will be instructed to destroy their copies of the manuscript after reviewing them. We will return only the original manuscript to you for revision or if rejected.

MANUSCRIPTS: All material should be typed double-spaced with margins at least one inch wide and pages numbered consecutively beginning with the title page. In addition to a paper copy, send an IBM- or Macintosh-compatible file on a floppy disk or CD, in Word or Wordperfect. *Title Page* should include title (of at most 100 characters and spaces), full names of authors as you wish them to be published, names and cities of institutional affiliation(s) of authors and of institution(s) where the studies were performed, and name, full address, telephone number, fax number and e-mail address of the person to whom correspondence, proofs, and reprint requests are to be sent. Four to six *key words* should be listed on the title page. These words will assist indexers. Also, at bottom of title page include a short running title of 40 characters or less.

Abstract should be concise and no longer than 225 words. *Body* may or may not be divided into Introduction, Materials and Methods, Results and Discussion, depending on the length and nature of the paper. Introductory remarks should indicate clearly the significance of the work presented. *References* may be indicated in the text and listed in the reference list in whatever style the author prefers, but we prefer that titles of articles be omitted.

TABLES: Tables should be typewritten on separate sheets and identified by roman numerals (eg. Table III) and titles. Table notes should be keyed by superscript italic lower-case letters (eg. ^aControl). The approximate locations of *tables* and *figures* should be indicated in the margins of the manuscript.

ILLUSTRATIONS: Original artwork or glossy photostatic prints, together with two photocopies (like Xerox copies) should be provided. Each illustration should be numbered on the back in pencil, along with the authors' names. It is preferred that line drawings be made on paper that is not larger than 8½ by 13 inches, and that the drawing be its intended size in the printed paper. Most figures will occupy ½ to full column, that is 5 inches wide. Lines and lettering should be thick enough to allow reduction. A drawing of overall dimension of 8 by 10 inches that will be reduced to ¼ of its original size should be lettered with 18-point (capitals 6 mm high, lower-case 4 mm high) or larger lettering. Glossy photostatic prints are acceptable, and should be attached firmly to a sheet of paper the same size as the manuscript. Postacceptance: If possible send figures as an image file using TIFF or JPEG formatting scanned at a resolution of 600 dpi.

PHOTOGRAPHS: High-quality black and white glossy prints should be provided in triplicate, and may be provided as one print plus two photocopies if the photocopies are sufficiently clear to portray the original to referees. Photographs should be attached firmly to a sheet of paper the same size as the manuscript. Photographs that have been scanned and stored as a TIFF file with a resolution of 300 dpi may also be submitted.

REFEREES: Two anonymous referees will be sought for each paper. Authors are encouraged to suggest names and addresses of suitable referees. Referees will be given deadlines for mailing manuscripts back or phoning reviews in, and will be invited to provide editorial statements or Letters that deal with issues raised by submitted papers.

REPRINTS: An order form is enclosed with proofs sent to authors.

PAGE CHARGES: Page charge is \$20.00 per published page. It may be waived in the case of severe international exchange difficulties. An additional charge of \$15.00 will be levied for photographs that require screening (eg., E.M's, chromatograms, scans).

Mechanisms of Telomerase Binding to Telomeres

George Czerlinski^{1*} and Tjalling Ypma²

¹*Department of Biology*

²*Department of Mathematics*

Western Washington University

Bellingham, WA 98225

**Corresponding author; E-mail: george@submicron.com*

Abstract: There are essentially two alternative mechanisms for the binding of telomerase to telomeres, assuming that a protective component is initially bound to the telomerase binding region on the telomeres. Either the protective (or blocking) agent first dissociates and telomerase binds thereafter, or telomerase binds first and the protective agent then dissociates from the ternary complex. In the limit, this second possibility permits the ternary complex to become a transition complex (creating another possible mechanism). Numerical simulation of both rapid mixing and chemical relaxation is used to study these alternatives. We aim to determine how the mechanisms may be distinguished experimentally and identify an appropriate experimental design. We show that rapid mixing experiments are better than chemical relaxation experiments, since the latter are more affected by the statistics of single molecule kinetics. However, hidden fast steps can only be revealed by chemical relaxation. The detection of mechanistic changes hinges on linking fluorescence reporters to the reaction components, either directly (chemically) or indirectly (*via* an indicator reaction). Fluorescence is excited by two-photon absorption in a small reaction volume. Various detection strategies and design issues are examined, including limitations imposed by diffusion. Constant rather than stopped flow is shown to be preferable.

KEY WORDS: telomerase, telomeres, blocking-agent, rapid mixing, chemical relaxation, two-photon absorption

TELOMERASE, a reverse transcriptase, was discovered by Greider and Blackburn (1985). They obtained the enzyme from tetrahymena. Morin (1989) used the same method to confirm the presence of telomerase in certain human cells. In humans telomerase is only active in germ cells, stem cells and proliferating tumor cells (Blackburn, 1991). Ideas about the functioning of the enzyme were first described by Greider and Blackburn (1989). Exactly how the initial telomere-telomerase complex is formed remains unclear

(Baumann and Cech, 2001). There is some indication that the molecular weight of fully active human telomerase is very high (1000 kDa or more, Schnapp *et al.*, 1998). A recent review on telomerase was given by Thomas Cech (2004).

In the binding of telomerase to the (3'-) ends of chromosomes one may distinguish the three mechanistic alternatives introduced in Figure 1. All involve a protective agent (component 3 in Figure 1) which may be a compound like Pot1 (Baumann and Cech, 2001). In Model A the protective agent first dissociates and telomerase (component 2) binds thereafter. In Model B telomerase binds first and the protective agent then dissociates from the ternary complex. A limiting case is considered in Model C, where the intermediate complex becomes a transition complex. These last two cases are shown with poten-

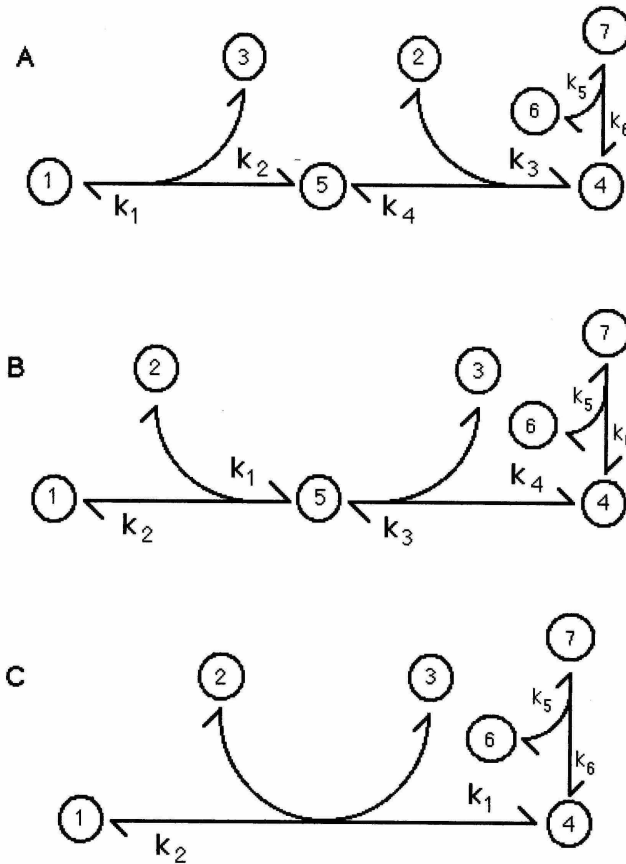


FIGURE 1. Two basic mechanisms of telomerase binding and a third limiting case are shown. The meaning of the circled numbers depends upon the mechanism/model as follows: For all three models: 1 = telomere-blocker complex, 2 = free telomerase, 3 = free blocker, 4 = telomere-telomerase complex. Component 5 is free telomere-ends for model A, but telomerase-telomere-blocker complex for model B, and absent from model C. For all models component 6 is free nucleotide with fluorophor attached and component 7 is its bound form (see text for more details).

tial energy profiles in Figure 2 which also shows an intermediate case with the short-lived complex in low concentration. We aim to determine how these mechanisms may be distinguished experimentally. The third step in these models (involving component 6) represents an indicator for the active telomere-telomerase complex.

It is difficult to study the mechanism of a reaction sequence which is highly localized on the cell nucleus. Even if we could move the chromosome ends into a very small space, we would not be able to use conventional mixing techniques. Fortunately, very small volumes can be observed with two-photon absorption under a microscope. One reactant remains fixed in space and the other reactant flows over it. The reaction system may be simplified by attaching chromosome ends to the object glass under the microscope and letting the telomerase solution flow over the attached reactant (with blocker bound). In principle we may use stopped flow or constant flow. This is the basic experimental setup

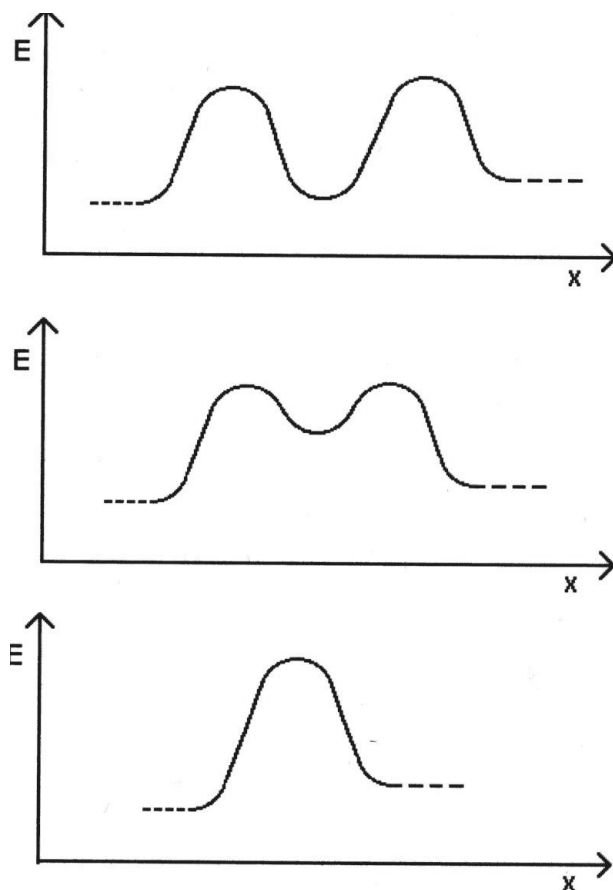


FIGURE 2: Potential energy profile for models B and C of Figure 1 plus an intermediate case (in the middle) which has a valley for the intermediate where the concentration is too low to be detected.

which we discuss in the method section to the extent needed for the kinetic modeling. To investigate any possible faster steps in the reaction sequence (such as the binding of component 6), we introduce chemical relaxation by temperature jump.

Our goal is to find the best experimental conditions for distinguishing between the mechanisms. To accomplish this goal we simulate the kinetics under a variety of conditions. The kinetic concentration profiles show us which components should be connected to suitable fluorophores for their actual detection.

Wenz *et al* (2001) conducted experiments which point to human telomerase acting as dimers. We will consider models with telomerase dimers in a later paper.

Methods

Basic Experimental Design

The basic design consists of a fluorescence microscope with a dichroic mirror to deflect the pulsed laser light onto the object carrier focused to the diffraction limit, resulting in two-photon absorption from a volume of less than $1 \mu\text{m}^3$ (Denk *et al*, 1991). The dichroic mirror is designed to transmit the fluorescence emitted from the fluorophors within the absorption volume, which contains the target polydeoxynucleotides either on the microscope objective or as telomere ends on a cell nucleus. The quartz object holder is temperature controlled such that switching between two fluids of different temperature can be quickly accomplished to produce the desired temperature jump to observe chemical relaxation. Pulses of infrared (laser) light may have to be used to raise the temperature quickly.

Definition of Reaction Parameters

Figure 1 details the three alternative binding models and identifies the components and rate constants. Rate constants k_1 , k_3 and k_5 are always bimolecular, k_2 , k_4 and k_6 are monomolecular in models A and B, while k_2 is bimolecular and k_6 is monomolecular in model C. For all three models, components 1, 4, 5 and 7 refer to the various complexes of telomere ends containing the telomerase binding site; these are fixed in space (*in situ*).

Concentrations are defined by lower case “c” with the component number (i) as subscript. Without superscript, c_i refers to the concentration as a function of time; superscript 0 (that is c_i^0) denotes initial concentrations; and superscript T (that is c_i^T) identifies total concentrations of any basic structure (time-independent). Often $c_i^T = c_i^0$.

Chemical Kinetics

All models begin with telomere ends saturated with blocker. This is accomplished in a pre-equilibrium with $c_5^0 \gg K_{2,1} = k_2/k_1$. The details are shown in Table I. The actual cylindrical volume of two-photon absorption is close to $0.5 \mu\text{m}^3$ and the excitation depth close to $1 \mu\text{m}$ leading to the radius given. The value for the bimolecular rate constant k_1 derives from the consideration that it may be diffusion limited and require rather precise orientation, as in the binding of NADH to liver alcohol dehydrogenase (Czerlinski, 1993). The value of k_2 then follows from $K_{2,1} = k_2/k_1$ with an equilibrium constant for relatively tight binding.

TABLE I. Parameter values for pre-equilibration

PARAMETER, UNITS	VALUE
Avogadro's Number, molecules/mole	6.022×10^{23}
Radius of 2-photon abs. cylin., μm	0.4
Depth of 2-photon abs. cylin., μm	1.00
Volume at chromosome ends, μm^3	0.500
# of DNA-ends in volume, molecules	50
c_1^0 , μM	0
c_3^0 , μM	5.0
c_5^0 , μM	0.166
$K_{2,1}$, μM	0.01
k_1 , $\mu\text{M}^{-1} \text{s}^{-1}$	0.1
k_2 , s^{-1}	0.001
c_{one} , μM	0.0033

(concentration of one molecule in microvolume)

Reaction Kinetics

We simulated the chemical kinetics of each of the models A, B and C, for both constant and stopped flow, denoting the cases by Ac, Bc, Cc for constant flow and As, Bs, Cs for stopped flow respectively. We conducted experiments with a variety of different values of c_3^0 listed in Tables II through IV, that is, different initial concentrations of blocker; the respective cases are referred to as As-1, As-2, As-3 etc. for the different initial values. For Model A we further tried two alternative values of k_2 (and thus $K_{2,1}$), while for Model B we used two alternative values of k_4 (and thus $K_{4,3}$).

The values for the equilibrium constants in Tables II to IV were selected relative to $K_{2,1}$ in Table I as follows: $K_{4,3}$ (Table II) = $10 K_{2,1}$ (Table I), with an alternative value for $K_{2,1}$ (Table II) = $10 K_{4,3}$ (Table II) to cover a wide range of possibilities. These equilibrium values are reversed in Tables III and IV. The value for $K_{6,5}$ (identical in all Tables) is consistent with currently available literature; the value for k_5 was chosen somewhat arbitrarily, but should be in the right range (Stryer, 1988). Values for the bimolecular rate constants in these tables were chosen such that k_1 (Table II) = k_1 (Table I), and k_3 (Table II) = $10 k_1$ (Table I). These values are reversed in Tables III and IV. Values for the monomolecular rate constants in Tables II and III follow from the values for the equilibrium constants and bimolecular rate constants.

The applicable differential equations and the mass conservation equations depend on the individual model and whether we use constant or stopped flow. For each of the models A, B and C, and for both constant and stopped flow, several differential equations and conservation equations hold; we selected and list only enough of these relationships to provide the unique, well-defined solution for each case. A complete set of differential equations can be derived by direct reference to Figure 1, but some of those equations will be redundant.

Constant Flow

For constant flow, in which the concentrations of components 2, 3 and 6 are held constant, the relevant constants, initial conditions (including alternative values of c_3^0), differential equations and conservation equations are displayed in Tables II through IV corresponding to models A through C respectively. These are open systems with only one conservation equation (for the components immobilized on the cell nucleus or by attaching them to the objective). Since the concentrations of components 2, 3 and 6 are held constant, the system of differential equations is linear in the remaining variables, greatly facilitating the computation.

Stopped Flow

For stopped flow c_2 , c_3 and c_6 are no longer held constant, requiring the introduction of additional equations to supplement those listed in Tables II to IV. These are closed systems governed by conservation equations; the conditions $c_i = c_i^0$ (for $i = 2, 3, 6$ and all t) of Tables II through IV are replaced by the relationships listed in Tables V through VII respectively. Again, two alternate values are used for the dissociation constant of component 3. To what extent stopped flow can actually be implemented will be discussed later.

In each case the differential equations form a stiff system which was solved numerically by the Matlab (Mathworks, 2004) routine ode23s (Shampine and Reichelt, 1997).

TABLE II. Model A, constant flow (Ac)

PARAMETER, UNITS	VALUE	ALT.
c_1^0 , μM	0.166	
c_2^0 , μM	1.0	
c_3^0 , μM (Ac-1, Ac-2)	0, 0.2	
c_6^0 , μM	1.0	
$c_i^0 = 0$ for $i = 4, 5, 7$		
$K_{6,5}$, μM	0.2	
k_5 , $\mu\text{M}^{-1} \text{s}^{-1}$	20	
k_6 , s^{-1}	4	
$K_{4,3}$, μM	0.1	
k_3 , $\mu\text{M}^{-1} \text{s}^{-1}$	1	
k_4 , s^{-1}	0.1	
$K_{2,1}$, μM	1	0.01
k_1 , $\mu\text{M}^{-1} \text{s}^{-1}$	0.1	0.1
k_2 , s^{-1}	0.1	0.001
$dc_1/dt = k_1 c_3 c_5 - k_2 c_1$		
$dc_5/dt = k_2 c_1 - k_1 c_3 c_5 + k_4 c_4 - k_3 c_2 c_5$		
$dc_7/dt = k_5 c_4 c_6 - k_6 c_7$		
$c_1^T (= c_1^0) = c_1 + c_4 + c_5 + c_7$		
for all t : $c_i = c_i^0$ for $i = 2, 3, 6$		
At equilibrium:		
$K_{2,1} = c_3 c_5 / c_1$, $K_{4,3} = c_2 c_5 / c_4$, $K_{6,5} = c_4 c_6 / c_7$		

TABLE III. Model B, constant flow (Bc)

PARAMETER, UNITS	VALUE	ALT.
$c_1^0, \mu\text{M}$	0.166	
$c_2^0, \mu\text{M}$	1.0	
$c_3^0, \mu\text{M}$ (Bc-1, Bc-2, Bc3)	0, 0.2, 2	
$c_6^0, \mu\text{M}$	1.0	
$c_i^0 = 0$ for $i = 4, 5, 7$		
$K_{6,5}, \mu\text{M}$	0.2	
$k_5, \mu\text{M}^{-1} \text{s}^{-1}$	20	
k_6, s^{-1}	4	
$K_{2,1}, \mu\text{M}$	0.1	
$k_1, \mu\text{M}^{-1} \text{s}^{-1}$	1	
k_2, s^{-1}	0.1	
$K_{4,3}, \mu\text{M}$	1	0.01
$k_3, \mu\text{M}^{-1} \text{s}^{-1}$	0.1	0.1
k_4, s^{-1}	0.1	0.001
$dc_1/dt = k_2 c_5 - k_1 c_1 c_2$		
$dc_5/dt = k_1 c_1 c_2 - k_2 c_5 + k_3 c_3 c_4 - k_4 c_5$		
$dc_7/dt = k_5 c_4 c_6 - k_6 c_7$		
$c_1^T (= c_1^0) = c_1 + c_4 + c_5 + c_7$		
for all $t: c_i = c_i^0$ for $i = 2, 3, 6$		
At equilibrium:		
$K_{2,1} = c_2 c_1 / c_5, K_{4,3} = c_3 c_4 / c_5, K_{6,5} = c_4 c_6 / c_7$		

TABLE IV. Model C, constant flow (Cc)

PARAMETER, UNITS	VALUE
$c_1^0, \mu\text{M}$	0.166
$c_2^0, \mu\text{M}$	1.0
$c_3^0, \mu\text{M}$ (Cc-1, Cc-2, Cc3)	0, 0.2, 2
$c_6^0, \mu\text{M}$	1.0
$c_i^0 = 0$ for $i = 4, 7$	
$K_{6,5}, \mu\text{M}$	0.2
$k_5, \mu\text{M}^{-1} \text{s}^{-1}$	20
k_6, s^{-1}	4
$K_{2,1}, \mu\text{M}$	0.1
$k_1, \mu\text{M}^{-1} \text{s}^{-1}$	1
k_2, s^{-1}	0.1
$dc_1/dt = k_2 c_3 c_4 - k_1 c_1 c_2$	
$dc_7/dt = k_5 c_4 c_6 - k_6 c_7$	
$c_1^T (= c_1^0) = c_1 + c_4 + c_7$	
for all $t: c_i = c_i^0$ for $i = 2, 3, 6$	
At equilibrium:	
$K_{2,1} = c_2 c_1 / (c_4 c_3), K_{6,5} = c_4 c_6 / c_7$	

TABLE V. Model A, stopped flow (As)

$$c_2^T = c_2 + c_4 + c_7$$

$$c_3^T = c_1 + c_3$$

$$c_6^T = c_6 + c_7$$

TABLE VI. Model B, stopped flow (Bs)

$$c_2^T = c_2 + c_4 + c_5 + c_7$$

$$c_3^T = c_1 + c_5 + c_3$$

$$c_6^T = c_6 + c_7$$

TABLE VII. Model C, stopped flow (Cs)

$$c_2^T = c_2 + c_4 + c_7$$

$$c_3^T = c_1 + c_3$$

$$c_6^T = c_6 + c_7$$

This is an implementation of a variable-steplength second order modified Rosenbrock method. Explicit expressions for the Jacobian matrix were provided. To verify the numerical results we repeated selected experiments using ode15s, and replacing the analytical Jacobian with a numerical approximation. In all cases the results obtained by the different methods were essentially identical. As an additional check the final values were verified by independently computing the equilibrium concentrations.

To obtain results for chemical relaxation initiated during the course of the flow at specified times, we assumed a sufficiently fast temperature perturbation (referred to as a “temperature jump”) which we simulate by instantaneously increasing all bimolecular rate constants (except k_2 in model C) by 30%. The numerical computation was then repeated and the data with unaltered rate constants subtracted from those with increased rate constants, resulting in the difference curves shown. Instead of temperature jump perturbation, one could also consider “concentration jumps” as introduced by Czerlinski (1966, p. 269). While the latter perturbation is straightforward for constant flow, the effects of diffusion have to be carefully considered for stopped flow, as we show below.

We use a logarithmic timescale for our graphs in order to be able to observe fast processes as well as slower ones. As a result, sideways shifts in the graphs correspond to changes in the order of magnitude of the corresponding reaction rates. To show how close the obtained curves are to single-molecule kinetics (Lu *et al.*, 1998) corresponding to one molecule in the observation volume (c_{one} in Table I; see also below), horizontal lines at $3 c_{\text{one}}$ and $10 c_{\text{one}}$ were added to the graphs.

Results and Discussion

Constant Flow

In the context of Model A (Figure 1A; Table II) it is not known whether $K_{2,1}$ ($= k_2/k_1$) is smaller or larger than $K_{4,3}$ ($= k_4/k_3$). Thus, Table II shows two alternative possibilities for the values of $K_{2,1}$. Figure 3 shows for Model A (with $c_3^0 = 0.2 \mu\text{M}$; model Ac-2) that in constant flow the curves for large $K_{2,1}$ differ from those for small $K_{2,1}$; the concentrations of components 4 and 7 are smaller for small $K_{2,1}$, as the latter prevents all of component 1 from dissociating. The rightward shift is due to the change in the value of k_2 from 0.1 s^{-1} to 0.001 s^{-1} (Table II). The concentration peak for component 5 disappears, but a small level of component 5 appears simultaneously with component 4.

Figure 4 shows that the sideways shift in the flow curves also occurs in the chemical relaxation curves for c_4 , c_5 and c_7 when relaxation is initiated at 100 s for Ac-2; this shift also occurs for Ac-1 and when relaxation is initiated at 10^4 s. The shift in Figure 4 arises from the fact that the reaction between components 4 and 7 is not accessible until 4 is actually formed. The dashed curve for component 1 in Figure 3 ($K_{2,1} = 0.01 \mu\text{M}$) shows that at 100 s only a small amount of this component has been consumed, leading to a

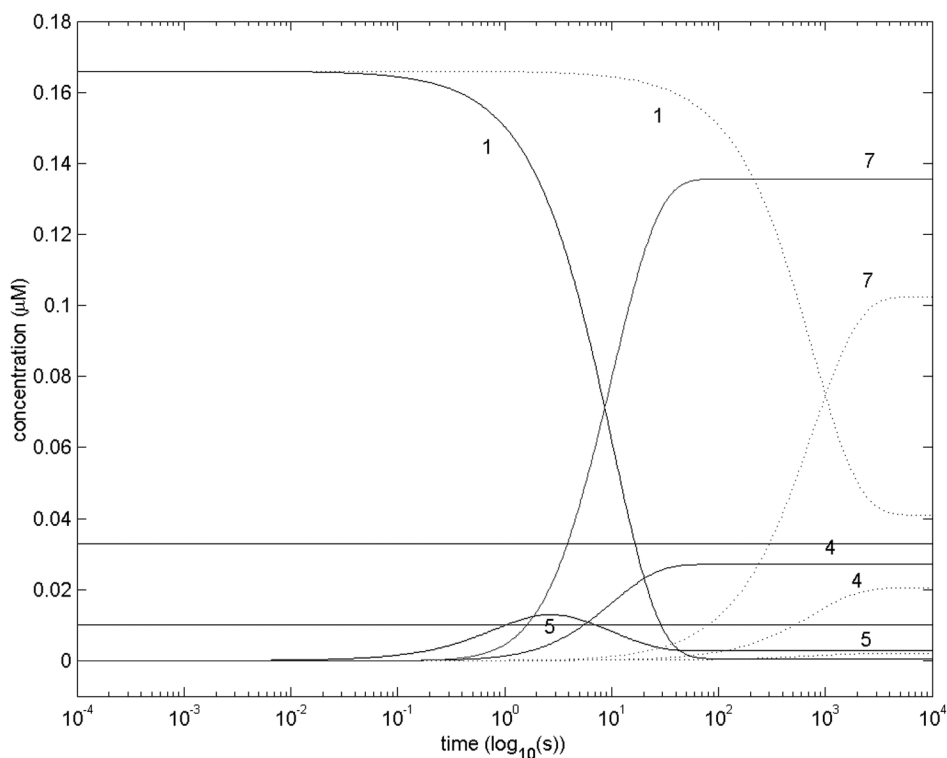


FIGURE 3. Model A, constant flow (Table II), $c_3^0 = 0.2 \text{ mM}$ (case Ac-2), with $K_{2,1} = 1$ as solid curve and $K_{2,1} = 0.01$ as dashed curve. The curves with constant $c_3^0 = 0 \text{ mM}$ (case Ac-1, not shown) are identical to the solid curve.

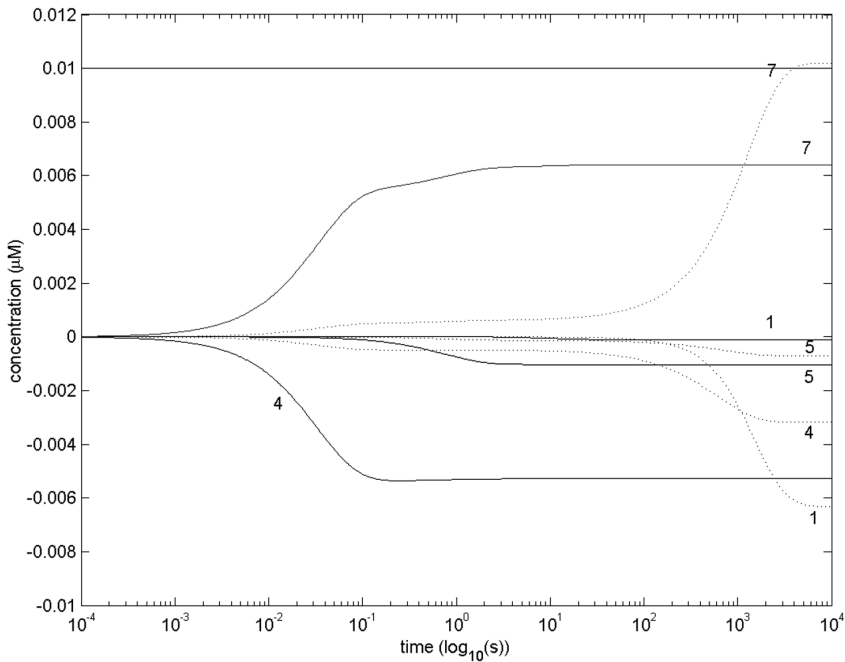


FIGURE 4. Model A, constant flow, as per Figure 3, with start of chemical relaxation (initiated for instance by temperature jump) at 100 s; curves show the deviations from the curves without perturbation. Please note that the line for $3 c_{\text{one}}$ coincides with the abscissa axis.

pronounced change in the dashed curve for component 1 in Figure 4. For $K_{2,1} = 0.01 \mu\text{M}$, all reactants are participating, showing that components 4 and 7 are in fast equilibrium at this time period. That is also why components 4 and 7 move nearly synchronously in Figure 4. The time period for visible presence of component 5 increases — as does the size of c_5 in constant flow — as the separation between $K_{2,1}$ and $K_{4,3}$ increases beyond the selected factor 10 shown here.

We deduce from the location of the horizontal lines in Figures 3 and 4 that single molecule kinetics may be largely neglected in flow experiments, but not in chemical relaxation experiments (where only the lines for $3 c_{\text{one}}$ are shown). This holds for all described simulations. Thus, many chemical relaxation curves would have to be measured for one set of data to obtain averaged curves which correspond to bulk concentrations.

Figures 5 to 7 are concerned with Model B (Figure 1B). Figure 5 shows that in constant flow there is very little difference between cases Bc-1 and Bc-2 for $K_{4,3} = 1$ (in both cases c_3^0 is small compared to $K_{4,3}$). Therefore, a third value for c_3^0 ($= 2 \mu\text{M}$) was chosen, although this high concentration is rather unlikely in nature. In all cases, component 5 reaches a pronounced concentration maximum after about 1 s. The difference between Models A and B lies in the fact that component 5 is free ssDNA in Model A and ternary complex in Model B.

Figure 6 shows the corresponding curves for Model B and $K_{4,3} = 0.01 \mu\text{M}$. While case Bc-1 shows the expected longer presence of component 5 and the expected shift of the rising curves for c_4 and c_7 relative to Figure 5, case Bc-2 is very different in the final time

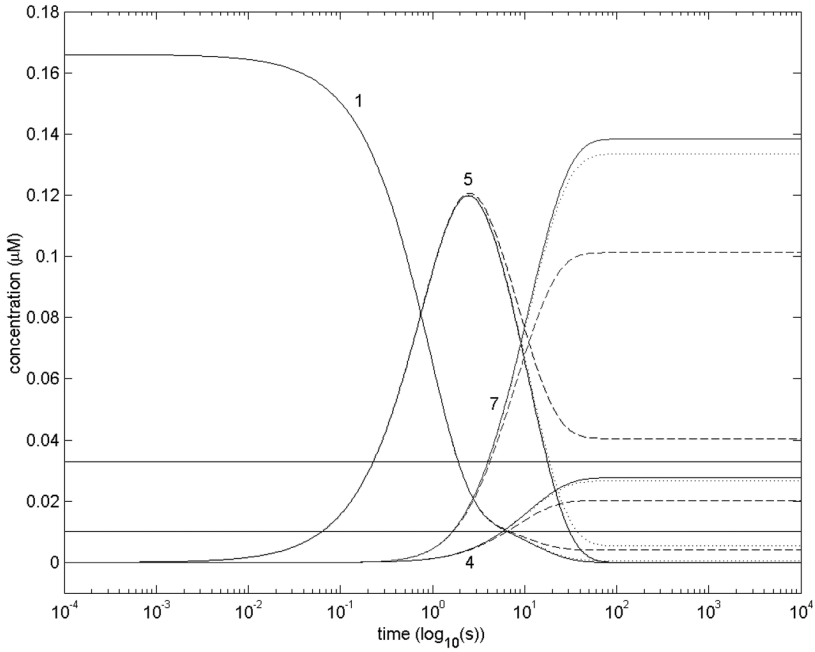


FIGURE 5. Model B, constant flow (Table III), constant $c_3^0 = 0$ (solid curves), 0.2 (dotted curves), 2.0 (dashed curves) μM with $K_{4,3} = 1$.

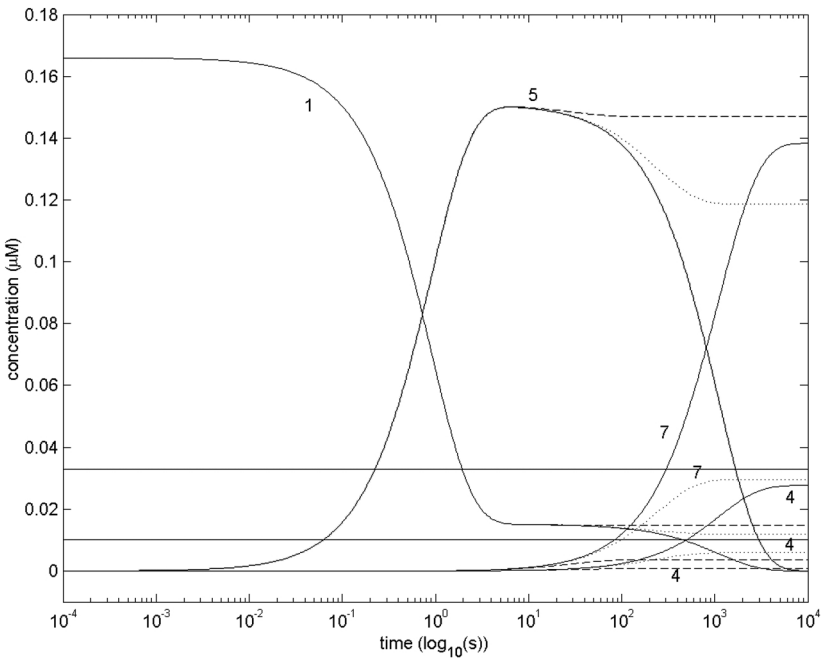


FIGURE 6. Model B, constant flow (Table III), constant $c_3^0 = 0$ (solid curves), 0.2 (dotted curves), 2.0 (dashed curves) μM , with $K_{4,3} = 0.01$.

period. Case Bc-3 produces almost no components 4 and 7. Because of the high concentration of the catalytically inactive ternary complex 5 over most of the time range, this alternate case is most likely not present in nature. The shape of the curves is clearly highly dependent upon the initial concentration of component 3: high $c_3^0 / K_{4,3}$ essentially stabilizes component 5.

Figure 7 shows the chemical relaxation results for $K_{4,3} = 1 \mu\text{M}$ and cases Bc-1, Bc-2 and Bc-3 with temperature jump at 100 s. The curves for Bc-1 and Bc-2 are almost identical, while those for Bc-3 are clearly different. A temperature jump at 1 s (not shown) reveals a transient appearance of component 5. The behavior is similar to that shown in Figure 4, except for the visible dependence upon the initial concentration of component 3. The value $K_{2,1} = 0.01 \mu\text{M}$ leads to a shift similar to that in Figure 4 (not shown).

Figure 8 refers to Model C. Compared to Model B there is no component 5 present. This would also be the limiting case for Model B at very low concentrations of component 5 (and thus sufficiently fast decomposition in both directions). As the two lower values for c_3^0 led to identical curves, we also used $c_3^0 = 2 \mu\text{M}$ (the values given for c_2^0 and $K_{2,1}$ dictate $c_3^0 \gg c_2^0$ for a significant change in final concentrations of components 4 and 7, as c_3^0 is low).

Figure 9 shows chemical relaxation with perturbation initiated at 100 s, under the conditions of Figure 8. Again, the curves for the two lower values of c_3^0 overlap, while the curves for $c_3^0 = 2 \mu\text{M}$ are clearly different. The difference for c_1 is substantial. One should note that high c_3^0 produced a visible relaxation curve for component 1, delayed from the initial change for components 4 and 7. At high c_3^0 there is a secondary change in 7 coinciding with the timing for the change in c_1 . A similar change in c_4 is barely visible.

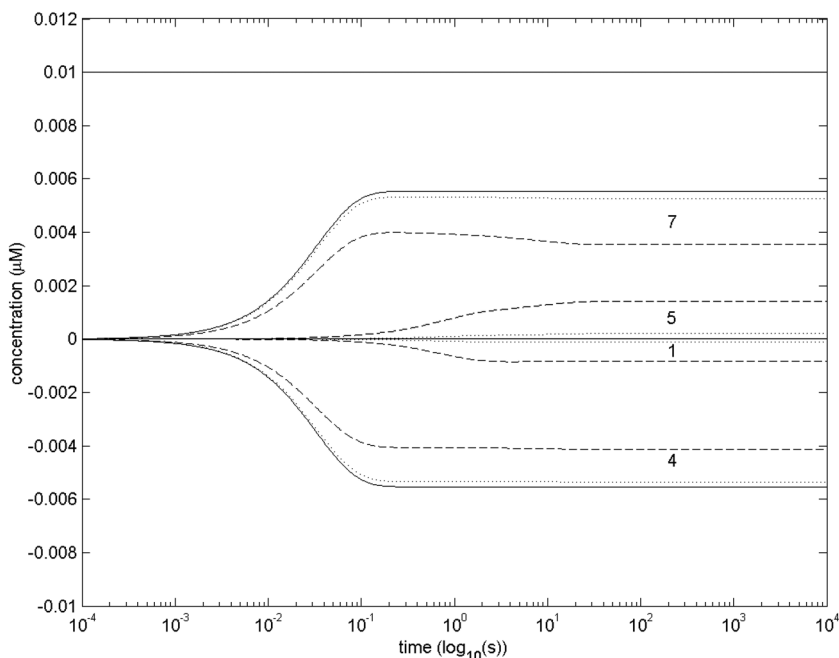


FIGURE 7. Chemical relaxation behavior for conditions of Figure 5, temperature jump initiated at 100 s.

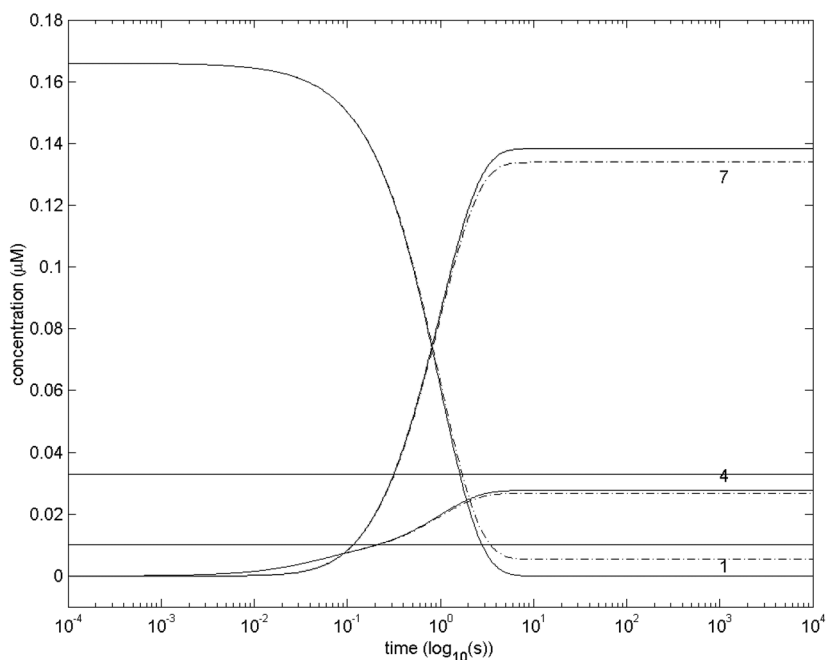


FIGURE 8. Model C, constant flow (Table IV), constant $c_3^0 = 0$ (solid curves), 2.0 (dashed curves) μM .

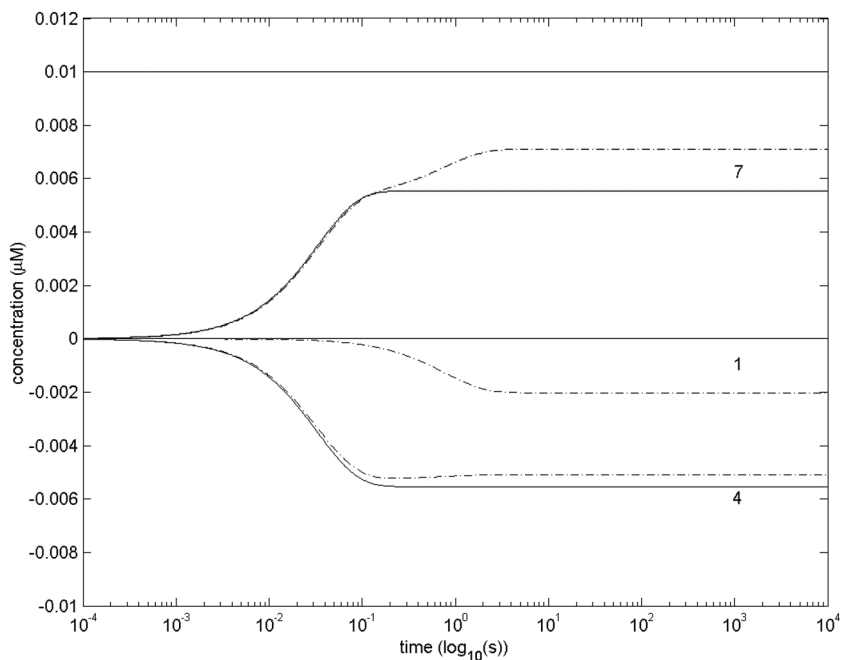


FIGURE 9. Temperature jump at 100 s for Model C, constant flow, conditions of Figure 8 with same notation of curves. Please note that the line for $3 c_{\text{one}}$ coincides with the abscissa axis.

Stopped Flow

Figure 10 refers to Model A and should be compared to Figure 3 involving constant flow under otherwise identical conditions. For $K_{2,1} = 1 \mu\text{M}$ there is very little difference between constant and stopped flow. But for $K_{2,1} = 0.01 \mu\text{M}$ the equilibrium values for components 1 and 7 are clearly different.

Chemical relaxation curves are shown in Figure 11 which should be compared to Figure 4. Structure and diversity are increased in Figure 11 over Figure 4. As indicated for Figure 4, the curves for $K_{2,1} = 0.01$ would be quite different for perturbation initiated at 10^4 s (curves for components 4 and 7 shifted back to the left). For $K_{2,1} = 0.01 \mu\text{M}$, in both stopped and constant flow most of component 1 is converted to other components for $c_3^0 = 0 \mu\text{M}$ (not shown), less for $c_3^0 = 0.2 \mu\text{M}$ (Figure 10) and only about 20% for $c_3^0 = 2 \mu\text{M}$ (not shown).

Figure 12 refers to Model B for $c_3^0 = 0 \mu\text{M}$. The difference between constant and stopped flow is rather small, but increases for larger c_3^0 (not shown).

Figure 13 refers to Model C for $c_3^0 = 0.2 \mu\text{M}$. The difference between constant flow and stopped flow is again rather small and negligible for practical purposes. Chemical relaxation data for this model are not shown, as there is again little difference between constant and stopped flow.

Figure 14 shows the behavior of Models A and B in stopped flow with $c_3^0 = 0 \mu\text{M}$ and $c_2^0 = 0.2 \mu\text{M}$ (reduced from the $1 \mu\text{M}$ used elsewhere in order to show the behavior of these curves together with the others; the concentration curves for component 2 have a similar shape for $c_2^0 = 1 \mu\text{M}$ but are vertically offset). The strongest difference between

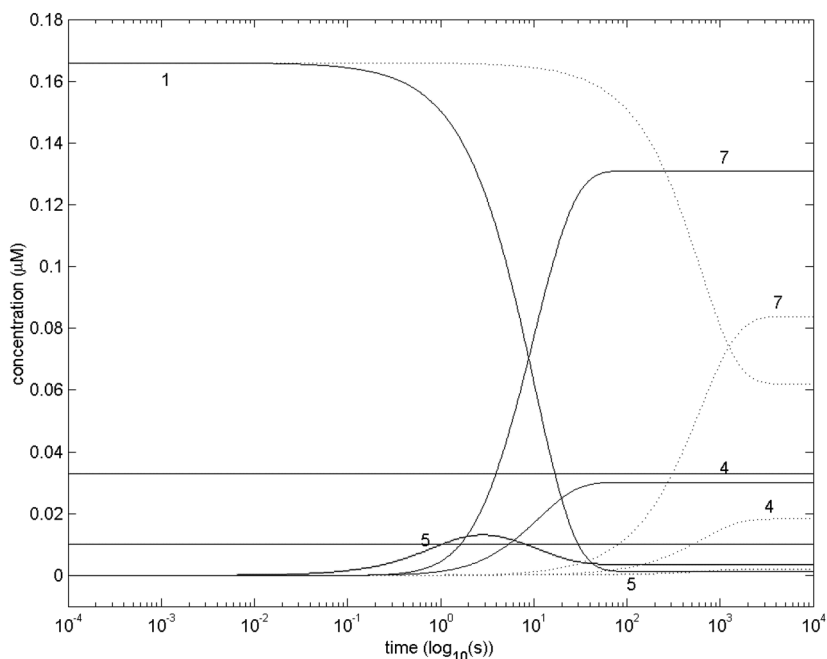


FIGURE 10. Model A, stopped flow (Table V) with $K_{2,1} = 1 \mu\text{M}$ (solid curves) and $K_{2,1} = 0.01 \mu\text{M}$ (dotted curves) for case As-2 only. Data not shown in Table V are in Table II.

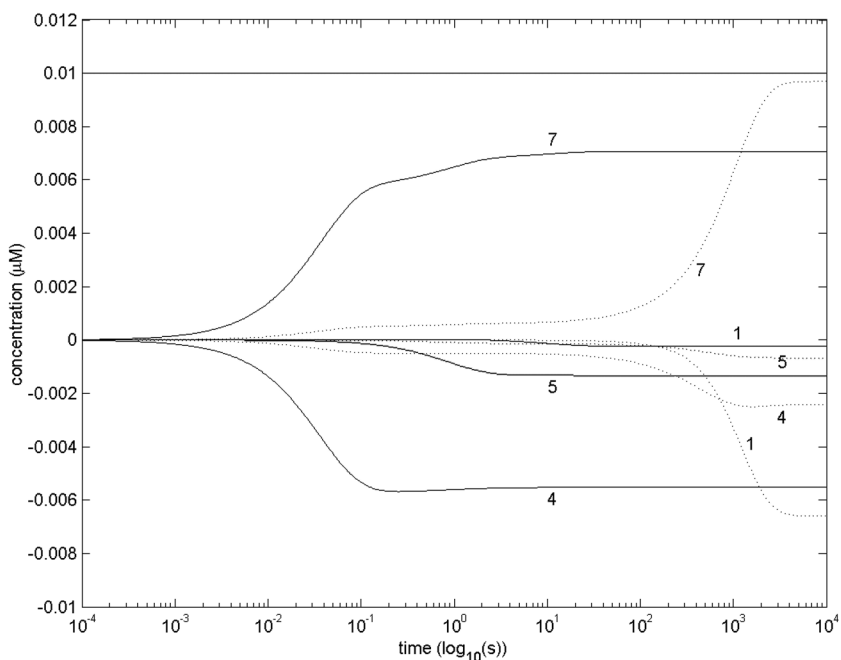


FIGURE 11. Difference curves after perturbation at 100 s, Model A, stopped flow (Table V) with $K_{2,1} = 1 \mu\text{M}$ (full curves) and $K_{2,1} = 0.01 \mu\text{M}$ (dotted curves) for case As-2 only. Please note that the line for $3 c_{\text{one}}$ coincides with the abscissa axis.

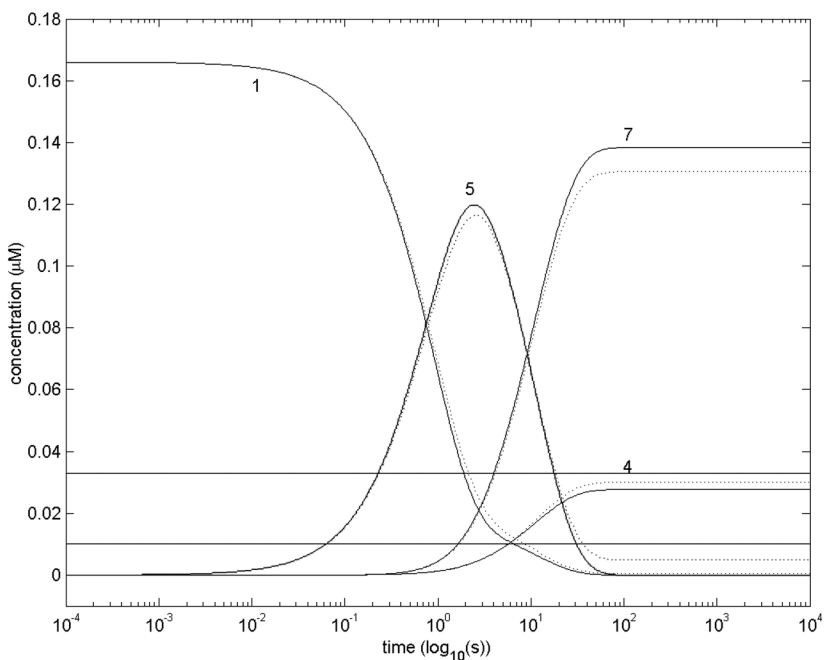


FIGURE 12. Model B, with $K_{4,3} = 1 \mu\text{M}$ for case Bc-1 and Bs-1 only, constant flow (solid curves) and stopped flow (dotted curves). Data not shown in Table VI are in Table III.

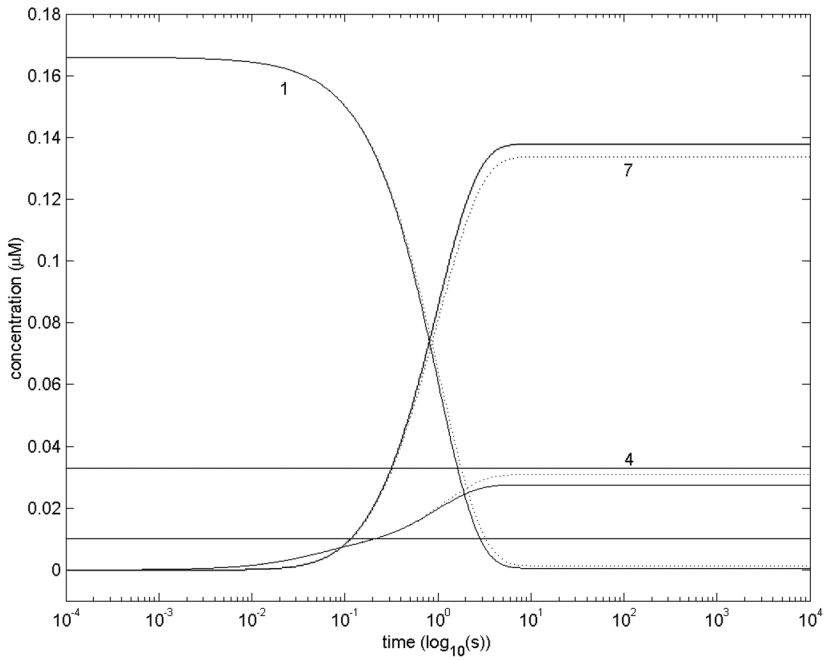


FIGURE 13. Model C with $c_3^0 = 0.2 \mu\text{M}$ only for constant flow (solid curves, case Cc-2) and stopped flow (dashed curves, case Cs-2). Data not shown in Table VII are in Table IV.

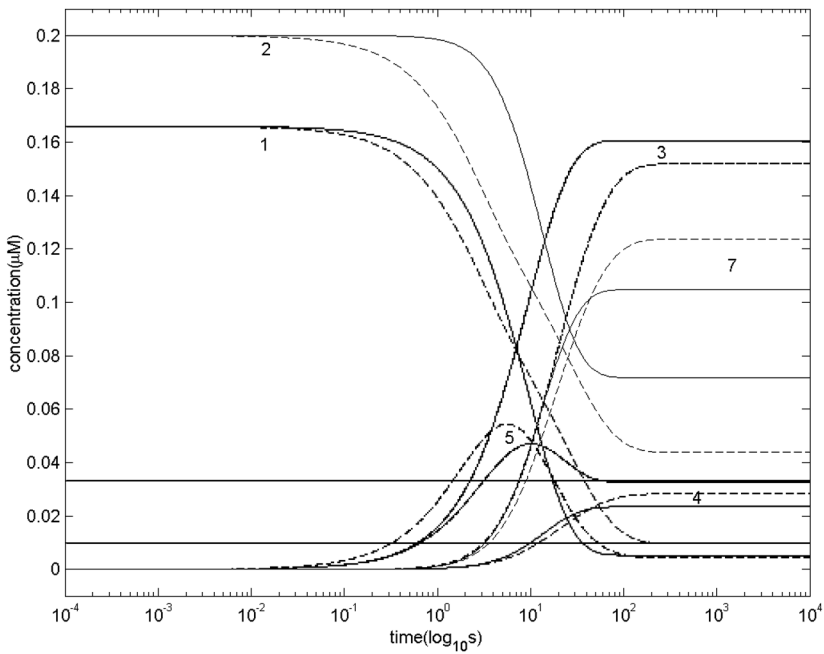


FIGURE 14. Stopped flow with $c_2^0 = 0.2 \mu\text{M}$ and $c_3^0 = 0 \mu\text{M}$. Solid curves refer to Model A (Table V), dashed curves to Model B (Table VI).

the models is in the shapes of c_1 and c_2 . The equilibrium values for component 5 are also strikingly different. Comparing the latter (solid curve) with the corresponding one in Figure 10, one sees that the equilibrium value and the transient maximum for component 5 are much lower in Figure 10 where $c_2^0 = 1 \mu\text{M}$.

Detection Strategy

The numerical simulations reveal that the models are best distinguished by the position of the concentration curves for components 3 and 5. If the curve for component 3 starts with the curve for component 5, Model A determines the system. If the curve for component 3 starts visibly later than the one for component 5, Model B determines the system (but see below). Model C is most likely present if there is no indication of component 5. As stopped flow and constant flow data are similar, data for constant flow under otherwise identical conditions are similar to Figure 14.

The simulated concentration data guide the use of specific fluorophors. We incorporated the fast reaction step with fluorophor-labeled dGTP (component 6) to provide an instant measure of the amount of telomerase-telomere complex formed. But this is not enough to distinguish between mechanisms. If component 1 is also fluorophor-labeled and its fluorescence changes measurably upon conversion, one could follow the decrease in this concentration and compare it with the appearance of the concentrations of components 4 and 7. If the latter correlates directly with the former, mechanism C is indicated. If the correlation is not present, either mechanism A or B are present.

Figure 14 shows that components 4 and 7 appear earlier for Model A than for Model B. One may expect such behavior on the basis of simply comparing the original models. However, much is dependent upon the conditions for the life of component 5. If the transient concentration of component 5 is relatively large, there will be a delay in the appearance of components 4 and 7. The conditions for the life of component 5 are largely effected by the size of c_2^0 and c_3^0 , plus their relation to the associated equilibrium constants. It is thus best to use a fluorescent indicator for free 5 in Model A (or for ternary complex 5 in Model B). One would then be able to quantitatively correlate all concentration changes along the path of fixed components. Obviously, one has to be careful that the indicator does not alter the kinetics significantly. If there is a free indicator binding with component 5, the conditions should be such that at most 20% of component 5 is bound to the indicator; otherwise, one would need to take into account the equilibrium constants involved in the binding of the indicator to component 5; for ease of detection this binding should be substantially faster than the binding of components 2 and 3.

One potential compound specific for free component 5 (unoccupied ssDNA) could possibly be a low molecular weight analogue of Pot1 (Loayza and de Lange, 2004), as Pot1 is specific for binding only to the ends of telomeres. Pot1 may be the protective agent (blocker) discussed above (Loayza and de Lange, 2004), deduced from work of Teixeira *et al* (2004).

Is there a way to distinguish between Models A and B without the use of an indicator for compound 5? In chemical relaxation one of us (Czerlinski, 1966) showed that the concentration dependence of the chemical relaxation times for Model B is inverse to those for Model A. By looking at Figure 14 it is also apparent that the transient concentration of component 5 decreases with increasing c_2^0 and c_3^0 for Model A, but increases with increasing c_2^0 and c_3^0 for Model B (not all data shown). This would be an indirect method of distinguishing between the two Models.

Consideration of Diffusion

So far we have ignored the fact that the observation volume in our mixing arrangement is not a closed system, but is surrounded by space without spatially fixed reactants. We have two cases. (1) Reactants are attached to the surface of an object glass. Then we have to take into account the fluid space above the fixed reactants. (2) Reactants are fixed near the surface of a cell nucleus. There is space all around the fixed reactants within the reaction volume. If one employs constant flow, the concentration at the reaction location can be kept constant, so we have an open system which is fully controlled. Stopped flow, on the other hand, requires consideration of reactants (components 2, 3 and 6) diffusing from outside the reaction volume into the reaction volume.

First, consider individual nucleotides on the surface of the cell nucleus diffusing to their reaction site. For simplicity we use the established diffusion constant of ATP (Diel *et al.*, 1991), $D = 3 \times 10^{-6} \text{ cm}^2 \text{ s}^{-1}$, and the relation $x^2 = 2 D t$ where x is the mean diffusion distance and t the characteristic diffusion time (Moore, 1960). With a diffusion channel length of $x = 10^{-6} \text{ cm}$ we compute $t = 1.67 \times 10^{-5} \text{ sec}$ which is negligibly short compared to the relaxation process of the steps involving nucleotide binding (Figure 4). This even holds if the diffusion constant is a factor of ten slower in the channel (Rostoftseva and Bezrukov, 1998). Telomerase and blocker may have a smaller diffusion constant D , but their kinetics is also slower than that of the nucleotide (Figure 3). Thus, diffusion through the pore will probably not affect the observed kinetics.

Next, consider reactants attached to the surface of an objective glass, case (1) above. The height of the flow volume above the surface is at least $10 \mu\text{m}$ (10^{-3} cm). One obtains $t = 0.167 \text{ s}$ from the cited formula. To obtain homogeneity after diffusion, t should be multiplied by 10. That is 1.67 s for nucleotides (component 6), and longer for the other free reactants (components 2 and 3). The data of Figure 14 show that we reach this limit for stopped flow operation. Obviously, the results are worse for case (2) above. However, if the actual kinetics is slower than assumed by us, we may be able to use stopped flow successfully. Reducing the size of the space around the reaction volume then becomes of paramount importance.

Optimizing the Design

While for constant flow we only need to consider the chemistry (and possibly small volume flow which can be arranged by a narrow flow channel), stopped flow requires the design of a stopped flow chamber with as small a volume as possible. One possible configuration is shown in Figure 15. Obviously, special tools are required to fabricate such small reaction chambers. Besides very small volumes consumed, stopped flow allows one to follow the changes in the concentrations of free components (2, 3, 6).

In early equipment tests one may use pH (and other) indicators together with suitable buffers to observe the stability of temperature as well as changes in temperature, selecting components with the proper reaction enthalpies (Czerlinski, 1966, pp. 218–227). In reverse, one may also use fluorescent pH indicator systems as fast optical temperature indicators, possibly even for temperature control (stability as well as fast rise time for temperature jumps).

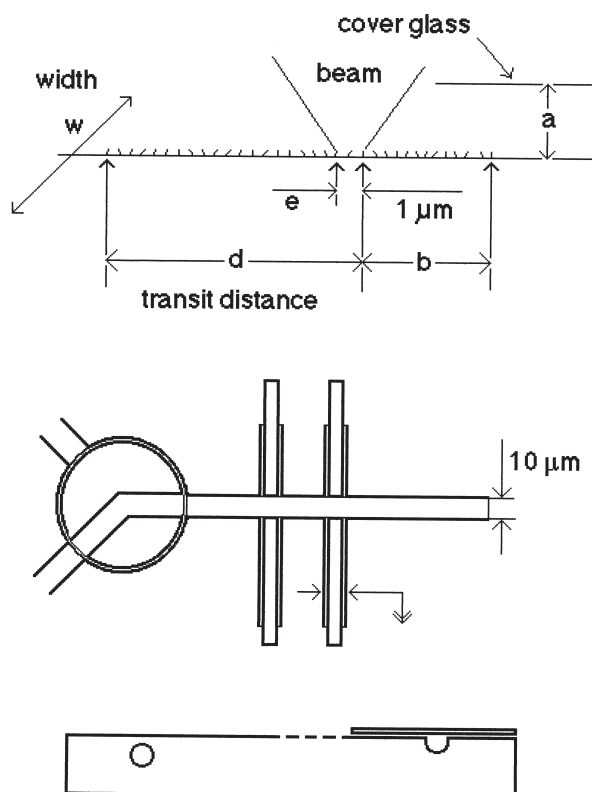


FIGURE 15. Object glass designs for small volumes. The top part shows a vertical cross-section in the plane of the central flow section where observation takes place; “beam” refers to the fluorescence emission beam collected by the microscope objective. Fluorescence excitation and emission beams propagate coaxially. The short lines on the objective indicate the desoxyribonucleotide chains attached to the surface of the objective. The flow moves from left to right. Distance d refers to the flow transit distance to the end of observation. Distance b covers the remainder of the attached chains. Distance e covers the width of the observation beam at the site of fluorescence emission, while a refers to the distance between top surface of objective to bottom surface of cover glass and w denotes the width of the object glass covered with the desoxyribonucleotide chains. A design for the smallest possible cell for stopped flow operation is shown in the middle portion. The four plungers are all moved together, providing a no-displacement closing valve system. The two-way valve on the left may have to be located further away than shown, as the central flow channel should only have a diameter of $10\ \mu\text{m}$. Such a small diameter bore may require advanced technology. The lower part shows a vertical cross-section in the circular plane of the bore. No cover glass is used on the left, but is required on the right to close off the groove. The required plungers are not shown here, but are different for the two types of bores.

References

- Baumann, P., Cech, T.R. (2001) Pot1, the putative telomere end-binding protein in fission yeast and humans. *Science* 292: 1171–1175.
- Blackburn, E.H. (1991) Structure and function of telomeres. *Nature* 350: 569–573.
- Cech, T.R. (2004) Beginning to understand the end of the chromosome. *Cell* 116: 273–279.
- Czerlinski, G. (1966) *Chemical Relaxation*, Marcel Dekker, New York, p. 89, 107.
- Czerlinski, G. (1993) Resolving the fast equilibrations of ternary complexes in liver alcohol dehydrogenase. *J. Theor. Biol.* 165: 313–320.
- Denk, W., Strickler, J.P., Webb, W.W. (1991) 2-photon laser microscopy, U.S. Patent No. 5,034,613, issued July 23.
- Diel, H., Ihlefeld, H., Schwegler, H. (1991) *Physik fuer Biologen*, Springer-Verlag, Berlin, p. 391.
- Greider, C.W., Blackburn, E.H. (1985) Identification of a specific telomere terminal transferase activated in tetrahymena extracts. *Cell* 43: 405–413.
- Greider, C.W., Blackburn, E.H. (1989) A telomeric sequence in the RNA of tetrahymena telomerase required for telomere repeat synthesis. *Nature* 337: 331–337.
- Loayza, D., de Lange, T. (2004) Telomerase regulation at the telomere: a binary switch. *Cell* 117: 279–280.
- Lu, H.P., Xun, L., Xie, X.S. (1998) Single-molecule enzymatic dynamics. *Science* 282: 1877–1882.
- Matlab 7.0 (2004) The Mathworks, 24 Prime Park Way, Natick, MA.
- Moore, W.J. (1960) *Physical Chemistry*, 2nd Ed., Prentice Hall, Englewood-Cliffs, NJ, p. 449.
- Morin, G.B. (1989) The human telomere terminal transferase enzyme is a ribonucleoprotein that synthesises TTAGGG repeats. *Cell* 59: 521–529.
- Rostoftseva, T.K., Bezrukov, S.M. (1998) ATP transport through a single mitochondrial channel, VDAC, studied by current fluctuation analysis. *Biophys. J.* 74: 2365–2373.
- Schnapp, G., Rodl, H.-F., Rettig, W.J., Schnapp, A., Damm, K. (1998) One-step affinity purification protocol for human telomerase. *Nucl. Acids Res.* 26: 3311–3313.
- Shampine, L.F., Reichelt, M.W. (1997) The Matlab ODE Suite. *SIAM J. Sci. Comput.* 18: 1–22.
- Stryer, L. (1988) *Biochemistry*, 3rd Ed., Freeman & Co., New York, p. 191.
- Teixeira, M.T., Americ, M., Sperisen, P., Lingner, J. (2004) Telomere length homeostasis is achieved by a switch between telomerase-extendable and non-extendable states. *Cell* 117: 323–335.
- Wenz, C., Enenkel, B., Amacker, M., Kelleher, C., Damm, K., and Lingner, J. (2001) Human telomerase contains two cooperating telomerase RNA molecules. *EMBO J.* 20: 3526–3534.

Received December 1, 2005;
accepted January 12, 2006.

Effects of Post Low-dose X-ray Irradiation on Carbon Tetrachloride-induced Acatalasemic Mice Liver Damage

Takahiro Kataoka¹, Takaharu Nomura², Da-Hong Wang³,
Takehito Taguchi¹, and Kiyonori Yamaoka^{1*}

*Chairs of ¹Medical Radioscience and ³Public Health, Okayama University Medical School,
5-1 Shikata-cho, 2-chome, Okayama 700-8558, Japan,*

*²Low Dose Radiation Research Center, Central Research Institute of Electric Power Industry,
2-11-1 Iwado-kita, Komae-shi, Tokyo 201-8511, Japan*

**Author for correspondence; E-mail: yamaoka@md.okayama-u.ac.jp*

Abstract: The catalase activities in the blood and organs of the acatalasemic (C3H/AnLCs^b-Cs^b) mouse of the C3H strain are lower than those of the normal (C3H/AnLCs^a-Cs^a) mouse. We examined the effects of post low-dose (0.5 Gy) X-ray irradiation which reduced the oxidative damage under carbon tetrachloride-induced hepatopathy in acatalasemic or normal mice. As a result, the 0.5 Gy irradiation after carbon tetrachloride administration decreased the glutamic oxaloacetic and glutamic pyruvic transaminase activity in the acatalasemic mouse blood to a level similar to that of the acatalasemic mouse blood not treated with carbon tetrachloride; this is in contrast to a high-dose (15 Gy) irradiation. In the same manner, pathological disorder was improved by 0.5 Gy irradiation. The fat degeneration in normal mice was quickly reduced, in contrast to acatalasemic mice. These findings suggest that low-dose irradiation after carbon tetrachloride administration accelerates the rate of recovery and that catalase plays an important role in the recovery from hepatopathy induced by carbon tetrachloride, in contrast to high-dose irradiation.

KEY WORDS: acatalasemic mouse / CCl₄ / post low-dose irradiation / antioxidant substance

CATALASE IS an enzyme which catalyzes the resolving of hydrogen peroxide to water and oxygen. It is widely distributed in aerobic cells, such as animal, plant and microor-

Abbreviation: •CCl₃, trichloromethyl radical; GCS, glutamylcysteine synthetase; GOT, glutamic oxaloacetic transaminase; GPx, glutathione peroxidase; GPT, glutamic pyruvic transaminase; GR, glutathione reductase; GSH, glutathione; MDA, malondialdehyde; NADPH, nicotinamide adenine dinucleotide phosphate; O₂⁻, superoxide anion; SOD, superoxide dismutase; TBA, thiobarbituric acid; TBARS, thiobarbituric acid reactive substances; XOD, xanthine oxidase

ganisms, and it is contained in the livers, kidneys and red blood cells in mammals. The acatalasemic mouse is named so due to the loss of catalase. This mouse has a catalase activity about one tenth to one half of that in normal mouse, and provides hydrogen peroxide (H_2O_2) in these mice for carcinogenesis (1,2). As aging brings about decrease in antioxidant substances, the acatalasemic mouse is a useful model to study the relationship between active oxygen disease and low-dose irradiation.

We have reported that low-dose X-rays or low-level radon inhalation reduced the lipid peroxide to levels similar to those of juvenile animals. These mechanisms involve induction of superoxide dismutase (SOD), which destroys the superoxide anion (O_2^-), catalase, which destroys H_2O_2 and glutathione peroxidase (GPx), which also destroys H_2O_2 . These antioxidant substances increase after low-dose irradiation. Low-dose irradiation causes the production of a small amount of O_2^- *in vivo*; therefore, antioxidant substances are induced. These changes continue for a comparatively long time after low-dose irradiation, although the age, organ and the organization of the animals result in differences in the radiation receptivity (3–6).

It is well known that carbon tetrachloride (CCl_4) causes liver cirrhosis. The toxicity of CCl_4 is weak, and the hepatocellular damage by CCl_4 is peculiar to the liver. Transient hepatocellular damage, such as degeneration and necrosis, after the administration of CCl_4 is thought to be induced by the trichloromethyl radical ($\bullet\text{CCl}_3$). The mechanisms of CCl_4 -induced hepatotoxicity are generally considered to result from the conversion of CCl_4 into $\bullet\text{CCl}_3$ by the cytochrome P450 system in the endoplasmic reticulum of hepatocytes, in which the trichloromethyl radical and the highly reactive trichloromethyl peroxyradical are formed to initiate lipid peroxidation of the endoplasmic reticulum in the early stage of CCl_4 -induced toxicity (7–15). Transient hepatocellular disorders after CCl_4 administration are thought to be induced by $\bullet\text{CCl}_3$.

Moreover, we have reported that the peaks of hepatocellular disorder were reached at around 18 hrs after CCl_4 administration (16), and that the peaks of the activities of antioxidant enzymes were reached at around 4 hrs after low-dose irradiation (3).

Considering this background, in the present study we examined whether oxygen damage is inhibited by low dose X-ray irradiation after CCl_4 administration or not. We also investigated the various biochemical parameters, such as transaminase activities in these hepatopathic mice. To put it concretely, we examined the time and dose dependent changes in livers of mice subjected to X-ray irradiation immediately after CCl_4 administration (Experiment 1), and the dose dependent changes in mice livers 4 hrs after X-ray irradiation and 18 hrs after CCl_4 administration (Experiment 2).

Materials and Methods

Animals

Two strains of C3H mice originally provided by Feinstein *et al.*, normal (C3H/AnLCS^aCs^a) and acatalasemic (C3H/AnLCS^bCs^b) strains (17), nine weeks of age and 20–30 g of body weight were kept in an air-conditioned room (temperature 20°C and humidity 60%) at the Animal Center for Medical Research, Okayama University Medical School. They were fed on Oriental MF diet (Oriental Yeast Co., Tokyo) and tap water *ad libitum*. The number of mice per experimental group was 5. Approval from the affiliated bodies for animal experiments was received.

12.5 μl CCl_4 (20% in olive oil)/g weight was injected intraperitoneally to mice.

Each mouse was irradiated with a single dose of 0.5 Gy (low-dose) or 15 Gy (high-dose) at a dose rate of 0.75 Gy/min of X-rays (voltage: 150 keV, ampere: 15 mA, filters: Cu:Al=0.5 mm:1.0 mm) immediately (Experiment 1) or at 18 hrs (Experiment 2) after CCl_4 administration, using an X-ray generator (Hitachi MBR-1505R2). The age matched control mice were sham-irradiated. All the animals were sacrificed by cervical dislocation. Each experimental group consisted of 5 mice. In Experiment 1, blood was drawn at 18 hrs or 42 hrs after CCl_4 administration and X-ray irradiation (immediately). And in Experiment 2, X-ray irradiation was 18 hrs after administration and blood was drawn 4 hrs after the irradiation. Serum was separated by centrifugation at $3,000\times g$ for 15 min for the assay of the activities of glutamic oxaloacetic transaminase (GOT) and glutamic pyruvic transaminase (GPT). Livers were quickly excised for the analyses of the activities of catalase, SOD, GPx, the total glutathione content, glutamylcysteine synthetase (GCS) and the thiobarbituric acid reactive substances (TBARS) production. Parts of the livers were fixed in 10% neutral-buffered formalin for histological examinations.

Biochemical assays

Blood was collected using the above treatment, and serum was obtained by centrifugation at $3,000\times g$ for 15 min at 4°C . The activities of GOT and GPT were measured with the UV-rate method using GOT and GPT-test kits (Wako Pure Chemical Industry, Co., Ltd.) (18).

Lipid peroxide, malondialdehyde (MDA), was assessed with TBARS according to the method of Uchiyama and Mihara (19). The liver was homogenized in 154 mM KCl on ice and refluxed for 60 min at 95°C in the presence of 0.3% (w/v) thiobarbituric acid (TBA) and 7.5% (v/v) acetic acid at pH 3.5. The optical density of colored product was read at 532 nm with a spectrophotometer. 1,1,3,3-Tetraethoxy-propane was used for the standard curve, and the results were expressed as n mol of malondialdehyde per mg of protein. The protein content was measured according to method of Lowry *et al* (20).

The SOD activity was determined with the spin-trapping method, using a JES-TE100 electron spin resonance (ESR) device (JEOL) (21). The measuring procedure of this ESR method was as follows: 15 ml of 450 mM 5,5-dimethyl-1-pyrroline-*N*-oxide (DMPO), 85 μl of SOD extract specimen and 50 μl of 2 mM hypoxanthine were placed in a test tube. To the mixture was added 50 μl of xanthine oxidase (XOD) (0.2 units/ml). After agitation, the assay mixture was transferred into a special flat cell (product of JEOL). The DMPO- O_2^- -spin adduct was analyzed 45 sec after the addition of XOD with the aid of an ESR spectrometer. Manganese oxide was used as an internal standard. The spin number was calculated by comparing the signal strength with that of 2,2,6,6-tetramethyl piperidine-*N*-oxide, the spin number of which is known.

Catalase activity was measured at 240 nm by a spectrophotometer in terms of H_2O_2 reduction rate at 37°C (22). The mixtures for assays consisted of 50 μl of 1 M Tris-HCl buffer containing 5 mM ethylenediaminetetraacetic acid (EDTA) (pH 8.0), 900 μl of 10 mM H_2O_2 , 30 μl of deionized water, and 20 μl of the liver supernatant. The activity was calculated by using a molar extinction coefficient of $7.1\times 10^{-3} \text{ M}^{-1}\text{cm}^{-1}$. In all assays, the assay mixtures were incubated at 37°C and then at 30°C for 5 min each. The reactions were started by adding the liver supernatant prepared as described above.

GPx activity was assayed by coupling the reduction of tertbutyl hydroperoxide to the oxidation of reduced nicotinamide adenine dinucleotide phosphate (NADPH) by glutathione

reductase (GR) (23). The assay mixtures consisted of 100 μ l of 1 M Tris-HCl containing 5 mM EDTA (pH 8.0), 20 μ l of 0.1 M glutathione, 100 μ l of GR solution (10 units/ml), 100 μ l of 2 mM NADPH, 650 μ l of distilled water, 10 μ l of 7 mM tertbutyl hydroperoxide, and 10 μ l of liver supernatant. The oxidation of NADPH at 37°C was followed spectrophotometrically at 340 nm. One unit of activity is defined as the amount of GPx required to oxidize 1 μ mol of NADPH per min.

The total glutathione content was measured using a modified spectrophotometric technique (24). Briefly, 0.25 g of liver was suspended in 2.5 ml of 0.1 M phosphate buffer (pH 7.4), mixed with 1.25 ml of ice-cold 10% trichloroacetic acid (TCA) solution, then homogenized in a teflon-grass homogenizer. The homogenates were centrifuged at 14,000 \times g for 15 min. Subsequently, 0.5 ml of the supernatant was treated with 3 ml of ice-cooled diethylether, and the diethylether layer was removed with a pipette. This procedure was repeated 5 times to remove the excess TCA. The final supernatant was assayed for total glutathione content. The sample solution (2.5 μ l) was mixed with 1 mM 5,5'-dithiobis (2-nitrobenzoic acid) (DTNB), 733 μ l of 0.3 mM NADPH and 10 μ l of GR (2 units/ μ l). The rate of change in absorbance was measured at 412 nm. Glutathione standards (1–20 μ g/ml) were analyzed in the same manner.

The activity of γ -GCS, the rate-limiting enzyme for *de novo* glutathione (GSH) biosynthesis was measured by means of a coupled enzyme assay that evaluates nicotinamide adenine dinucleotide phosphates (NADH) oxidation (25). The reaction mixture consisted of 600 μ l of pre-mixture solution containing 100 mM Tris-HCl (pH 8.2), 150 mM KCl, 20 mM $MgCl_2$, 50 mM EDTA, and 0.2 mM NADH, 100 μ l of 0.1 M ATP, 100 μ l of 0.1 M phosphoenol pyruvate, 50 μ l of 0.1 M *L*-glutamete, 5 μ l of pyruvate kinase solution (5 units), 5 μ l of lactate dehydrogenase solution (10 units), 50 μ l of 0.1M *L*- α -aminobutyric acid and 90 μ l of the liver supernatant. The NADH oxidation at 37°C was followed by measuring the absorbance at 340 nm. The activity was calculated using a molar extinction coefficient of $6.22 \times 10^3 \text{ M}^{-1} \text{ cm}^{-1}$ and expressed as μ mol of NADH oxidized / min / mg protein.

Histopathological examination

The left and central lobes of the liver were fixed in 10% formalin, processed with a graded mixture of ethanol and xylene and embedded in paraffin. Five μ m thick tissue sections were prepared and stained with hematoxlin-eosin (HE). The other parts were placed in a deep freezer at -80°C for the assays, as described below. Small tissue specimens (4 \times 4 \times 2 mm) were collected from the liver, which showed gross fat degeneration. They were fixed by immersion for 12 hrs in 4% phosphate-buffered formalin at room temperature. After rinsing in phosphate-buffered saline for 2 hrs, the tissue was immersed into an octo-compound for a period of 2 hrs by twice changing the 100% catalysed plastic containers. Two μ m thick sections were cut with a Sorvall microtome using glass knives, stretched on a water bath (23°C), put on a slide, and dried at room temperature. Lipids were demonstrated using Sudan Black B, the sections were rinsed briefly in 70% ethanol and stained in a filtered Sudan Black B solution containing 0.25% Sudan Black B in 70% ethanol. The sections were differentiated in 70% ethanol. Counterstaining was performed by using 1% neutral red for 5 min, and the sections were mounted in glycerin-gelatin (26).

Statistical analysis

The data values are presented as the mean \pm the standard error of mean (SEM). The statistical significance of differences was determined with Student's *t*-test for comparison between two groups or by two-way analysis of variance (ANOVA) and Dunnett's tests for multiple comparison.

Results

Experiment 1: Time and dose dependent changes in mice livers by X-ray irradiation immediately following CCl₄ administration

Changes caused by 0.5 Gy irradiation

Within 18 hrs after CCl₄ administration, the GPx activity significantly increased in normal mice subjected to sham irradiation. On the other hand, no significant differences were observed in the activities of GOT, GPT, SOD, catalase and GCS and the lipid peroxide level and total glutathione content in either acatalasemic or normal mice subjected to 0.5 Gy irradiation. Within 42 hrs of CCl₄ administration, the activities of GOT and GPT significantly decreased in both acatalasemic and normal mice. In the same manner, no significant differences were observed in the activities of the SOD and GCS and lipid peroxide level and total glutathione content with 0.5 Gy irradiation (Table I, II).

Changes caused by 15 Gy irradiation

Within 18 hrs of CCl₄ administration, the activities of GOT and GPT and the lipid peroxide level significantly increased in both acatalasemic and normal mice given 15 Gy irradiation after CCl₄ administration. On the other hand, the activities of SOD, catalase, GPx and GCS, and total glutathione content significantly decreased. Within 42 hrs of CCl₄ administration, the lipid peroxide level significantly increased in both acatalasemic and normal mice, and the activities of SOD and catalase and total glutathione content significantly decreased (Table I, II).

Histological observation caused by 0.5 Gy or 15 Gy irradiation

At 18 hrs following CCl₄ administration, liver tissues exhibited fat degeneration surrounding the central vein but no significant differences in either acatalasemic or normal mice among sham-, 0.5 Gy or 15 Gy irradiation groups. However, at 42 hrs after CCl₄ administration, the fat degeneration in livers of both acatalasemic and normal mice from the sham- or 0.5 Gy irradiated groups was reduced compared with that of each group, as shown by the results of blood biochemistry (Table I). Moreover, the fat degeneration in normal mice quickly decreased, compared with the acatalasemic mice.

At 18 hrs after CCl₄ administration, the liver tissues of mice subjected to sham-, 0.5 Gy or 15Gy irradiation exhibited centrilobular necrosis of the parenchymal hepatocytes both in acatalasemic and normal mice. At 42 hrs after CCl₄ administration, centrilobular necrosis was greater than at 18 hrs after CCl₄ administration in the sham-, 0.5 Gy or 15 Gy irradiated groups. (Figure 1-1 to Figure 1-4).

TABLE I. Temporal changes in aminotransferases in blood of acatalasemic or normal mice at each sham-, 0.5 Gy or 15 Gy X-ray irradiation following CCl₄ administration.

GOT activity [kU/L]	Mice	No Treatment	Treatment	Time after CCl ₄ administration	
				18 hrs	42 hrs
Normal	Control	0.84±0.09	CCl ₄	8.09±0.57	-
			CCl ₄ +Sham	7.32±0.54	5.66±0.48*
			CCl ₄ +0.5Gy	9.32±0.61	4.12±0.41***
			CCl ₄ +15Gy	11.93±0.69**	10.14±0.64*
Acatalasemic	Control	2.20±0.15***	CCl ₄	11.03±0.66	-
			CCl ₄ +Sham	10.80±0.66	7.67±0.55**
			CCl ₄ +0.5Gy	12.12±0.70	6.10±0.49***
			CCl ₄ +15Gy	14.35±0.76	12.48±0.71*
Normal	Control	0.97±0.10	CCl ₄	10.85±0.66	-
			CCl ₄ +Sham	9.60±0.62	7.85±0.56*
			CCl ₄ +0.5Gy	10.37±0.64	5.52±0.47***
			CCl ₄ +15Gy	12.90±0.72	11.27±0.67
Acatalasemic	Control	2.17±0.15***	CCl ₄	12.97±0.72	-
			CCl ₄ +Sham	11.76±0.69	9.94±0.63*
			CCl ₄ +0.5Gy	13.10±0.72	7.04±0.53**
			CCl ₄ +15Gy	15.25±0.78*	13.76±0.74

Each value indicates the mean ± SEM. The number of mice per experimental point is 5. *P < 0.05, **P < 0.01, ***P < 0.001 vs. CCl₄ administration, +++P < 0.001 vs. normal mice.

TABLE II. Temporal changes in antioxidant-associated substances in liver of acatalasemic or normal mice at each sham-, 0.5 Gy or 15 Gy X-ray irradiation following CCl₄ administration.

	Mice	Treatment	Time after CCl ₄ administration	
			18 hrs	42 hrs
Lipid peroxide level [nM/mg protein]	Normal	CCl ₄ +Sham	0.57±0.03	1.12±0.13
		CCl ₄ +0.5Gy	0.57±0.04	1.00±0.14
		CCl ₄ +15Gy	1.48±0.14***	1.36±0.16*
	Acatalasemic	CCl ₄ +Sham	0.69±0.07	1.30±0.16
		CCl ₄ +0.5Gy	0.84±0.12	1.05±0.16
		CCl ₄ +15Gy	1.65±0.12***	1.63±0.12*
SOD activity [U/mg protein]	Normal	CCl ₄ +Sham	52.4±10.5	38.6±2.7
		CCl ₄ +0.5Gy	50.8±2.9	37.1±5.8
		CCl ₄ +15Gy	24.9±3.3***	22.4±2.1***
	Acatalasemic	CCl ₄ +Sham	47.2±5.1	40.1±2.3
		CCl ₄ +0.5Gy	46.0±4.2	39.2±3.6
		CCl ₄ +15Gy	25.6±6.1***	18.4±1.2***
Catalase activity [U/mg protein]	Normal	CCl ₄ +Sham	241±28	151±19
		CCl ₄ +0.5Gy	243±26	190±11**
		CCl ₄ +15Gy	111±37***	114±8*
	Acatalasemic	CCl ₄ +Sham	107±13	86±13
		CCl ₄ +0.5Gy	109±7	108±7*
		CCl ₄ +15Gy	60±8***	59±7*
GPx activity [U/mg protein]	Normal	CCl ₄ +Sham	39.2±5.3	25.0±4.0
		CCl ₄ +0.5Gy	55.3±5.9**	33.0±4.0*
		CCl ₄ +15Gy	26.9±4.1**	31.8±6.1
	Acatalasemic	CCl ₄ +Sham	42.0±4.4	29.0±3.0
		CCl ₄ +0.5Gy	47.2±6.9	35.0±3.8*
		CCl ₄ +15Gy	27.4±3.9***	29.7±5.6
t-GSH level [nM/mg protein]	Normal	CCl ₄ +Sham	12.1±2.1	9.7±0.8
		CCl ₄ +0.5Gy	12.0±1.2	7.8±1.0
		CCl ₄ +15Gy	5.2±0.4***	4.5±0.4***
	Acatalasemic	CCl ₄ +Sham	12.7±1.1	9.2±0.7
		CCl ₄ +0.5Gy	12.0±1.4	7.8±1.3
		CCl ₄ +15Gy	5.7±0.7***	4.4±0.7***
GCS activity [U/mg protein]	Normal	CCl ₄ +Sham	12.8±1.1	11.7±0.8
		CCl ₄ +0.5Gy	14.4±1.3	10.7±1.1
		CCl ₄ +15Gy	10.7±1.1*	10.3±0.9
	Acatalasemic	CCl ₄ +Sham	12.1±1.5	11.1±0.6
		CCl ₄ +0.5Gy	13.2±1.6	10.0±1.0
		CCl ₄ +15Gy	10.1±0.8*	9.7±1.0

Each value indicates the mean ± SEM. The number of mice per experimental point is 5. *P < 0.05, **P < 0.01, ***P < 0.001 vs. CCl₄+Sham.

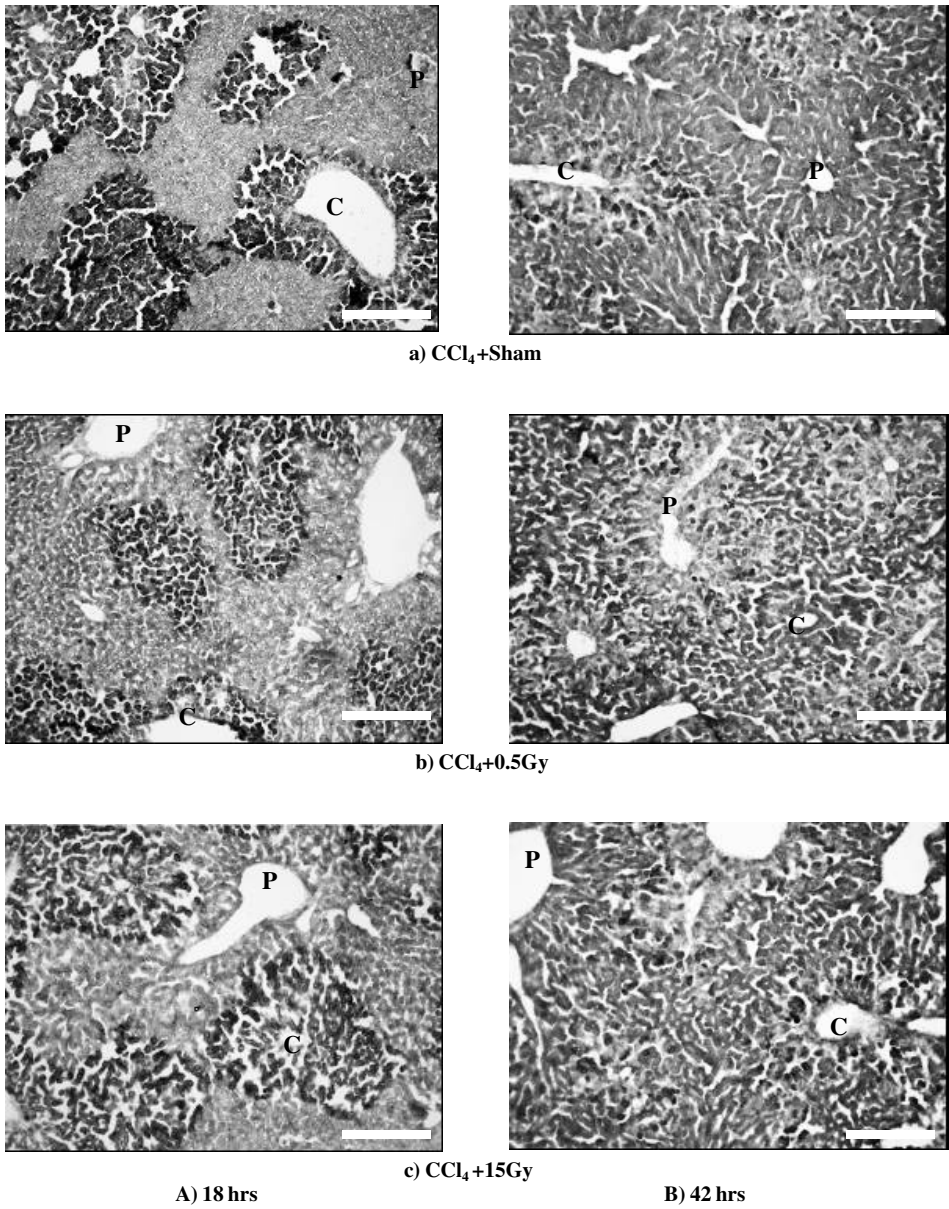
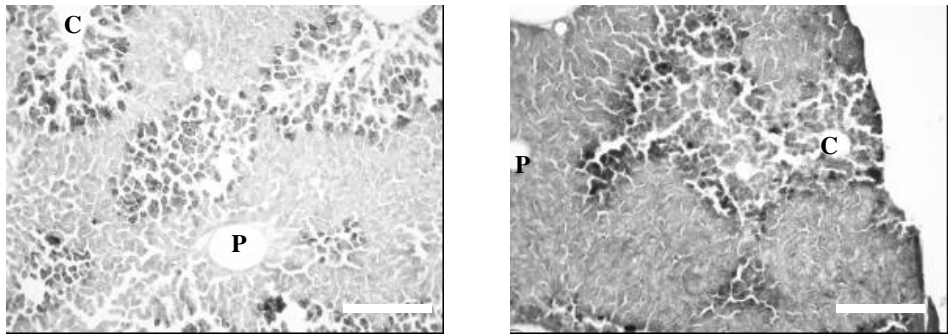
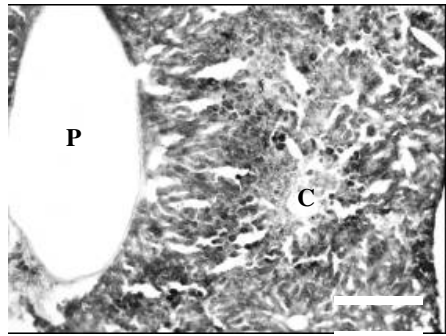
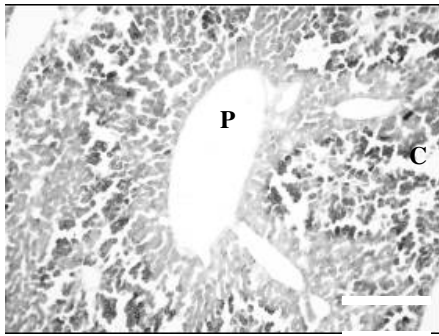


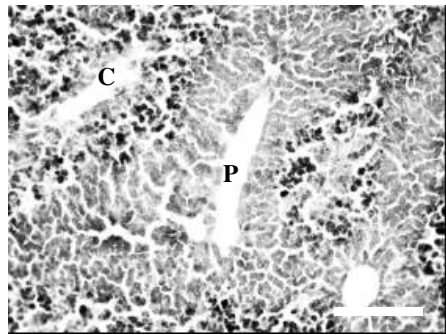
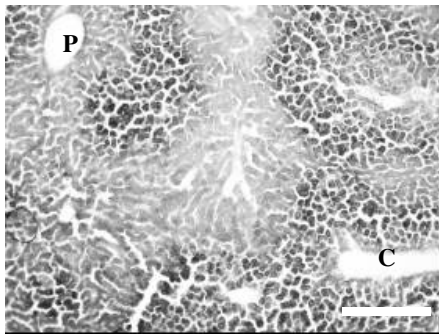
FIGURE 1-1. Differences in liver histopathology of acatalasemic mice under sham-irradiation (a), 0.5 Gy irradiation (b) or 15 Gy irradiation (c) at 18 hrs (A), and 42 hrs (B) after CCl₄ administration. The length of scale bar is 300 μ m. For all figures Sudan Black B (black colored) staining was used for the detection of fat degeneration surrounding the central vein (C) and the portal vein (P).



a) CCl₄+Sham



b) CCl₄+0.5Gy



A) 18 hrs

c) CCl₄+15Gy

B) 42 hrs

FIGURE 1-2. Differences in liver histopathology of normal mice under sham-irradiation (a), 0.5 Gy irradiation (b) or 15 Gy irradiation (c) at 18 hrs (A) and 42 hrs (B) after CCl₄ administration. The scale and staining techniques are the same as in Figure 1-1.

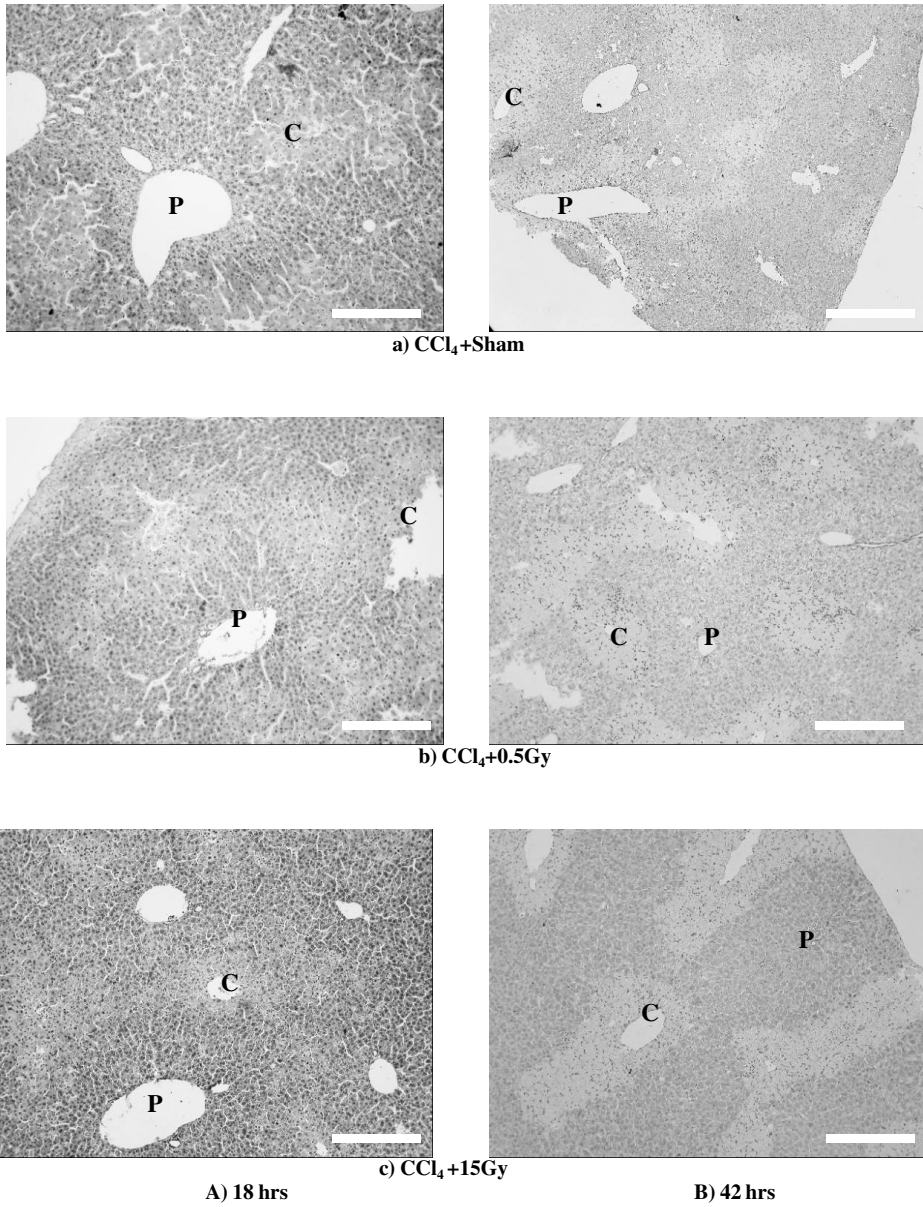


FIGURE 1-3. Differences in liver histopathology of acatalasemic mice under sham-irradiation (a), 0.5 Gy irradiation (b) or 15 Gy irradiation (c) at 18 hrs (A) and 42 hrs (B) under CCl_4 administration. All figures are stained with hematoxylin-eosin for the detection of fat degeneration surrounding the central vein (C) and the portal vein (P). The scale is the same as Figure 1-1.

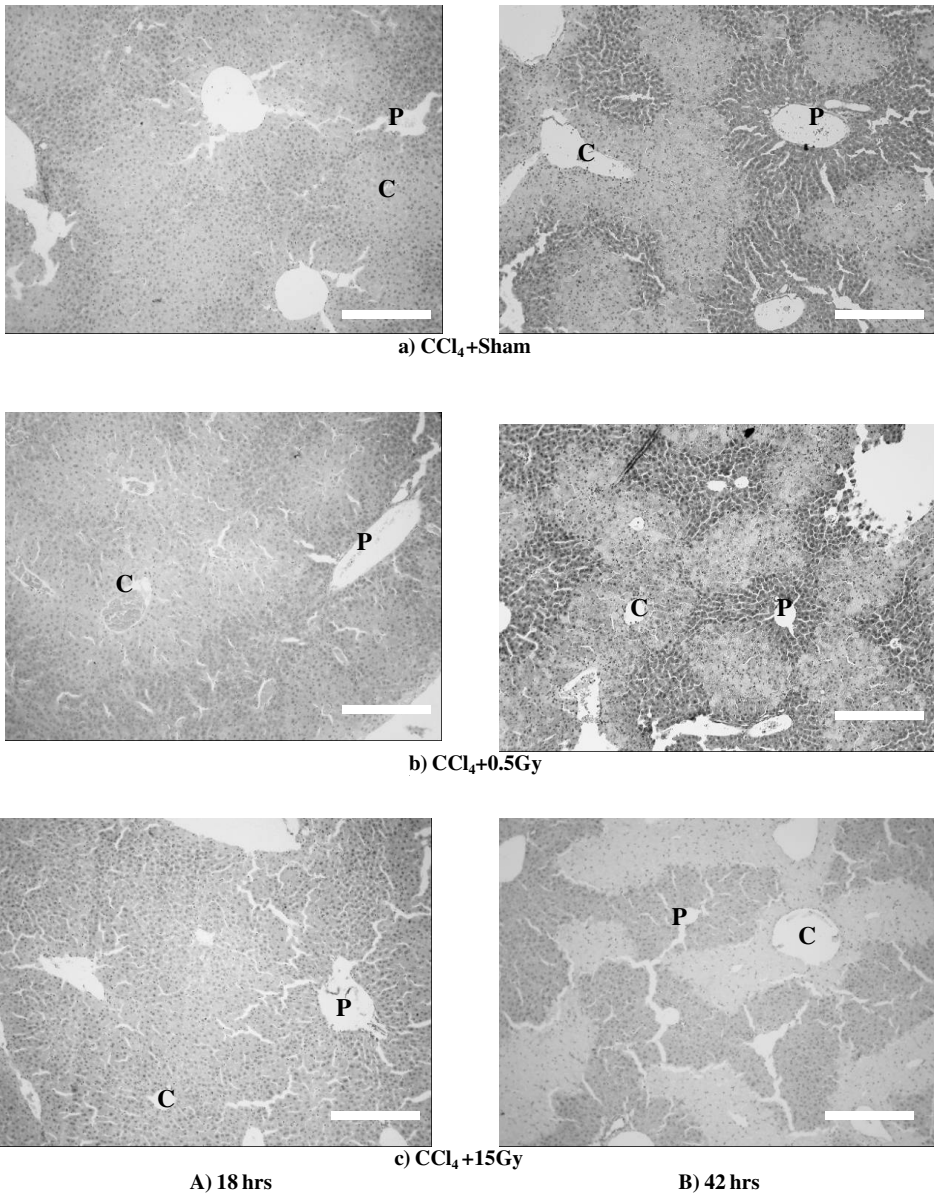


FIGURE 1-4. Differences in liver histopathology of normal mice under sham- (a), 0.5 Gy (b) or 15 Gy irradiation (c) at 18 hrs (A) and 42 hrs (B) after CCl₄ administration. All sections were stained with hematoxylin-eosin for the detection of fat degeneration surrounding the central vein (C) and the portal vein (P). The scale is the same as Figure 1-1.

Experiment 2: Dose dependent changes in mice livers at 4 hrs after X-ray irradiation 18 hrs after CCl₄ administration

Differences between the acatalasemic mouse and normal mouse

Under the conditions of non-irradiation and no CCl₄ treatment, no significant differences were observed in the lipid peroxide level and the activities of SOD, GPx and GCS and the total glutathione content between acatalasemic mice and normal mice, whereas the acatalasemic mice showed a significantly lower catalase activity and significantly higher activities of GOT and GPT than those of the normal mice (Table III, IV).

Changes caused after CCl₄ administration

The activities of GOT, GPT, SOD, catalase, GPx and GCS, and total glutathione content were significantly decreased and the lipid peroxide level significantly increased in both acatalasemic and normal mice after the administration of CCl₄ (Table III, IV).

Changes caused by 0.5 Gy irradiation after CCl₄ administration

There were significant decreases in the activities of GOT and GPT in both acatalasemic and normal mice, and significant increases in the activities of SOD, catalase and GCS in acatalasemic mice and the catalase activities in normal mice exposed to 0.5 Gy irradiation (Table III, IV).

Changes caused by 15 Gy irradiation after CCl₄ administration

There was a significant increase in catalase activity in normal mice, whereas no significant differences were observed in the activities of SOD, catalase, GPx and GCS, total glutathione content, and lipid peroxide level in the acatalasemic mice (Table III, IV).

Histological observation

Under sham irradiation with no CCl₄ administration, there was no fat degeneration in either the acatalasemic or the normal mice. After CCl₄ administration, the liver tissues exhibited fat degeneration surrounding the central vein, but there were no obvious changes in the extent of the fat degeneration among the sham-, 0.5 Gy or 15 Gy irradiated mice, shown by the results of blood biochemistry.

Under sham-, 0.5 Gy or 15 Gy irradiation of mice following CCl₄ administration, liver tissues exhibited centrilobular necrosis of the parenchymal hepatocytes. The extent of centrilobular necrosis under 0.5 Gy irradiation was greater than under sham irradiation but smaller than under 15 Gy irradiation. However, there were no obvious changes in the extent of the fat degeneration among the sham-, 0.5 Gy or 15 Gy irradiation, reflecting the results of blood biochemistry (Figure 2-1 to Figure 2-2).

TABLE III. Temporal changes in aminotransferases in blood of acatalasemic or normal mice at each sham-, 0.5 Gy or 15 Gy X-ray irradiation following CCl₄ administration.

	Treatment	Mice	
		Normal	Acatalasemic
GOT activity [kU/L]	Control	0.84±0.09	2.20±0.15 ⁺⁺⁺
	CCl ₄ +Sham	5.62±0.47	7.74±0.56
	CCl ₄ +0.5Gy	4.57±0.43 [*]	6.61±0.51 [*]
	CCl ₄ +15Gy	7.52±0.55 [*]	9.65±0.62 [*]
GPT activity [kU/L]	Control	0.97±0.10	2.17±0.15 ⁺⁺⁺
	CCl ₄ +Sham	7.36±0.54	9.14±0.60
	CCl ₄ +0.5Gy	5.27±0.46 ^{**}	7.62±0.55 ^{**}
	CCl ₄ +15Gy	7.98±0.55	10.14±0.64 [*]

Each value indicates the mean ± SEM. The number of mice per experimental point is 5. ⁺⁺⁺P < 0.001 vs. normal mouse. ^{**}P < 0.01, ^{*}P < 0.05 vs. control.

TABLE IV. Temporal changes in antioxidant-associated substances in liver of acatalasemic or normal mice at each sham-, 0.5 Gy or 15 Gy X-ray irradiation following CCl₄ administration.

	Treatment	Mice	
		Normal	Acatalasemic
Lipid peroxide level [nM/mg protein]	Control	0.39±0.06	0.49±0.08
	CCl ₄ +Sham	1.04±0.20 ^{***}	1.50±0.26 ^{***}
	CCl ₄ +0.5Gy	0.80±0.08 [#]	1.28±0.18
	CCl ₄ +15Gy	1.01±0.12	1.17±0.20
SOD activity [U/mg protein]	Control	48.6±3.8	55.5±3.7
	CCl ₄ +Sham	20.7±5.0 ^{***}	20.4±3.9 ^{***}
	CCl ₄ +0.5Gy	22.0±2.4	29.1±6.4 [#]
	CCl ₄ +15Gy	15.2±2.4	20.7±3.4
Catalase activity [U/mg protein]	Control	250±25.0	95±14.5 ⁺⁺⁺
	CCl ₄ +Sham	107±23.2 ^{***}	68±13.3 [*]
	CCl ₄ +0.5Gy	205±14.1 ^{###}	110±10.0 ^{###}
	CCl ₄ +15Gy	167±30.9 [#]	53±11.0
GPx activity [U/mg protein]	Control	33.7±5.1	42.0±5.0
	CCl ₄ +Sham	22.2±4.2 ^{***}	17.7±2.6 ^{***}
	CCl ₄ +0.5Gy	27.6±5.5	27.7±5.5
	CCl ₄ +15Gy	24.9±5.6	23.0±4.3
t-GSH level [µg/mg protein]	Control	11.1±1.6	12.0±2.0
	CCl ₄ +Sham	6.2±0.8 ^{***}	4.7±0.8 ^{***}
	CCl ₄ +0.5Gy	6.6±1.2	6.0±1.1
	CCl ₄ +15Gy	5.2±0.8	4.3±0.7
GCS activity [µg/mg protein]	Control	15.9±2.2	13.8±2.2
	CCl ₄ +Sham	9.8±2.0 ^{***}	7.7±0.7 ^{***}
	CCl ₄ +0.5Gy	12.0±2.3	11.5±1.6 ^{###}
	CCl ₄ +15Gy	8.5±1.1	8.0±1.1

Each value indicates the mean ± SEM. The number of mice per experimental point is 5. ⁺⁺⁺P < 0.001 vs. normal mouse. ^{***}P < 0.001, ^{*}P < 0.05 vs. control, ^{###}P < 0.001, [#]P < 0.05 vs. CCl₄+Sham.

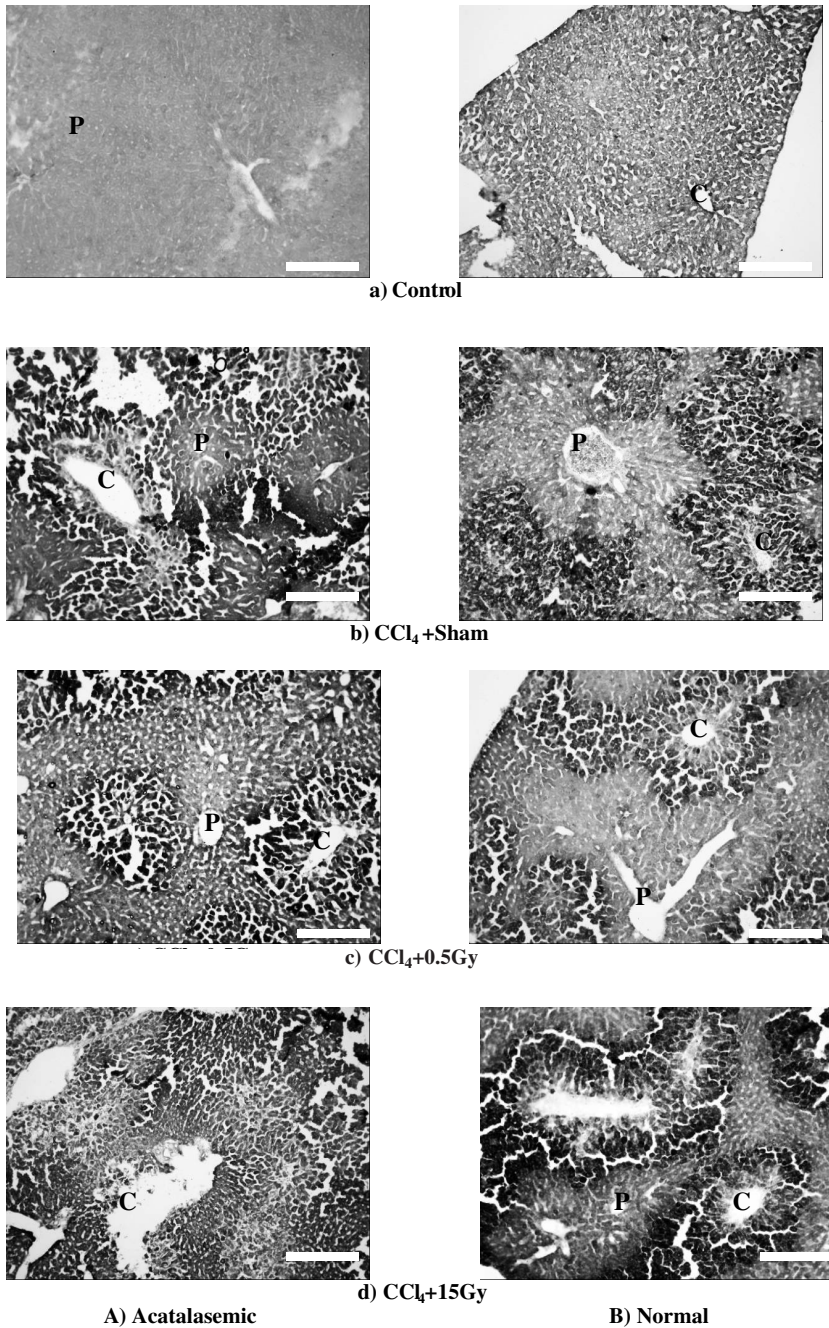


FIGURE 2-1. Differences in liver histopathology between acatalasemic (A) and normal (B) mice under non-treated control (a), sham- (b), 0.5 Gy (c) or 15 Gy irradiation (d) conditions following CCl₄ administration. The scale and staining techniques are the same as in Figure 1-1.

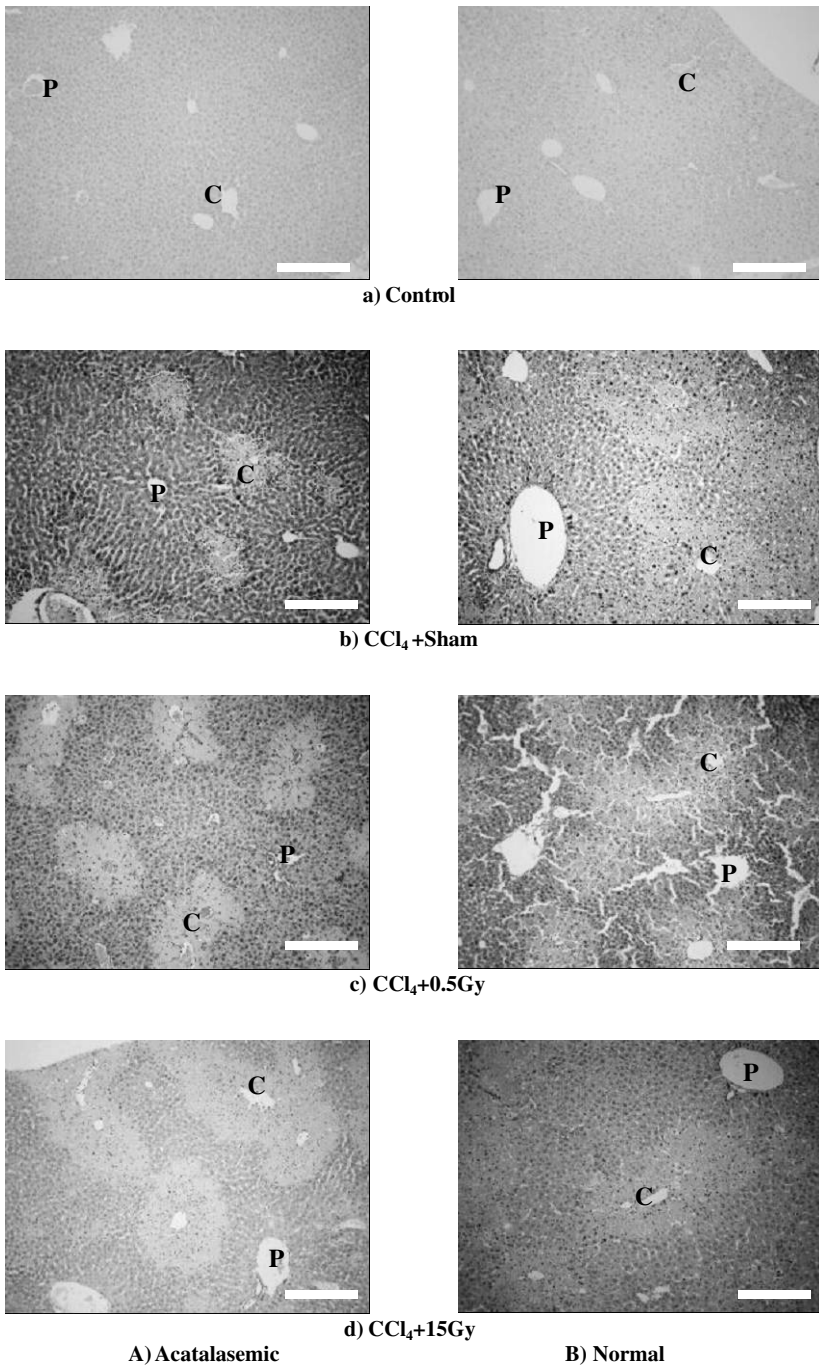


FIGURE 2-2. Differences in liver histopathology between acatalasemic (A) and normal (B) mice under non-treated control (a), sham- (b), 0.5 Gy (c) or 15 Gy irradiation (d) conditions following CCl₄ administration. The scale and staining techniques are the same as in Figure 1-3.

Discussion

In this study, liver damage by CCl_4 was confirmed, because the activities of GOT and GPT in the serum of both the acatalasemic and normal mice increased after CCl_4 administration. Cytochrome P450 in the microsomes, which takes part in drug metabolism and steroid metabolism caused the production of the trichloromethyl radical ($\bullet\text{CCl}_3$), and therefore resulted in liver damage. As radiation induced the superoxide anion radical (O_2^-), it was expected that the activities of GOT and GPT were increased by the irradiation after CCl_4 administration. However, at 18 hrs after CCl_4 administration, there were no significant differences among the sham-, 0.5 Gy or 15 Gy irradiated groups. It may be that 0.5 Gy irradiation induced a small amount of active oxygen *in vivo*, but 15 Gy irradiation induced a large amount of active oxygen. As a result, the activities of GOT and GPT with 15 Gy irradiation after CCl_4 administration were significantly higher than with 0.5 Gy irradiation after CCl_4 administration. At 42 hrs after CCl_4 administration and 0.5 Gy irradiation, the activities of GOT and GPT in the acatalasemic and normal mice were significantly lower than with sham-irradiation. However, there was no recovery of the liver damage with 15 Gy irradiation (Experiment 1). Moreover, at 22 hrs after CCl_4 administration, the activities of GOT and GPT in the acatalasemic and normal mice with sham irradiation were higher than with 0.5 Gy irradiation, due to elevated oxidative enzyme (3,5,6,27-29) which played a role in an earlier recovery of liver damage (Experiment 2).

It is known that low-dose (0.5 Gy) irradiation produces adequate oxygen stress and antioxidant enzymes were increased and the lipid peroxide level was decreased (3,5,28, 30,31). Moreover, we have reported that prior low-dose X-ray irradiation inhibits CCl_4 -induced hepatopathy in acatalasemic mice (32). These findings may indicate that antioxidant enzymes, which were elevated by 0.5 Gy irradiation, reduced the fat liver caused by CCl_4 administration. In this study, at 18 hrs or 42 hrs after CCl_4 administration, the activities of SOD, catalase, GPx and GCS, and total glutathione content were significantly decreased by 15 Gy irradiation, but at 42 hrs, the activities of catalase and GPx were significantly increased by 0.5 Gy irradiation (Experiment 1). At 22 hrs after CCl_4 administration, the activities of SOD, catalase, GPx and GCS were significantly increased by 0.5 Gy irradiation (Experiment 2). This suggested that the antioxidant enzymes were increased independently of CCl_4 administration.

At 18 hrs or 42 hrs after CCl_4 administration, the lipid peroxide level was significantly increased by 15 Gy irradiation, but there was no change between sham- and 0.5 Gy irradiation. It suggested that 15 Gy irradiation induced lipid peroxide by CCl_4 , and that 0.5 Gy irradiation did not (Experiment 1). At 22 hrs after CCl_4 administration, the lipid peroxide levels in both acatalasemic and normal mice were significantly increased, but 0.5 Gy irradiation after CCl_4 administration decreased the lipid peroxide level. It suggested that 0.5 Gy irradiation induced antioxidant enzymes and lipid peroxide levels were decreased (Experiment 2).

On pathological examination, under the conditions of sham-, 0.5 Gy or 15Gy irradiation after CCl_4 administration, no significant differences were observed in the lipid peroxide level in spite of the reduction of the GOT and GPT activities. It suggested that the inhibitory effect of post low-dose X-ray irradiation on CCl_4 administration was not clear, and that fat liver degeneration was induced by 15 Gy irradiation. However, at 42 hrs after CCl_4 administration, liver fat degeneration was smaller than those at 18 hrs (Experiment 1). This

was in accord with the GOT and GPT activities. The nuclei in the cells surrounding the central vein were dividing, and fat degeneration improved. Because the O₂ pressure of the central vein was lower than that of the portal vein, the cells around the fat degeneration quickly improved. The fat degeneration in normal mice quickly decreased, in contrast to the acatalasemic mice. It suggested that lack of catalase delayed the recovery of fat degeneration.

As a result, low-dose irradiation accelerated the rate of recovery. The recovery of the acatalasemic mice was lower than that of the normal mice. This may be because of the decreased catalase activities. These findings suggest that catalase plays an important role in the recovery of CCl₄-induced hepatopathy.

References

1. Tottori, Y. (1987) Activity and stability of catalase in the organs of acatalasemic mice. *Okayama Igakkai Zasshi*. 99: 1623–1632.
2. Ogata, M. (1991) Review article; A catalasemia. *Hum. Genet.* 86: 331–340.
3. Yamaoka, K., Edamatsu, R. and Mori, A. (1991) Increased SOD activities and decreased lipid peroxide levels in rat organs induced by low doses X-irradiation. *Free Radic. Biol. Med.* 11: 299–306.
4. Yamaoka, K., Komoto, Y., Suzuka, I., Edamatsu, R. and Mori, A. (1993) Effect of radon inhalation on biological function; lipid peroxide, SOD activity and membrane fluidity. *Arch. Biochem. Biophys.* 302: 37–41.
5. Yamaoka, K., Edamatsu, R., Ito, T. and Mori, A. (1994) Effects of low dose X-irradiation on biomembrane in brain cortex of aged rats. *Free Radic. Biol. Med.* 16: 529–534.
6. Yamaoka, K., Kojima, S., Takahashi, M., Nomura, T. and Iriyama, K. (1998) Change of glutathione peroxidase synthesis along with that of superoxide dismutase synthesis in mice spleens after low-dose X-ray irradiation. *Biochim. Biophys. Acta*, 1381: 265–270.
7. Slater, T.F. (1972) *Free Radical Mechanisms in Tissue Injury*, Pion Limited, London, pp. 91–170.
8. Recknagel, R.O., Glende, Jr. E.A. and Hruszkewycz, A.M. (1977) Chemical mechanisms in carbon tetrachloride toxicity. *Free Radicals in Biology*, Vol. III (W.A. Pryor, ed.), Academic Press, New York, 97–132.
9. Reynolds, E.S. and Moslen, M.T. (1980) Free-radical damage in liver. *Free Radicals in Biology*, Vol. IV (W.A. Pryor, ed.), Academic Press, New York, pp. 49–94.
10. Slater, T.F. (1982) Activation of carbon tetrachloride, chemical principles and biological significance., *Free Radicals, Lipid Peroxidation and Cancer*, (D.C.H. McBrien and T.F. Slater, eds.), Academic Press, London, pp. 243–274.
11. Recknagel, R.O. (1967) Carbon tetrachloride hepatotoxicity. *Pharmacol. Rev.* 65: 145–208.
12. Slater, T.F. (1966) Necrogenic action of carbon tetrachloride in the rat; a speculative mechanism based on activation. *Nature* 209: 36–40.
13. Pacek, J.E., Slater, T.F. and Willson, R.L. (1978) Reaction of the carbon tetrachloride-related peroxy free radical ($\cdot\text{CCl}_3$) with amino acids; pulse radiolysis evidence. *Life Sci.* 23: 2617–2620.
14. Slater, T.F. (1984) Free radical mechanisms in tissue injury. *Biochem. J.* 222: 1–15.
15. Recknagel, R.O., Glende, E.A., Dolak, J.A. and Waller, R.E. (1989) Mechanisms of carbon tetrachloride toxicity. *Pharmacol. Ther.* 43: 139–154.
16. Goor, H.V., Gerrits, P.O. and Grond, J. (1986) The application of lipid-soluble stains in plastic-embedded section. *Histochemistry.* 85: 251–253.
17. Feinstein, R.N., Braun, J.T. and Howard, J.B. (1967) Acatalasemic and hepocatalasemic mouse mutants. *Arch. Biochem. Biophys.* 120: 165–169.

18. Kannen, A., Wroblewski, F. and La Due, J.S. (1995) Transaminase activity in human blood. *J. Clin. Invest.* **34**: 126–131.
19. Uchiyama, M. and Mihara, M. (1987) Determination of malondialdehyde precursor in tissues by thiobarbituric acid. *Anal. Biochem.* **86**: 271–278.
20. Lowry, O.H., Rosebrough, N.J., Farr, A.L. and Randall, R.J. (1951) Protein measurement with the folin phenol reagent. *J. Biol. Chem.* **193**: 265–275.
21. Hiramatsu, M., Kohon, M., Edamatsu, R., Mitsuta, K. and Mori, A. (1992) Increased superoxide dismutase activity in aged human cerebrospinal fluid and rat brain determined by electron spin resonance spectrometry using the spin trap method. *J. Neurochem.* **58**: 1160–1164.
22. Aebi, H., Wyss, S.R., Scherz, B. and Gross, J. (1976) Properties of erythrocyte catalase from homozygotes and heterozygotes for Swiss-type acatalasemia. *Biochem. Genet.* **14**: 791–807.
23. Yamamoto, Y. and Takahashi, K. (1993) Glutathione peroxide isolated from plasma reduces phospholipid hydroperoxide. *Arch. Biochem. Biophys.* **305**: 541–545.
24. Delides, A., Spooner, R.J., Golgberg, D.M. and Neal, F.E. (1976) An optimized semi-automatic rate method for serum glutathione reductase activity and its application to patients with malignant disease. *J. Clin. Pathol.* **29**: 73–77.
25. Moore, W.R., Anderson, M.E., Meister, A., Murata, K. and Kimura, A. (1989) Increased capacity for glutathione synthesis enhances resistance to radiation in *Escherichia coli*. a possible model for mammalian cell, protection. *Proc. Natl. Acad. Sci. USA* **86**: 1461–1464.
26. Wang, D.H., Ishii, K., Zhen, L.X. and Taketa, K. (1996) Enhanced liver injury in acatalasemic mice following exposure to carbon tetrachloride. *Arch. Toxicity.* **70**: 189–194.
27. Kojima, S., Matuki, O., Nomura, T., Kubodera, A., Honda, Y., Honda, S., Tanooka, H., Wakasugi, H. and Yamaoka, K. (1998) Induction of mRNAs for glutathione synthesis-related proteins in mouse liver by low doses of γ -rays. *Biochim. Biophys. Acta.* **1381**: 312–318.
28. Matsuki, O., Nomura, T., Kojima, S., Kubodera, A. and Yamaoka, K. (1998) Effect of small-dose γ -ray on endogenous antioxidant enzymes in mice. *Radioisotopes.* **47**: 291–299.
29. Kojima, S., Matsumori, S., Ishida, H. and Yamaoka, K. (2000) Possible role of elevation of glutathione in the acquisition of enhanced proliferation of mouse splenocytes exposed to small-dose γ -rays. *Int. J. Radiat. Biol.* **76**: 1641–1647.
30. Yamaoka, K., Mori, S., Nomura, T., Taguchi, T., Ito, T., Hanamoto, K. and Kojima, S. (2002) Elevation of antioxidant potency in mice brain by low-dose X-ray irradiation and its effect on Fe-NTA-induced brain damage. *Physiol. Chem. Phys. & Med. NMR* **34**: 103–112.
31. Yamaoka, K., Nomura, T., Wang, D.H., Mori, S., Taguchi, T., Ishikawa, T., Hanamoto, K. and Kira, S. (2002) Adjustment function among antioxidant substances in acatalasemic mice brain and its enhancement by low-dose X-ray irradiation *Physiol. Chem. Phys. & Med. NMR* **34**: 113–120.
32. Yamaoka, K., Kataoka, T., Nomura, T., Taguchi, T., Wang, Da-Hong, Mori, Shuji., Hanamoto, K. and Kira, S. (2004) Inhibitory effects of prior low-dose irradiation on carbon tetrachloride-induced hepatopathy in acatalasemic mice. *J. Rad. Res.* **45**: 89–95.

*Received August 9, 2005;
accepted October 27, 2005.*

Water And Electrolyte Changes in Skeletal and Cardiac Muscles of Rats During Prolonged Hypokinesia

Yan G. Zorbas¹, Kostas K. Kakuris^{2*}, Eugenios A. Neofitos²
and Nikolaos I. Afoninos²

¹Higher Institute of Biochemistry, Gomel, Belarus

²European Foundation of Environmental Sciences, Athens, Greece

*Author for correspondence. Email: kkakuris@yahoo.com

Abstract: The objective of this study was to show that hypokinesia (diminished movement) could affect differently water and electrolyte content in muscles having minimum differences in their function and morphology. To this end, we studied water and electrolyte content in skeletal and cardiac muscles, fluid excretion, electrolyte absorption, and electrolyte levels in plasma, urine and feces of rats during prolonged hypokinesia (HK).

Studies were conducted on one-hundred-twenty-six 13-weeks old male Wister rats during a pre-hypokinetic period and a hypokinesia period. Animals were equally divided into two groups: vivarium control rats (VCR) and hypokinetic rats (HKR). Hypokinetic animals were kept in small individual cages which restricted their movements in all directions without hindering food and water intake. Control rats were housed in individual cages under vivarium control conditions.

Sodium (Na⁺) and potassium (K⁺) absorption, electrolyte and water content in cardiac muscles (right and left ventricle), thigh extensor (quadriceps femoris muscle) and long muscle of the back (biceps femoris muscle), urine volume, and electrolyte levels in plasma and urine and feces did not change in VCR when compared to their pre-hypokinetic levels. The absorption of Na⁺ and K⁺, water and electrolyte content in cardiac and skeletal muscles decreased significantly, while urine volume, plasma electrolyte levels and urine and fecal electrolyte excretion increased significantly in HKR compared with their pre-HK values and with their respective vivarium control (VCR). Water and electrolyte content decreased more significantly in skeletal than in cardiac muscles. Water and electrolyte levels decreased more in the thigh extensor and in the right ventricle than in the long muscle of the back, the left ventricle or the septum.

Muscles suffering from higher water and electrolyte loss against the background of lower water and electrolyte content show lower water and electrolyte deposition. Lower electrolyte and water content in skeletal than in cardiac muscle shows that water and electrolyte content decreases more in skeletal than cardiac muscles. Skeletal muscle showed lower water and electrolyte content than cardiac muscle indicating that the risk for decreased muscle water and electrolyte content is inversely related to the muscle function and morphology, i.e., the more

weight-bearing supporting function and morphology muscles have, the higher the risk for lower muscle water and electrolyte content. It was concluded that the greater muscle function and morphology, the lower electrolyte and water deposition, the higher water and electrolyte losses, and the lower water and electrolyte content.

KEY WORDS: water and electrolyte depletion, water and electrolyte deposition, muscle water and electrolytes, water and electrolyte losses, sedentary conditions, hypokinetic water and electrolyte interactions.

BY DEFINITION hypokinesia (diminished movement) is characterized by decreased muscular activity. Hypokinesia (HK) is a factor of catabolism induction (1–3) and may develop when there is a drastic reduction of physical load on the skeletal muscle system. Prolonged HK may be present due to age, disease, disability and sedentary living and working conditions. Among the effects of HK, the changes in fluid and electrolyte homeostasis and in particular the dissociation between the fluid and electrolyte loss and fluid-electrolyte depletion has been of the greatest interest (4–6), largely due to higher fluid and electrolyte loss with fluid and electrolyte depletion and the recent interest on fluid and electrolyte homeostasis under sedentary living and working conditions.

Decreased water and electrolyte content in muscles (5–13) is associated with the increase of water and electrolyte loss (5–11). Increase of water and electrolyte loss with a decrease of water and electrolyte content in muscle is a well recognized change which is inherent to prolonged HK (5–11). Increased fluid and electrolyte loss with decreased electrolyte and water content indicates the presence of decreased fluid and electrolyte utilization (5–13) which is attributable to several factors and primarily to the decreased muscle cell mass (5, 6). The decreased fluid and electrolyte utilization must affect the efficiency of electrolyte and water accumulation in muscle (5–13). The effect of prolonged HK on water and electrolyte content may vary in muscles with different function and morphology, and thus its effect on muscle electrolyte and water deposition (5–13).

Decreased water and electrolyte content in muscles is associated with an increase of plasma water and electrolytes as well (10–13). Absence of a relationship between lower muscle water and electrolyte content and higher plasma water and electrolyte level has been shown (5–13). An increase of plasma water and electrolyte level with a decrease of muscle water and electrolyte content is attributable to the decrease of water and electrolyte deposition; this is because when water and electrolyte deposition decreases, plasma water and electrolyte level increases (5–13). During HK, in contrast to the normal muscular activity, decreased muscle water and electrolyte content is accompanied by an increase rather than a decrease of plasma water and electrolyte levels. This indicates the presence of other mechanisms than those involved in higher plasma water and electrolyte level with lower muscle water and electrolyte level during normal muscular activity.

Studies during HK have shown that changes in distribution of water and electrolytes in muscles may occur (14–16). This redistribution of water and electrolytes in muscles could serve as an indicator of the water and electrolyte deposition and the functional and morphological changes which may develop in muscles (14–16). Hypokinesia affecting muscle function and morphology, will inevitably lead to redistribution of water and electrolytes in muscles and thus to water and electrolyte deposition and functional and morphological changes in muscles (14–16). Water and electrolyte changes in muscles with minor differences in morphology and function could serve as an indicator of the water and electrolyte

deposition and the functional and morphological changes in muscle having different function and morphology. To this end, studies must be performed on electrolytes and water content in muscle with different function and morphology for determining the magnitude of water and electrolyte deposition and functional and morphological changes in muscle with different function and morphology.

The objective of this study was to show that HK could affect differently water and electrolyte content in muscle with minimum differences in their function and morphology. Measurements of water and electrolyte content in skeletal and cardiac muscles, electrolyte absorption, fluid excretion, plasma electrolyte levels and electrolyte losses in urine and feces were made in animals during HK.

Materials and Methods

Experiments were performed on one hundred-twenty-six 13-week-old healthy male Wistar rats which were obtained from a Local Breeding Animal Laboratory. Rats on arrival were given an adaptational dietary period of 9-days during which the rats were fed a commercial laboratory diet. At the start of the study, rats were about 90-days old and weighed 376 to 398 g. Rats were housed in individual metabolic cages without restriction of muscular activity where light (0.7:00 to 19:00 h), and ambient temperature (25 to 27 °C) and relative ambient humidity (60%) was automatically controlled. Studies were approved by the Committee for the Protection of Animals.

An assignment of rats into two groups was conducted randomly and their conditions were:

Group one: sixty unrestrained rats were housed in individual cages under vivarium control conditions for 90-days. They served as vivarium control rats (VCR).

Group two: sixty restrained rats were kept in small individual cages for 90-days. They served as hypokinetic rats (HKR).

Protocol

Hypokinetic studies were preceded by a pre-HK period of 9-days that involved biochemical examinations, training, testing and conditioning of animals to their laboratory conditions (1,2). The preparation period carried out for collecting pre-HK values about skeletal and cardiac muscle water-electrolyte levels, electrolyte absorption, fluid excretion and electrolyte levels in plasma and urine and feces. This was aimed at minimizing stress induced by restriction of muscular activity (1,2).

Production of hypokinesia

To simulate HK rats were kept in small individual cages. The dimensions of the cages (195 x 80 x 95 mm) allowed for restricting movements in all directions without hindering food and water intakes. Hypokinetic animals could assume a postural position that allowed them to groom. When necessary, dimensions of the individual cages could be reduced using special wood inserts. The cages were constricted so that their dimensions could be changed according to the size of the individual rat so that a relative constant level of restricted muscular activity could be maintained.

Food and water consumption

The daily food consumption was measured and 90% of the daily amount (12 g) was mixed with deionized distilled water (1:2 wt/vol) to form slurry which was divided into two meals. Animals were pair-fed daily in the morning, at the rate of 40 to 60 g food per day. The control rats were allowed to eat approximately the same amount of food as hypokinetic animals. The dietary food was supplied daily in individual feeders formed by little troughs and wood partitions. Food for the entire investigation was from the same production lots which contain all essential nutrients. The laboratory food contained 38% carbohydrate, 19% protein, 4% fat, 22% cellulose, vitamins A, D, E, 0.7% sodium chloride, 0.8% potassium, 0.9% calcium, 0.9% phosphorus and 0.5% magnesium. Food intake was measured by daily weighing (Mettler PL 200 balance) of the slurry food containers. Rats received daily deionized-distilled water *ad libitum*. Water dispensers (120 to 150 mL) were secured onto a wooden plate installed on the front cage panels and filled daily. All animals were weighed daily between the 8 and 9 a.m. to measure their body weight.

Electrolyte absorption measurements

During the pre-HK period and HK period, electrolyte absorption was measured in hypokinetic and control animals. The electrolyte amount in food was calculated directly by keeping an exact duplicate of the consumed food of each rat. The total electrolyte losses in 24 h urine and fecal samples were measured. Measuring electrolyte absorption [(intake-losses of electrolytes in urine and feces)/intake], required the consumption of a calculated electrolyte amount, followed by the 24 h urine and fecal collection, with calculation of the percentage of electrolyte retained in the body, i.e., absorption of electrolyte is equal to the [(intake-loss of electrolytes in urine and feces)/intake] and expressed as percentage. The electrolyte amounts in the 24 h urine and fecal collections during pre-HK were considered to be the pre-HK values of urine and fecal electrolyte excretion of each rat. Electrolyte values were then subtracted from electrolytes in the 24 h urine and fecal collections during the HK period. The differences were compared with the total amount of electrolyte consumed with food and expressed as a percentage of electrolyte absorption.

Plasma, urine and fecal sample collections

Urine and fecal sample were collected from each rat every day and were pooled to form 6-day composites, while plasma samples were collected every 6-days. A 6-day (consecutive days) pooled samples were collected. Mean \pm SD's of the measurements are presented during pre-HK and HK period. Blood samples in an amount of 2.0 mL were obtained from anaesthetized rats *via* a cardiac puncture. To obtain plasma, blood samples were transferred to polypropylene tubes containing sodium heparin. Samples were centrifuged immediately at 10,000 x g for 2 min at room temperature and separated using glass capillary pipets that had been washed in hydrochloric acid and deionized water. Aliquots for plasma K⁺ and Na⁺ measurements were stored at -20 °C. Twenty-four-hour urine samples uncontaminated by stools were obtained. A stainless steel urine-feces separating funnels (Hoeltge, model HB/SS, Hoeltge Inc., Cincinnati, OH, USA), were placed beneath each rat to collect uncontaminated 24 hour urine samples. To ensure 24 hour urine collections, creatinine excretion was measured. Urine samples were collected in a beaker with layers of mineral oil to prevent evaporation. Beakers were replaced daily. Urine samples refrigerated.

erated at 4 °C until needed for analysis of K⁺ and Na⁺ level. Fecal samples were dried, wet ashed with nitric and perchloric acid and diluted as necessary with deionized distilled water and analyzed. A marker was used for complete feces recovery. Samples of each rat were assayed in the same run.

Tissue preparations, electrolyte extraction and analysis

Samples were collected during pre-HK and HK period and mean \pm SD of muscle water and electrolyte content are presented. Muscle water and electrolyte levels are reported in the average of seven rats. Seven rats from each group were exsanguinated under ether anaesthesia by cardiac puncture. Rats were sacrificed on the 1st, 7th and 9th day of the pre-HK period and on the 7th, 15th, 30, 50, 70 and 90th day of HK period and myocardium (right and left ventricle), thigh extensor (quadriceps femoris muscle) and long muscles of the back (biceps femoris muscle) were removed. Muscles were thoroughly cleaned of connective tissues, fatty inclusions and large vessels and dried to a constant weight. Muscles were weighed on Teflon liners and put in a drying chamber at 105 °C. After muscle samples had been dried to a constant weight, they were transferred to quartz tubes for mineral extraction by means of concentrated HNO₃ (nitric acid), and distilled off in a quartz apparatus. After ashing, muscle residue was dissolved in 0.05 M HCl (hydrochloric acid) and, as a chloride solution, analyzed for muscle water-mineral level.

Measurements were done in duplicate and appropriate standards were used for all measurements: K⁺ and Na⁺ levels in cardiac muscles (right and left ventricle), thigh extensor (quadriceps femoris muscle) and long muscles of the back (biceps femoris muscle) of rats, and in plasma and urine were measured using a Perkin-Elmer 420 Model flame photometer (Perkin-Elmer Corp., Norwalk, CT). Water level in myocardium, thigh extensor and long muscles of the back of rats were measured using the method of drying tissue to a constant weight at a temperature of 105 °C. This method makes it possible to show the hydration level in the measured cardiac and skeletal muscles.

Data analyses

The results were analyzed with a 2-way ANOVA (hypokinetic vs. active controls) X 2 (pre-intervention vs. post-intervention) with repeated measures on the last factor. A Tukey-Kramer post-hoc test was used to establish which means were significantly different from each other. A format analysis was done to establish the shape of changes. A correlation coefficient was used to examine correlation between electrolyte absorption, and water and electrolyte levels in muscle, and electrolyte levels in plasma, urine and feces. Predetermined level of significance was set at $p < 0.05$. Results are reported as mean \pm SD.

Results

Pre-hypokinetic muscle water-electrolytes, plasma, urine and fecal electrolytes and urine volume

At the end of the pre-HK period, the urine volume, the urine and fecal electrolyte excretion, the electrolyte absorption (Table I), the plasma electrolyte concentrations (Table II) and the skeletal and cardiac muscle electrolyte content (Table III) and the muscle water

TABLE I. Urine and fecal sodium and potassium excretion, urine volume and electrolyte absorption measured in rats at pre-hypokinesia and during control and hypokinetic conditions.

Days	Fecal		Urine		Urine Volume, ml/24h/days	Electrolyte Absorption, %/days
	Sodium, mEq/days	Potassium, mEq/days	Sodium, mEq/days	Potassium, mEq/days		
Vivarium Control Rats (VCR), n=7						
Pre-HK	3.81 ± 0.21	5.40 ± 0.25	1.55 ± 0.22	3.25 ± 0.43	10.9 ± 1.2	60 ± 4
7th	3.76 ± 0.22	5.37 ± 0.23	1.53 ± 0.21	3.23 ± 0.46	10.7 ± 1.3	62 ± 3
15th	3.78 ± 0.20	5.38 ± 0.24	1.54 ± 0.22	3.24 ± 0.44	10.8 ± 1.2	61 ± 5
30th	3.75 ± 0.25	5.37 ± 0.25	1.52 ± 0.23	3.21 ± 0.35	10.7 ± 1.4	63 ± 4
50th	3.78 ± 0.17	5.38 ± 0.23	1.53 ± 0.24	3.23 ± 0.36	10.6 ± 1.3	61 ± 5
70th	3.76 ± 0.23	5.36 ± 0.25	1.54 ± 0.20	3.22 ± 0.45	10.7 ± 1.2	62 ± 4
90th	3.74 ± 0.18	5.37 ± 0.24	1.53 ± 0.23	3.23 ± 0.44	10.8 ± 1.4	61 ± 3
Hypokinetic Rats (HKR), n=7						
Pre-HK	3.80 ± 0.17	5.40 ± 0.23	1.56 ± 0.20	3.26 ± 0.43	10.8 ± 1.4	61 ± 5
7th	5.21 ± 0.25*	7.46 ± 0.35*	2.11 ± 0.23*	4.40 ± 0.45*	15.1 ± 1.5*	15 ± 3*
15th	5.08 ± 0.23*	7.15 ± 0.44*	2.03 ± 0.25*	4.25 ± 0.44*	14.0 ± 1.3*	17 ± 4*
30th	5.80 ± 0.17*	8.19 ± 0.53*	2.25 ± 0.20*	4.70 ± 0.36*	16.6 ± 1.5*	11 ± 5*
50th	5.61 ± 0.25*	7.67 ± 0.45*	2.13 ± 1.24*	4.47 ± 0.45*	15.2 ± 1.3*	15 ± 4*
70th	6.47 ± 0.26*	9.20 ± 0.43*	2.35 ± 0.21*	4.97 ± 0.39*	17.0 ± 1.5*	07 ± 3*
90th	6.26 ± 0.18*	8.79 ± 0.44*	2.28 ± 0.25*	4.68 ± 0.44*	16.3 ± 1.4*	10 ± 4*

All values are presented as mean ± SD. *p<0.05 significant differences between control and hypokinetic groups of rats.

content (Table IV) were not significantly different between the control and hypokinetic groups of rats.

Hypokinetic changes in plasma and urine and fecal electrolytes and urine volume

Electrolyte absorption, urine volume, plasma electrolyte concentration, urine and fecal electrolyte levels did not change in VCR when compared to their pre-HK values (Tables I and II). However, electrolyte absorption decreased significantly ($p<0.05$), and urine volume, plasma electrolyte concentration, and urine and fecal electrolyte excretion increased significantly ($p<0.05$) in HKR when compared to their pre-HK values and their respective vivarium control (VCR) (Tables I and II). A significant correlation $r = 0.93$ was found between the decreased electrolyte absorption and increased, diuresis, plasma electrolyte levels and urine and fecal electrolyte excretion.

Hypokinetic water and electrolyte changes in myocardium and skeletal muscles

Water and electrolyte content in the myocardium (right and left ventricles) and skeletal muscles (thigh extensor and long muscle of the back) did not change in VCR compared with their pre-HK values (Tables III and IV). Conversely, water and electrolyte content in the myocardium and the skeletal muscles decreased significantly ($p<0.05$) in HKR when compared to their pre-HK values and their respective vivarium controls (VCR) (Tables III

TABLE II. Plasma sodium and potassium concentrations measured in rats at pre-hypokinesia and during control and hypokinetic conditions.

Days	Plasma	
	Sodium, mEq/L	Potassium, mEq/L
Vivarium Control Rats (VCR), n=7		
Pre-HK	145 ± 1.2	4.9 ± 0.15
7th	144 ± 1.1	4.7 ± 0.13
15th	144 ± 1.2	4.8 ± 0.14
30th	143 ± 1.1	4.7 ± 0.15
50th	144 ± 1.2	4.8 ± 0.13
70th	143 ± 1.2	4.6 ± 0.15
90th	144 ± 1.1	4.7 ± 0.14
Hypokinetic Rats (HKR), n=7		
Pre-HK	146 ± 1.2	5.0 ± 0.13
7th	156 ± 1.3*	5.6 ± 0.15*
15th	155 ± 1.2*	5.5 ± 0.14*
30th	158 ± 1.3*	5.9 ± 0.13*
50th	156 ± 1.2*	5.7 ± 0.15*
70th	160 ± 1.3*	6.2 ± 0.13*
90th	158 ± 1.2*	5.9 ± 0.14*

All values are presented as mean ± SD. *p<0.05 significant differences between control and hypokinetic groups of rats.

and IV). However, the electrolyte and the water content decreased more significantly ($p<0.05$) in the skeletal muscles than in the cardiac muscle (Tables III and IV). Water and electrolyte content decreased more in thigh extensor than in the long muscle of the back and more in the right ventricle than in the left ventricle and the septum; however, these values were not significantly different. A significant correlation $r = 0.93$ was found between the decreased electrolyte absorption and decreased muscle water and electrolyte content.

Discussion

Pre-hypokinetic muscle water-electrolytes, plasma, urine and fecal electrolytes and urine volume

During the pre-hypokinetic treatment period, electrolyte absorption, water and electrolyte levels in cardiac and skeletal muscles, urine volume, plasma electrolyte levels and electrolyte excretion in urine and feces did not change. Electrolyte absorption, urine excretion, water and electrolyte content in cardiac and skeletal muscles and electrolyte levels in plasma, urine and feces were in balance with the ingested water and electrolytes. This is because the consumed water and electrolytes were retained by the body and were taken up for deposition in muscles (5–13). This shows that electrolytes and water released in

TABLE III. Sodium and potassium content of the cardiac and skeletal muscles measured in rats at pre-hypokinesia and during control, and hypokinetic conditions.

Days	Cardiac Muscles Right Ventricle, and Left Ventricle, mEq/kg wet tissue		Skeletal Muscles Thigh Extensor and Long Back Muscle, mEq/kg wet tissue	
	Vivarium Control Rats (VCR), n=7			
Sodium				
Pre-HK	65.5 ± 0.37	58.6 ± 0.30	29.5 ± 0.44	25.3 ± 0.33
7th	65.7 ± 0.35	58.8 ± 0.26	29.7 ± 0.32	25.6 ± 0.41
15th	65.8 ± 0.42	59.0 ± 0.35	29.8 ± 0.51	25.5 ± 0.38
30th	65.7 ± 0.40	58.8 ± 0.33	29.7 ± 0.43	25.8 ± 0.40
50th	65.9 ± 0.47	59.0 ± 0.27	30.0 ± 0.47	25.7 ± 0.53
70th	65.8 ± 0.33	58.8 ± 0.30	29.8 ± 0.52	26.0 ± 0.41
90th	65.9 ± 0.45	59.0 ± 0.41	30.0 ± 0.43	26.2 ± 0.50
Potassium				
Pre-HK	113.8 ± 0.48	116.4 ± 0.44	160.8 ± 0.52	156.4 ± 0.47
7th	114.2 ± 0.32	116.6 ± 0.52	161.0 ± 0.43	156.6 ± 0.50
15th	113.8 ± 0.39	116.8 ± 0.41	160.7 ± 0.50	156.8 ± 0.41
30th	114.0 ± 0.50	117.0 ± 0.54	161.2 ± 0.41	157.0 ± 0.54
50th	114.2 ± 0.44	116.8 ± 0.57	160.8 ± 0.56	156.8 ± 0.42
70th	114.5 ± 0.43	117.0 ± 0.50	161.4 ± 0.52	157.0 ± 0.47
90th	114.1 ± 0.54	116.8 ± 0.53	161.0 ± 0.46	157.1 ± 0.43
Hypokinetic Rats (HKR), n=7				
Sodium				
Pre-HK	65.4 ± 0.41	58.7 ± 0.54	29.3 ± 0.43	25.5 ± 0.51
7th	58.0 ± 0.53*	53.2 ± 0.35*	25.3 ± 0.41**	22.4 ± 0.47**
15th	59.7 ± 0.47*	53.7 ± 0.54*	26.2 ± 0.45**	23.0 ± 0.48**
30th	57.2 ± 0.42*	52.4 ± 0.46*	24.8 ± 0.51**	21.5 ± 0.54**
50th	58.1 ± 0.55*	53.3 ± 0.51*	23.4 ± 0.43**	22.6 ± 0.41**
70th	55.6 ± 0.46*	51.8 ± 0.54*	22.3 ± 0.47**	20.4 ± 0.48**
90th	56.5 ± 0.50*	52.5 ± 0.40*	23.2 ± 0.51**	21.6 ± 0.46**
Potassium				
Pre-HK	113.8 ± 0.53	116.7 ± 0.43	160.5 ± 0.41	156.3 ± 0.50
7th	97.1 ± 0.48*	102.3 ± 0.43*	132.0 ± 0.52**	128.7 ± 0.43**
15th	99.3 ± 0.43*	104.7 ± 0.52*	134.7 ± 0.40**	130.1 ± 0.38**
30th	94.3 ± 0.35*	99.8 ± 0.38*	129.2 ± 0.43**	125.2 ± 0.50**
50th	96.6 ± 0.41*	101.2 ± 0.45*	131.6 ± 0.52**	127.4 ± 0.36**
70th	92.8 ± 0.37*	97.6 ± 0.50*	121.8 ± 0.38**	122.2 ± 0.45**
90th	94.2 ± 0.42*	99.8 ± 0.36**	126.6 ± 0.41**	125.6 ± 0.43**

All values are presented as mean ± SD. *p<0.05 significant differences between control and hypokinetic groups of rats. **p<0.05 significant differences between skeletal muscles and cardiac muscles.

TABLE IV. Water content of the cardiac and skeletal muscles measured in rats at pre-hypokinesia and during control and hypokinetic conditions.

Days	Skeletal Muscles Right Ventricle, and Left Ventricle, mEq/kg wet tissue		Skeletal Muscles Thigh Extensor and Long Back Muscle, mEq/kg wet tissue	
	Vivarium Control Rats (VCR), n=7			
Pre-HK	77.35 ± 0.43	78.41 ± 0.52	79.50 ± 0.53	78.21 ± 0.48
7th	77.50 ± 0.56	78.65 ± 0.41	79.74 ± 0.42	78.48 ± 0.56
15th	77.47 ± 0.54	78.50 ± 0.52	79.61 ± 0.47	78.35 ± 0.54
30th	77.67 ± 0.48	78.82 ± 0.46	79.86 ± 0.48	78.67 ± 0.40
50th	77.60 ± 0.50	78.73 ± 0.50	79.70 ± 0.53	78.53 ± 0.52
70th	77.87 ± 0.47	78.86 ± 0.53	79.95 ± 0.46	78.79 ± 0.40
90th	77.75 ± 0.44	78.71 ± 0.44	79.88 ± 0.52	78.64 ± 0.53
Hypokinetic Rats (HKR), n=7				
Pre-HK	77.31 ± 0.35	78.44 ± 0.51	79.48 ± 0.42	78.21 ± 0.35
7th	66.40 ± 0.51*	69.58 ± 0.53*	64.90 ± 0.51**	68.87 ± 0.40**
15th	67.13 ± 0.42*	70.80 ± 0.41*	65.11 ± 0.45**	69.21 ± 0.36**
30th	64.21 ± 0.50*	67.57 ± 0.43*	61.48 ± 0.32**	65.42 ± 0.41**
50th	65.05 ± 0.46*	68.25 ± 0.52*	62.24 ± 0.40**	66.22 ± 0.40**
70th	62.28 ± 0.51*	65.41 ± 0.40*	59.11 ± 0.53**	62.13 ± 0.43**
90th	63.30 ± 0.42*	66.13 ± 0.52*	60.33 ± 0.41**	63.10 ± 0.42**

All values are presented as mean ± SD. *p<0.05 significant differences between control and hypokinetic groups of rats. **p<0.05 significant differences between skeletal muscles and cardiac muscles.

consequence of normal muscular activity are readily returned to muscles, and deposited in muscles (5–13). During pre-HK, normal muscular activity did not affect muscle water and electrolytes and hypokinetic and control rats did not show changes in electrolyte absorption, urine excretion and water and electrolyte content in muscles, and electrolyte levels in plasma, urine and feces.

Hypokinetic muscle water and electrolyte utilization, plasma and electrolyte excretion, and fluid loss

During normal muscle activity, muscle electrolyte depletion is usually associated with decreased plasma electrolyte level. In contrast, during HK muscle electrolyte depletion is always associated with higher plasma electrolytes (5–13). During pre-HK, plasma electrolytes were not increased because electrolytes were deposited in muscles, while during HK they increased because they failed to deposit in muscle (5–13). During HK, no matter how much electrolytes animals ingest, the plasma electrolyte level is always increased with electrolyte depletion (4–6). The increase of plasma electrolyte concentration in the face of a decrease of muscle electrolyte content shows that electrolytes could not be deposited in muscles; this indicates that hyperelectroemia is attributable to decreased electrolyte deposition, because when muscle electrolyte content decreased, plasma electrolyte concentration increased (5–13). In fact, a significant correlation exists between

the decreased muscle electrolyte content and the increased plasma electrolyte levels. The decreased electrolyte deposition promotes electrolyte shifting in plasma and contributes to the increased plasma electrolyte concentration (5–13). The persistence of an increased plasma electrolyte level with a decrease of muscle electrolyte content indicates the involvement of mechanisms other than those involved with hypoelectroemia during normal muscular activity and muscle electrolyte depletion, which could have contributed to the higher plasma electrolyte levels during HK. This is of course not consistent with the current findings where the decreased muscle electrolyte level is usually associated with decreased plasma electrolyte level. The increased plasma electrolyte concentration with decreased muscle electrolyte content is not unique to prolonged HK. Patients with renal failure and higher or lower electrolyte consumption show hyperelectroemia also. However, evidence is emerging to indicate that increased plasma electrolyte concentration with decreased muscle electrolyte content is associated with decreased muscle electrolyte deposition (5–13).

During pre-HK, muscle water and electrolyte content remained stable because the consumed water and electrolytes were taken up by muscles and utilized to a great extent by the body which protected muscles from any changes. During HK, however, animals always showed a lower muscle water and electrolyte content compared with control animals. During pre-HK, water and electrolyte intake usually normalize water and electrolyte depletion, while during HK no matter how much water and electrolytes animals ingest, the water and electrolyte level in muscles is always depressed (4–6). Water and electrolyte content decreased mostly in skeletal muscle and least in cardiac muscle which is in accordance to the findings where electrolyte and water content decreases most in muscle that have a weight-bearing supporting morphology and function (14–16). The severity of decreased muscle water and electrolyte content was different in skeletal muscle and cardiac muscle which have a different weight-bearing supporting function and morphology. The muscle water and electrolyte content decreased more in muscles with higher supporting function and morphology than in muscles with lower supporting function and morphology. The reason remains unclear why muscle water and electrolyte level decrease differently in skeletal and cardiac muscles with different function and morphology. There are grounds to indicate, that the lower muscle water and electrolyte content leads to the lower water and electrolyte absorption and to the higher water and electrolyte losses and thus to lower electrolyte and water level in muscles; this is because the lower the muscle water and electrolyte content the higher the water and electrolyte losses and the higher the muscle water and electrolyte level the lower the water and electrolyte losses (5–13). This is ensured by several factors and primarily by the decreased water and electrolyte deposition (5–13) which is primarily attributable to the decreased cell mass (5, 6). The differences in water and electrolyte loss with different muscle water and electrolyte content are attributable to the differences in water and electrolyte deposition in muscles with different supporting function and morphology (5–13).

With a decrease of water and electrolyte content in skeletal and cardiac muscles, rats have shown an increase of water and electrolyte loss (5–13). A fraction of the water and electrolyte loss with muscle electrolyte and water depletion may be associated with weight losses, muscle atrophy, hypokinetic stress (1, 2) and endogenous steroid stimulation (17, 18). A common consequence of body weight losses, muscle atrophy, hypokinetic stress (1, 2) and excess of endogenous steroids (17, 18) is that the water and electrolyte

absorption from intestine is drastically depressed. This would prevent normal water and electrolyte absorption with muscle water and electrolyte depletion resulting in higher water and electrolyte losses. The fact that muscle water and electrolyte content remained depressed till the end of HK shows that little if any water and electrolyte had been deposited in muscles. Thus, the differences in water and electrolyte depletion in different muscle groups show the differences in the magnitude of water and electrolyte deposition in muscles. Because water and electrolytes were decreased more in the skeletal than cardiac muscles, it indicates that the differences of water and electrolyte level in muscles with minimal differences in morphology and function are attributable to the differences of water and electrolyte deposition in muscles (5–13).

Decreased muscle water and electrolyte content was always accompanied by increased water and electrolyte losses. This is due to the decreased water and electrolyte deposition which is ensured primarily by the decreased muscle cell mass (5, 6), injury of the skeletal muscle cell, decreased electrolyte and cellular metabolism, (5, 6), impaired endocrine control mechanisms (17, 18) and other contributing factors. The severity of decreased water and electrolyte deposition was different in muscles with different function and morphology; but it was at maximum in the skeletal muscles which have a weight-bearing supporting function and morphology (14–16). The mechanisms by which water and electrolyte deposition decreases more in skeletal than the cardiac muscle is not clear; however, it has been shown that differences in magnitude of functional and morphological changes in muscles is the main factor for lower water and electrolyte deposition in skeletal than in cardiac muscles (14–16). The lower water and electrolyte deposition in skeletal than in cardiac muscle is attributable to greater water and electrolyte changes in skeletal than cardiac muscles, and indicates that water and electrolyte deposition decreases analogous to the changes in muscle morphology and function (14–16). The magnitude of decreased water and electrolyte deposition in skeletal than cardiac muscle shows the severity of changes in muscle with different morphology and function and the intensity of decreased mechanical load in skeletal than in cardiac muscles (14–16).

The distribution coefficient of water and electrolytes between muscles and plasma is the integral index of muscle function and morphology (19, 20). Being involved in fine regulated processes of active membrane transport and maintenance of osmotic equilibrium between the extracellular and intracellular fluids, electrolytes are distributed in muscles analogous to the function of the system of membranomyo-fibril conjugation, degree of cell metabolic activity and chemical condition of the cytoplasmic template that carries predetermined charges (19, 20). Because HK affects muscle function and morphology (1, 2) this must have contributed to changes of electrolytes and water in skeletal and cardiac muscles. In fact there was a decrease of muscle water and electrolyte content which was greater in skeletal than in cardiac muscles. Thus, the greater decreases of water and electrolyte content in skeletal muscle than in myocardium could be attributable to the greater decreases in function and morphology of skeletal than cardiac muscle. Decreased synthesis of proteins, primarily in skeletal muscles (1, 2), may have led to the decreases of water and electrolyte content in skeletal and cardiac muscles as well. This develops as a vicious circle due to which there is a greater protein depletion, and even greater water-electrolyte depletion, in muscles. Muscle protein synthesis needs K^+ (21), however, muscle K^+ decreases more in skeletal than cardiac muscles; this in turn can decrease

protein synthesis more in skeletal than cardiac muscles which decreases water and electrolyte level more in the former than the latter (21).

It is known that the muscular system is the principal water reservoir in the body, so that a decrease of water content in the muscles would indicate muscle dehydration (10–13). In fact hypokinetic rats have shown a decrease of water content in skeletal and cardiac muscle. Because HK is a factor of catabolism induction, animals are experiencing catabolism (1, 2). This could have affected the muscle water deposition and thus water level in skeletal and cardiac muscles. Decreases of water content in skeletal and cardiac muscles could also be associated with protein catabolism, muscle atrophy, body weight loss and muscle mass loss (1, 2). Moreover, since muscle saturation with electrolytes depends on muscle saturation with water (10–13) decreased muscle electrolyte content could be attributable to the decreased water level in skeletal and cardiac muscle. Thus, the greater decreases of water content in skeletal than in cardiac muscles could have led to the greater decreases of electrolyte content in skeletal muscle than myocardium (14–16). The greater decreases of water content in skeletal than cardiac muscles could be attributable to the greater decreases of muscle water deposition in skeletal than cardiac muscles (14–16).

If muscles had shown no differences in water and electrolyte deposition, skeletal and cardiac muscles would have fared equally well, however, skeletal muscles fared worst than cardiac muscles; this is because water and electrolyte content decreased more in skeletal muscle than myocardium. The reason for this may be related to the differences in the magnitude of water and electrolyte deposition in muscle with different function and morphology (14–16). It was for this reason that skeletal muscles responded with lower electrolyte and water deposition than cardiac muscles and the water and electrolyte content decreased more in skeletal muscles than myocardium. Because skeletal muscles showed lower water and electrolyte content than cardiac muscles, it indicates that skeletal muscles show lower water and electrolyte deposition than cardiac muscles. Probably, skeletal muscles have a more labile and less responsive electrolyte and water deposition control mechanism than myocardium. Evidence, is emerging to indicate that during prolonged HK skeletal muscles show lower water and electrolyte deposition than cardiac muscles (14–16). The results obtained from this study indicate that the water and electrolyte deposition decreases more in muscles with weight-bearing supporting function and morphology than in cardiac muscles.

The pathogenetic and metabolic mechanism by which water and electrolyte losses with muscle water and electrolyte depletion developed is not clear. Decreased muscular activity and functional load on the skeletomuscular system resulted in the higher water and electrolyte losses with decreased muscle water and electrolyte content. The decreased electrolyte and water deposition could have contributed to a large extent to the higher water and electrolyte loss with decreased muscle water and electrolyte content (5–13). The systems called upon to maintain muscle water and electrolyte level alters muscle water and electrolyte deposition enough to have muscle electrolyte and water content conform to the decreased muscular activity and diminished mechanical load on the skeletal muscular system (14–16). Increased water and electrolyte loss with decreased muscle water and electrolyte content could have been in essence a hypokinetic reaction and the result of the decreased water and electrolyte deposition. Decreased muscle water and electrolyte content could have been the result of higher water and electrolyte loss with

muscle water and electrolyte depletion due to the decreased muscular activity and functional load on skeletomuscular system.

Conclusion

The combination of lower muscle water and electrolyte content and higher electrolyte and water losses indicates lower muscle water and electrolyte deposition. Dissociation between decreased muscle water and electrolyte content and increased water and electrolyte loss indicates decreased water and electrolyte deposition as the main mechanism of muscle water-electrolyte depletion. The lower water and electrolyte content in skeletal than in cardiac muscles shows that water and electrolyte content decreases more in skeletal than cardiac muscles. Water and electrolyte content decreasing more in skeletal than cardiac muscles suggests that the risk for lower muscle electrolyte and water content is inversely related to the muscle function and morphology, i.e., the more weight-bearing supporting function and morphology muscles have, the higher the risk for lower muscle water and electrolyte content. The decreased water and electrolyte level in muscles with different morphology and weight-supportive function shows that water and electrolyte content decreases more in muscles with heavier support function than in cardiac muscles. It was concluded that the greater muscle morphology for weight-supporting function, the lower water and electrolyte deposition, the higher water and electrolyte losses, and the lower the water and electrolyte content.

References

1. Fedorov, I.V. (1982) *Metabolism under Hypokinetic Conditions*, Izdatelstvo Nauka Press, Moscow, pp 254.
2. Fedorov, I.V. (1980) Biochemical basis of pathogenesis of hypokinesia. *Kosmicheskaya Biol.* 3: 3–10.
3. Kovalenko, E.A. and Gurovsky, H.H. (1982) *Hypokinesia*, Meditsina Press, Moscow, p. 320.
4. Zorbas, Y.G., Yaroshenko, Y.Y., Kuznetsov, N.K. and Verentsov, G.E. (1998) Daily magnesium supplements effect on magnesium deficiency in rats during prolonged restriction of motor activity. *Metabolism* 47: 903–907.
5. Krotov, V.P. (1981) Kinetics and regulation of fluid-electrolyte metabolism in animals and man during hypokinesia, PhD thesis, Interkosmos' Council, Academy of Sciences USSR and Directorate of Kosmic Biology and Medicine, Ministry of Health USSR, Moscow, Russia.
6. Volozhin, A.V. (1987) Pathogenesis of disturbances of calcium metabolism in mineralized tissues during long-term hypokinesia, PhD thesis, Interkosmos' Council, Academy of Sciences USSR and Directorate of Kosmic Biology and Medicine, Ministry of Health USSR, Moscow, Russia.
7. Zorbas, Y.G., Ivanov, A.L. and Fujiyama, Y.F. (1990) Electrolyte content in organs and tissues of rats during and after hypokinesia. *Materia Medica Polona* 22: 263–266.
8. Zorbas, Y.G., Yaroshenko, Y.Y., Kuznetsov, N.K., Madvedev S.N. and Federenko, Y.F. (1997) Electrolyte concentration in skeletal muscles and plasma of rats during and after exposure to hypokinesia and hyperhydration. *Physiol. Chem. Phys. & Med. NMR* 29: 243–259.
9. Zorbas, Y.G., Kakurin, V.J., Kuznetsov, N.A. and Deogenov, V.A. (2004) Electrolyte content determination in skeletal bone of rat for disclosing mineral depletion during prolonged hypokinesia. *Trace Elements and Electrolytes* 21: 220–228.

10. Zorbas, Y.G., Ivanov, A.L. and Federenko, Y.F. (1995) Electrolyte and water content in organs and tissues of rats during and after exposure to prolonged restriction of motor activity. *Rev. Esp. Fisiol. (J. Physiol. Biochem.)* 51: 155–162.
11. Zorbas, Y.G., Alexeyev, N.B. and Nikolessu, Z.A. (1990) Water mineral metabolism in muscle and tissues of rabbits under hypokinesia. *Materia Medica Polona* 22: 267–275.
12. Krotov, V.P. (1972) Study of water-electrolyte metabolism during restricted motor activity. *Kosmicheskaya Biol.* 6: 66–74.
13. Osipov, Yu. Yu. and Shaskov, V.S. (1970) Water-electrolyte metabolism in animals subjected to restricted mobility. *Kosmicheskaya Biol.* 7: 17–21.
14. Nestorov, V.P. and Tigranyan, R.A. (1979) Effects of cosmic flight conditions on electrolyte concentration of skeletal muscles of rats. *Kosmicheskaya Biol.* 13: 66–68.
15. Mikhaleva, N.P., Yefimenko, G.D., and Bobrovnitskiy, I.P. (1978) Electrolyte content of the myocardium, skeletal muscles and blood of rats during prolonged hypokinesia and readaptation. *Kosmicheskaya Biol.* 12: 80–81.
16. Zorbas, Y.G., Ivanov, A.L. and Fujiyama, Y.N. (1990) Electrolyte composition of skeletal muscles after hypokinesia. *Materia Medica Polona* 22: 286–288.
17. Vasil'yev, V.N. (1981) Adrenosympathetic activity in the presence of different functional states of man, PhD thesis, Interkosmos' Council, Academy of Sciences USSR and Directorate of Kosmic Biology and Medicine, Ministry of Health USSR, Moscow, Russia.
18. Vasil'yev, V.N. (1981) Adrenosympathetic activity in the presence of different functional states of man, PhD thesis, Interkosmos' Council, Academy of Sciences USSR and Directorate of Kosmic Biology and Medicine, Ministry of Health USSR, Moscow, Russia.
19. Katz, B. (1968) *Nerves, Muscles and Synapses*. Meditsina Press, Moscow.
20. Nestorov, V.P. (1985) *Structure and Functions of Biological Membranes*. Meditsina Press, Moscow.
21. Mirskiy N.P. and Osawa, S.N. (1963) In: *Functional Morphology of Cell*. Nauka Press, Moscow, pp 9–68.

*Received January 10, 2005;
accepted April 9, 2006.*

What Befalls the Proteins and Water in a Living Cell When the Cell Dies?

Gilbert N. Ling* and Ya-zhen Fu**

**Damadian Foundation for Basic and Cancer Research
Tim and Kim Ling Foundation for Basic and Cancer Research
110 Marcus Drive, Melville, NY, USA 11747*

Email: gilbertling@dobar.org

*** Institute of Biophysics, Academia Sinica, Beijing, Peoples Republic of China 100101*

Abstract: The solvency of solutes of varying molecular size in the intracellular water of freshly-killed Ehrlich carcinoma cells fits the same theoretical curve that describes the solvency of similar solutes in a 36% solution of native bovine hemoglobin — a protein found only in red blood cells and making up 97.3% of the red cell's total intracellular proteins. The merging of the two sets of data confirms the prediction of the AI Hypothesis that key intracellular protein(s) in dying cells undergo(es) a transition from: (1) one in which the polypeptide NHCO groups assume a fully-extended conformation with relatively strong power of polarizing and orienting the bulk-phase water in multilayers; to (2) one in which most of the polypeptide NHCO groups are engaged in α -helical and other “introvert” conformations (see below for definition) with much weaker power in polarizing-orienting multilayers of bulk-phase water. This concordance of the two sets of data also shows that what we now call **native** hemoglobin — supposedly denoting hemoglobin found in its natural state in **living red blood cells** —, in fact, more closely resembles the water-polarizing, and -orienting intracellular proteins in **dead cells**. Although in the dead Ehrlich carcinoma cells as well as in the 36% solution of native hemoglobin, much of the protein's polypeptide NHCO groups are engaged in α -helical and other “introvert” conformation (Perutz 1969; Weissbluth 1974), both systems produce a weak but nonetheless pervasive and “long-range” water polarization and orientation. It is suggested that in both the dead Ehrlich carcinoma ascites cells and in the 36% native bovine hemoglobin solution, enough polypeptide NHCO groups assume the fully-extended conformation to produce the weak but far-reaching multilayer water polarization and orientation observed.

KEY WORDS AND TERMS: active living state, *ad infinitum* adsorption, association-induction hypothesis, AI Hypothesis, ATP as EWC, auto-cooperative transition, cardinal adsorbent, cell physiology, dead state, Ehrlich ascites cells, electron-withdrawing cardinal adsorbent, EWC, fully-extended protein, gelatin, hemoglobin, the living state, long-range dynamic structure of water, q-value of NaCl, native hemoglobin, denatured hemoglobin, non-evaporating water, non-freezing water, polarized-oriented multilayer theory, PM theory, poly(ethylene glycol), polypeptide, protein hydration, protoplasm, red blood cell, resting living state, ρ -value, Size Rule, water,

IN THE CONVENTIONAL membrane-pump theory, a living cell represents a membrane-enclosed solution of free solutes and the so-called *native* proteins in ordinary liquid water. Incessant activities of a battery of submicroscopic pumps postulated to reside in the cell membrane determine largely the cell's chemical makeup. On cell death, the pumps stop pumping. The asymmetric molecular and ionic distribution dissipates and the cell water and its dissolved substances mix with, and become an indistinguishable part of the cell's dead aqueous environment. As such, the theory does not anticipate any profound changes in the cell proteins nor in the bulk-phase cell water.

However, this membrane-pump theory has long ceased to be a valid theory. The details of its exhaustive disproof, reviewed again and again (see Ling 1997, and Chapter 12 of Ling 2001) are, unbelievable as it might seem, virtually unknown to the great majority of those who would like to know or should know.

However, it is not all darkness. There is also a brighter side. That is, at this very moment, there already exists (though also hidden) a theory of cell physiology, which has already reached maturity and successfully stood over 40 years of world-wide experimental testing.

This verified, new unifying theory bears the title, the **Association-induction hypothesis** or **AI Hypothesis** for short. Its continuing growth and leap-frog confirmation have been documented in four full-length monographs, whose publication span four decades (Ling 1962, 1984, 1992, 2001.)

In the following, we shall begin by reviewing briefly the relevant parts of the association-induction hypothesis that describe what and why this theory predicts that there is a profound change in the conformation of the key cell proteins and in the physical state of the bulk phase water when a cell dies.

Theory

Historically, the membrane (pump) theory has been by far the dominant theory of the living cell. However, Martin Fischer (1908, 1909); Benjamin Moore and Herbert E. Roaf (1908); Moore, Roaf and Webster (1912); W.W. Lepeschkin (1928); Ross A. Gortner (1930); E. Ernst (1963, see also Ernst and Scheffer, 1928); Dimitri N. Nasonov (1930, 1962) and A.S. Troshin (1966) all have their own ideas or theories on one subject or another. In addition to those specific ideas, they all shared a skepticism about the validity of the membrane-pump theory and a belief in the importance of protoplasm, which once Thomas Huxley eloquently called the physical basis of life (Huxley 1869.) One reason for the dominance of the membrane (pump) theory was that it was or at least appeared to be a coherent general or unifying theory. That is, until it was proven altogether wrong and a new unifying theory, the association-induction hypothesis, emerged and gradually affirmed.

In introducing and further developing the concept of a "living substance" or protoplasm, Ling's association-induction hypothesis is itself a continuation of the work of these deserving but alas, almost forgotten investigators, whose names are mentioned above and others who are unintentionally left out. Coming late on the scene — as it was the case with the association-induction hypothesis —, also has provided an advantage denied all

our predecessors: the great progress that had been made in fundamental physics and chemistry as well as biological sciences. It is obvious that without its help, the association-induction hypothesis would not have come into existence.

In the association-induction hypothesis, the early concept of protoplasm being the physical basis of life is fully retained. However, major changes have also been made and new concepts incorporated, so that the glaring weaknesses and mistakes in the old definition of protoplasm that have played a part in its misconceived total rejection, have been replaced to become a part of the self-consistent and coherent theory called the AI Hypothesis.

Thus, in the association-induction hypothesis, being alive signifies the existence of a closely-associated system of proteins-water-ions (or protoplasm), cooperatively-linked in a high (negative) energy and low-entropy state called the **living state**. An implication of this new definition is that just as a cell can live or die, so can the protoplasm making up different parts of the living cell. Cytoplasm, cell (or plasma) membrane, nucleus, nucleolus, Golgi apparatus, mitochondrial cristie, ribosome are the names given in the past to some of the protoplasmic components of the living cell.

As such, protoplasm is not just a “substance” defined by an unvarying chemical composition, no more so than a rainbow is merely a collection of different colored bands. Rather, protoplasm is a unique substance containing as its major components, water, small molecules and ions like K^+ (and/or) Na^+ and ATP but above all, proteins, a class of macromolecules found only in, and made by living cells. When this unique assembly of proteins, water, K^+ , ATP and other helpers exist in a (reversible) high-(negative)-energy, low-entropy state we call it the (resting) **living state** (Ling 1992, pp. 31–38; 2001, pp. 148–156.)

The maintenance of the protoplasm in the living state depends on the controlling influence of a consortium of small but critically important molecules or ions called **cardinal adsorbents** (Ling 2001, p. 166.) The cardinal adsorbent *par excellence* is, without question, the end product of energy metabolism, adenosine-triphosphate, or **ATP** mentioned earlier. In action, ATP is aided by what are collectively called **ATP helpers**. They include **congruous anions** (Ling 2001, p. 153) and an as yet-unidentified protein called **protein X** (see Figure 1) (Ling 2001, pp. 152–154.) Inconclusive preliminary search suggests that protein X might be or include *actin* (see Ling 2001, p. 154.) Together, ATP and its helpers keep the protoplasmic proteins in what I shall refer to as an open or **extrovert** conformation (illustrated in the right-hand-side picture in Figure 1) (see also Ling 1992, pp. 107; 2001, p. 77.)

To maintain the living state, ATP plays a *key* controlling role. For it is only when ATP is adsorbed on specific key sites on the protoplasmic protein called **cardinal sites** is the protoplasm alive. Only when ATP is abundant and suitably adsorbed are the negatively charged β -, and γ -carboxyl groups — carried respectively on aspartic and glutamic acid residues of the involved cell protein(s) — ready to preferentially adsorb K^+ ion over its alternatives: namely, Na^+ ion and fixed cations carried on lysine and arginine side chains (see right-side schematic illustration in Figure 1.) This explains why K^+ exists in much higher concentration in cells than in the surrounding medium and the bulk-phase water exists as strongly polarized and oriented multiple layers. And, why metabolic poisons like cyanide and iodoacetate kill cells by blocking the resynthesis of, and hence depleting ATP. Then K^+ is lost from the cell.

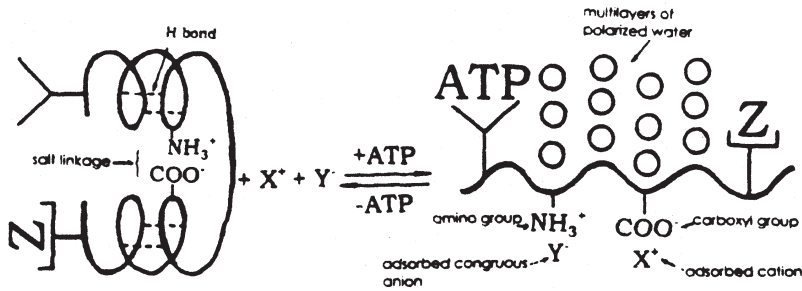


FIGURE 1. Diagrammatic illustration of reversible cooperative transition of a microscopic portion of living protoplasm. The transition is from an extrovert high (negative) energy — low entropy *resting living state* (right-hand side figure) to an introvert low (negative) energy — high entropy *active or dead state* (left-side figure.) This transition is under the control of the premier *cardinal adsorbent*, ATP — with the aid of *congruous anions* (Y^-) and *protein X*. In the extrovert conformation of the resting living state, the β - and γ -carboxyl groups are free to adsorb free ions X^+ (e.g., K^+) and the backbone NHCO groups are free to polarize and orient multi-layers of water molecules. In the introvert active or dead state, the β - and γ -carboxyl groups are locked in salt-linkages with fixed cationic groups and the backbone NHCO groups form α -helical or other intra- or inter-macromolecular H-bonds. (from Ling 2001)

In addition, Figure 1 also shows that in the *extrovert* conformation, a significant portion of the backbone carbonyl and imino groups of the protoplasmic proteins exist in the **fully-extended conformation** (Ling 1992, p. 121; 2001, p. 75.) The NH and CO groups of the fully-extended protein backbone polarize and orient multiple layers of water molecules near and far.

Assuming the dynamic structure (Ling 2001, p. 77) of **polarized-oriented multilayers**, the bulk-phase cell water has normal or reduced solubility for molecules and ions — collectively referred to as **solutes** — according to what is known as the **size rule** (Ling 1970, pp. 147–148; 1987; 1992, p. 77; 2001, p. 92.) That is, the larger the solute molecule, the smaller its *equilibrium distribution coefficient* or *q-value* in the cell or model water. Since hydrated Na^+ ion is large, its concentration in cell water is low. Nor can Na^+ ion successfully compete against K^+ ion for adsorption on the β - and γ -carboxyl groups. Accordingly, Na^+ ion is found at low concentration in most normal living cells as observed. In the AI hypothesis, neither the selective accumulation of K^+ nor the partial exclusion of sodium ion from the normal resting cell requires a *continuous* expenditure of energy. Rather, they represent different aspects of a *metastable* equilibrium state. Nonetheless, the maintenance of this *metastable* equilibrium state requires ATP. However, it only depends on the presence of ATP *per se* and its adsorption as such on key *cardinal sites*. It does not require its continuing splitting and delivering a package of energy stored in the so-called high energy. Long ago, Morales and Podolsky (1956) have shown that no such high energy phosphate bond exists (see Ling 2001, Table 3 on p. 112.)

According to the AI hypothesis, when the cell dies, the protoplasmic **system** of proteins-water-ions undergoes a **cooperative transition** (Ling 1962, pp. 162–163; 1964, 1980, 2001, p. 295; Karreman 1980) from the high- (negative)- energy-low entropy **resting living state** (Ling 1962, title of book; Ling 1992, pp. 32–33; 2001, Figure 3.2 on p. 33) to a low-(negative)-energy, high-entropy **dead state**. The dead state is a further

dissipative step down beyond that of the **active living state** (see Figure 3.2 on p. 33 in Ling 1992.)

As illustrated on the left-side schematic diagram of Figure 1, the protein involved assumes in the dead state what is called an **introvert conformation**. In this conformation, the negatively-charged β -, and γ -carboxyl groups are no longer free but are engaged in *salt-linkages* with an equivalent number of fixed ϵ -amino groups and guanidyl groups from lysine and arginine side chains respectively. In concert with the anchorage of the charged side chains brought about by salt-linkage formation, the backbone carbonyl and imino groups also become immobilized by engaging in intra- and/or inter-macromolecular H-bonds leading to the formation of the α -helical or β -pleated sheet conformation respectively. The transition from the *extrovert* to the *introvert* conformation in the dying cell liberates K^+ ions previously adsorbed singly on the β -, and γ -carboxyl groups; it also liberates water molecules adsorbed in polarized-oriented multilayers on the backbone CO and NH sites of the same or other intracellular proteins.

The progress made so far in establishing the **polarized oriented multilayer theory** (PM theory) of cell water (Ling 1965, 1970, 1972, 2003) — a subsidiary of the AI hypothesis — has involved the study of *inanimate models* side-by-side with the study of living cells. Chosen on the basis of fundamental principles of the PM theory, these models are divided into the two categories already alluded to above: **extrovert models** and **introvert models**.

Extrovert models comprise certain types of what has unfortunately been known as **denatured** proteins and oxygen-carrying linear polymers which exist in the full-extended conformation. Examples of extrovert models include urea, guanidine HCl and NaOH-denatured protein and nitrogen-carrying linear polymers, including poly(ethylene oxide), poly(vinyl methyl ether), polyvinylpyrrolidone and polyvinyl alcohol. For the newly gained prominence of polyvinyl alcohol (gel) in its spectacular confirmation of the PM theory, see Discussion below. (Also see Ling 1992, p. 81 for a description of Ling's theory why gelatin differs from most other proteins and that of his latest definition of *colloid*, which is the namesake of gelatin.) In contrast and irony, what we traditionally call native proteins are, as a rule, *introvert* models.

With these basic concepts in place, we now examine what the AI Hypothesis predicts on the conformation of the intracellular proteins and on the state of water in living cells before and after cell death: *in its resting living state*, some major intracellular proteins exist in the fully-extended extrovert state and the bulk-phase water in a cell resembles water in the presence of a suitable concentration of **denatured** proteins like gelatin and NaOH-denatured proteins; in a **dead** cell, some intracellular proteins assume the introvert state and the bulk phase water resembles water in the presence of a suitable concentration of the so-called **native** proteins.

In the last 35 years or so, a great deal of time has been spent in establishing that a host of cell physiological properties and behaviors, traditionally attributed to membrane pumps, membrane pore sizes, etc., actually originate from the distinctive properties of cell water (Ling 1992.) And in support of the theory, the investigators have been able to demonstrate highly similar behaviors and properties of bulk-phase water in living cells and bulk-phase water in the presence of extrovert models, but not so at all or weakly so by water in the presence of equal or even higher concentrations of introvert models of native proteins. (The interested reader should consult Chapter 5 of Ling 1992, especially

Table 5.5 for a complete summary of the extensive evidence referred to and the names of the investigators who created them.)

To put to a test the predicted similarity in the physico-chemical attributes of water in dead cells and water in the presence of (introvert) protein in the so-called native state, we select for testing the *solveny of the bulk-phase water for solutes of different molecular sizes*. This basic property of bulk-phase water was chosen on account of its simplicity and incisiveness in telling us *quantitatively* what is normal liquid water and what is not.

Now, hemoglobin makes up 97.3% of the total intracellular proteins of a mature mammalian red blood cell. Ideally, the comparison should be made, for example, between killed red blood cells and a solution of native hemoglobin at the concentration it is found in the red blood cell, i.e., 36%. However, there was a practical reason against it. At the time of our current study, we had not studied solute distribution in normal red blood cells. But we had completed the study of the solute distribution in three other kinds of living cells, frog muscle, frog ovarian eggs and Ehrlich carcinoma cells — though to this date, only the results on the frog muscle have been published (Ling *et al.* 1993.)

So, as the next best, we compared the solveny properties of a solution of native bovine hemoglobin — the study of which had also been more or less completed and eventually published (Ling and Hu 1988, 2004) —, with the solveny properties of killed Ehrlich carcinoma cancer cells.

Materials and Methods

(1) Cell preparation, incubation and extraction

Ehrlich carcinoma cells in the ascites form were carried in ICR mice and harvested 14 days after intraperitoneal inoculation. The ascites fluid collected was mixed with an equal volume of what will be referred to as the incubation solution, i.e., a modified Krebs's Ringer solution (composition to be described below) and the suspension centrifuged at 500 rpm on an International Centrifuge for 5 minutes to separate the cancer cells from red blood cells, which remained suspended. For very bloody ascites fluids, this step might be repeated one or even more times. The weights of the ascites cells collected at the bottom of the pre-weighed centrifuge tubes were determined. An equal weight of incubation solution was added to produce a 50% cell suspension. A 2-ml aliquot of this 50% suspension was then diluted with 20 ml of an incubation solution in a 500 ml Erlenmeyer flask. To keep the pH near neutral, this flask was equilibrated with a mixture of 3% CO₂ and 97% O₂, or a mixture of 3% CO₂ and 97% N₂. The flasks were then shaken at 75 excursions per minute in a constant temperature bath maintained at 25°C. The incubation lasted 20 hours. The permeability barrier of the killed ascites cells are much weakened; this duration of incubation is more than long enough to insure distribution equilibrium even for very large solute molecules determined from prior study of the time of equilibration of the same solutes in intact Ehrlich cancer cells.

The incubation solution used was a modified Krebs's Ringer solution containing the following: NaCl (135 mM); KCl (5 mM); NaH₂PO₄ (1.16 mM); Na₂HPO₄ (1.8 mM); NaHCO₃ (3.6 mM); D-glucose (5.6 mM); MgCl₂ (0.9 mM); CaCl₂ (1.30 mM.) In addition, to the solution might also be added Penicillin G (0.01%), Streptomycin sulfate (0.01%).

We killed the cancer cells by including in the incubation solution 1 mM NaCN and 5

mM iodoacetamide (which is a faster acting poison than sodium iodoacetate) replacing an equivalent amount of NaCl. To test the time required to kill the cells, we used a vital dye method (Erythrocin B, 0.28% in 0.154 M sodium chloride) and counted each time a total of 600 to 800 live and dead cells at 0, 1 and 2 hours of incubation. The results showed that at 0 hour incubation the total percentage of live cells was 91.7%. The surviving cells dropped precipitously to 3.05% after 1 hour of incubation, and to 0.84% after 2 hours of incubation respectively. These data reassured us that very early on during the 20 hour-long incubation, all or virtually all cells were dead.

In regular runs, the incubation solution contained probe solutes of different concentrations (replacing osmotic equivalents of NaCl in the incubation solution) in addition to 1 mM NaCN and 5 mM iodoacetamide. At the end of incubation, the cell suspension in the incubation solution was introduced into one or two 10-ml plastic syringe barrels. The tip of the syringe barrel was inserted snugly into the open end of a 500-microliter polypropylene micro-centrifuge tube. The assemblies were centrifuged at 2000 rpm for 10 minutes in an International Centrifuge. Aliquots of the supernatants were collected (for later analysis of its solute concentration) before the syringe barrels were separated from the micro-centrifuge tubes. Now loaded with dead ascites cells, the microcentrifuge tubes were capped and centrifuged at 15,000 rpm for 10 minutes in a Sorval RC-2 centrifuge to get rid of most of the entrapped incubation solution, which was then aspirated off and discarded. The cells at the bottom of the microcentrifuge tubes were divided into two portions.

One portion of the separated cells was introduced into pre-weighed aluminum pans. The dry weight and water content of the cells were obtained by weighing the loaded pan before and after drying in an oven at 100°C for 24 hours. The other portion of cells was blown into preweighed 15 ml Nalgene centrifuge tubes and the loaded tubes weighed again to obtain the wet cell weight. 3 ml of a 5.1% trichloroacetic acid was added to each tube and mixed with the aid of a Vortex shaker. The tubes were kept overnight in a cold room for solute extraction before centrifugation at 5000–10000 rpm for 5 to 10 minutes to spin down the precipitated cell debris. The clear supernatant solutions were diluted before assaying for the concentration of the probe solutes in the cell water.

(2) Assay of non-radioactive and radioactive solutes.

For solute extraction from cells, we used either 5% trichloroacetic acid (TCA) already mentioned above, or boiling water extraction followed by deproteination with the aid of Ba(OH)₂ and ZnSO₄ according to the method of Somogyi (1930.) L-lyxose was determined by the method of Roe and Rice (1948.) D-mannitol, D-sorbitol and perseitol were determined by the method of Burton (1957.) Sucrose, raffinose, and melezitose were analyzed for their reducing-sugar content by the method of Roe (1934) after hydrolysis by heating for 10 minutes at 80° C in an extract containing 21% HCl. For assay of radioactively labeled solutes, TCA extracts or supernatant containing similar TCA concentration were mixed with Bray's scintillation fluid (Bray 1960) and assayed on a beta-scintillation counter according to the method described by Ling and Hu (1988.)

(3) Determination of the extra-cellular space

It is not easy to determine accurately the extra-cellular space in dead ascites cells because the probe solutes often used to estimate the extracellular space of a population of normal cells do not stay outside the cells but penetrate into the cell interior to varying degrees.

Thus a compromise was chosen. The compromise involves the following assumption. The extracellular space in a centrifuged collection of dead cancer cells is the same as that for a similar population of live cancer cells spun down for the same length of time at the same gravitational force and in the same kind of centrifuge tubes.

To obtain the extracellular space of a population of live Ehrlich carcinoma ascites cells we first cleared the cell suspension of red blood cells by the centrifugation procedure described above. The ascites cancer cells spun down were then suspended in the modified Krebs's Ringer solution containing approximately 0.02 microcuries of ^3H -inulin to give approximately 20,000 counts per minute when assayed in the beta-counter. After mixing, the cells were introduced into the same type of syringe barrel-microcentrifuge assembly described above. The assembly was then spun down at 2000 rpm for 4 minutes and aliquots of the supernatant collected and its radioactivity assayed. Cells in the microcentrifuge tubes were spun down at 15,000 rpm for 10 minutes in the same Sorval RC-2 centrifuge used for other studies described above. Resuspended into 2 ml of Krebs's solution, the cells were then quickly spun down and aliquots of the supernatant solution weighed and counted. From the counts of the two supernatant solutions and the weight of the cells resuspended, we obtained for eight samples the following weight percentages of fluid in the extracellular space: 4.0; 5.6; 5.0; 6.7; 6.9; 4.6; 5.0; and 5.1, averaging $5.4\% \pm 1.0\%$ (mean \pm SD).

(4) Calculations of solute concentration in cells and its q- or ρ -value

From the determination of the water content, the non-radioactive or radioactive solute concentration in the total water content of the cell pallet ($[\text{S}]_{\text{cp}}$) and in the water of the supernatant solutions ($[\text{S}]_{\text{s}}$), the solute concentration in the cell water all in units of micromoles per ml or weight percentage and represented as $[\text{S}]_{\text{cw}}$ is calculated according to the following equation:

$$[\text{S}]_{\text{cw}} = \{[\text{S}]_{\text{cp}} - 0.063 [\text{S}]_{\text{s}}\} / \{1 - 0.063\}. \quad (1)$$

Next, we explain the meaning of the figure, 0.063. As mentioned above, we obtained from radioactive inulin assay, an average of extracellular space of 5.4%, which we rounded off to 5% in grams of water per gram of *whole cells*. To convert this figure to that of percentage volume of extracellular space per gram of *cell water*, the 5% figure is divided by the average water content, equal to 80% and we obtained the figure, 0.063 cited above.

The final goal of our calculations was to obtain either the *true equilibrium distribution coefficient* or **q-value** or failing that, the *apparent equilibrium coefficient* or **ρ -value**. Under the most favorable conditions, the q-value and ρ -value are equal. The q-value, of course, equals $[\text{S}]_{\text{cw}}$ divided by $[\text{S}]_{\text{s}}$. Note that $[\text{S}]_{\text{cw}}$ refers exclusively to solute in the cell water and it does not include solute that might be adsorbed on the cell proteins for example. The usual criterion to determine that a solute inside a cell is exclusively or nearly exclusively in the cell water is its rectilinear distribution. Any significant amount of adsorption would cause the distribution curve over a wide range of concentration to deviate from that of a straight line. Therefore, unless we have demonstrated such a straight line in the data from a spread of experimental points in a plot of $[\text{S}]_{\text{cw}}$ against $[\text{S}]_{\text{s}}$, the ratio obtained would be designated as a ρ -value.

(5) Sources of the values of molar volumes or molecular volumes

The molar volume or molecular volume is equal to the molecular weight of a solute divided by the density of that solute in its liquid state near its boiling point. None of the solutes we used for this study exists in the liquid state at ambient temperature and no such density data are available to make a precise determination of the molecular volume possible. As reported in a preceding paper (Ling *et al.* 1993), when liquid density is available even though it is not near the solute's boiling point, we used it anyway to calculate an approximately correct value. When liquid density (at any temperature) is not available, we used the solid density, or failing that, we computed molecular volumes as the sum of the "volume equivalents" of the elements as given by Kopp: hydrogen, 5.5; carbon 11.0; oxygen (-O-), 7.8, each multiplied by the number of atoms of that respective element in the solute molecule (see Glasstone 1946, p. 525.)

(6) Chemicals

We obtained the following chemicals from Sigma Chemical Co., St. Louis, MO : L-lyxose, Catalog No. L-7126, Lot 26F-0479; D-sorbitol, Catalog No. S-1876, Lot 34F-0016; D-mannitol, Catalog No. M-4125, Lot 81F-0517; D-melezitose, Catalog No. M 5375, Lot 35F-0328; iodoacetamide, Catalog No. I 6125, Lot 36F-5626, inulin (from dahlia tuber) Catalog No. I-3954, Lot 66c-7130, poly(ethylene glycol) (M.W. 3300) Catalog No., P 3640, Lot 16F-0477. The following two chemicals were from Aldrich Chemical Co., Milwaukee, WI., perseitol, Catalog No. 13661-1; D- raffinose Catalog No. 20667-9, Lot. 00302 BM. From Fisher Scientific Co., we obtained sucrose, Lot 851322. Labeled ^3H -inulin, Batch 1496-222 and labeled poly(ethylene glycol) [$1,2\text{-}^{14}\text{C}$] (M.W. 4000), Batch 1291-178 were both from New England Nuclear, Boston, MA.

Results

In Figure 2, the q -value and/or p -values of solutes in the water of dead Ehrlich ascites cells are represented as open circles and plotted against their various molecular volumes. Since the solutes with molar volume smaller than 1000 cc are all more or less constant in their equilibrium distribution coefficient at around 1.0 and to save space, only a duplicate set of data were obtained from all of these smaller solutes (see Table I.) However, for solutes with molar volume larger than 1000 cc, the equilibrium distribution coefficients are altogether different; they fall on a steep declining curve and small errors which would have no significant impact on the lower end of the spectrum, would have marked adverse effect here. To avoid that, all the data collected on the equilibrium distribution coefficients of probe molecules larger than 1000 cc are *true equilibrium distribution coefficients* or q -values; they were obtained from more experimental points covering a wide range of the probe molecule concentrations as indicated in Table II and plotted in Figure 3.

In Figure 2, we also replotted the q -values — represented as solid triangles — of similar and different solutes in a solution containing 36% (w/v) of native bovine hemoglobin previously reported by Ling and Hu (Ling and Hu 1988, 2004.)

The solid line that runs reasonably close to **both sets** of data points is the same theoretical curve computed in 1992 according to Ling's theoretical equation with variable

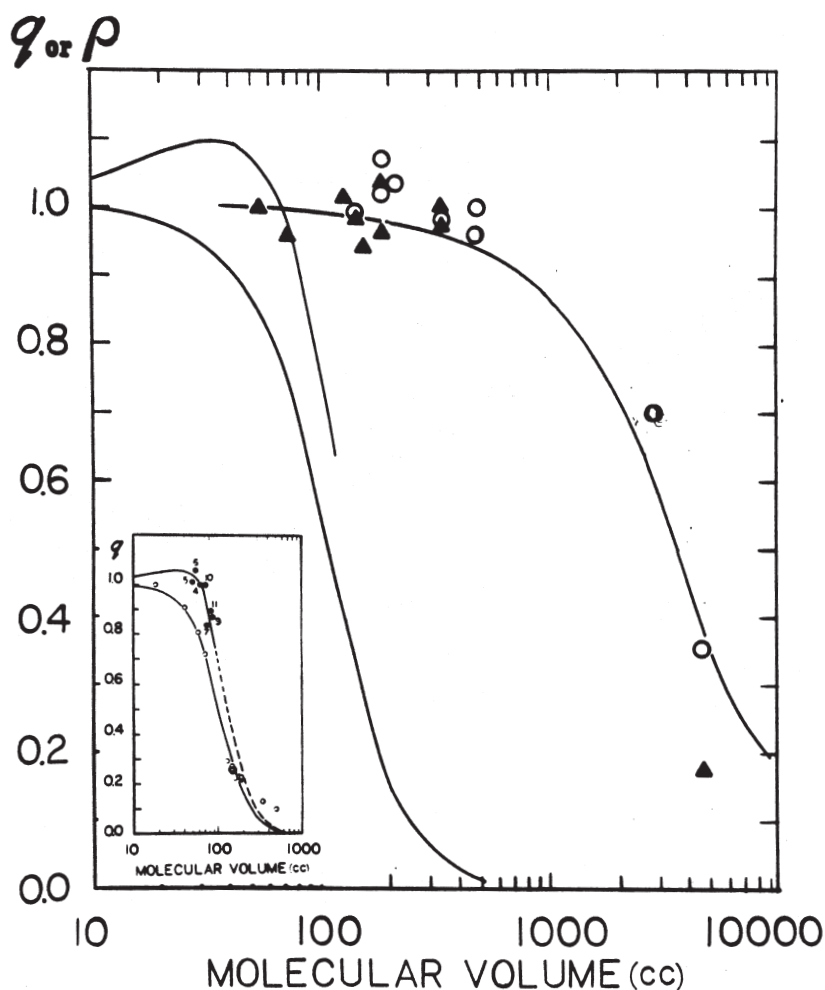


FIGURE 2. The q -values or ρ -values of neutral solutes of different molecular volumes in a solution of 36% native hemoglobin (solid triangles) and in the water in dead Ehrlich ascites cells (open circles.) The q - or ρ -values are plotted against the respective molecular volumes of the solutes. The native protein data as well as the theoretical curve based on Equation A1 in Endnote 1 drawn originally to fit the native hemoglobin data were from previously published data of Ling and Hu (1988 and 2004) and from Ling *et al.* (theoretical curve 1993) respectively. The inset showing q vs v plot of living frog muscles and the outlines of the theoretical curves shown in the inset are also drawn on the main graph to accentuate the profound difference between the solute-distribution profiles of live and dead cells. (It should be pointed out that there is an insignificant small difference in the u_{vp} used to calculate the right-hand side curve (3.8 cal/mole) and u_{vp} used in a prior publication of Ling and Hu (2004) from a later more up-to-date data on the q -value of PEG-4000 in a 36% hemoglobin solution (4.25cal/mole). This 3.3% difference is trivial and to be ignored.)

TABLE I. The q-values or ρ -values of solutes of different molecular volumes of water in dead Ehrlich ascites cells.

Solute	Water content (%)	Mol. Vol. (cc.)	ρ or q^*
L-Lyxose	88.1	149	0.99 (0.99; 0.98)
D-Sorbitol	86.4	189.8	1.02 (1.04; 1.00)
D-Mannitol	86.3	189.8	1.07 (1.06; 1.08)
Perseitol	87.0	219.6	1.03 (1.05; 1.00)
Sucrose	86.0	338.8	0.98 (1.02; 0.93)
Raffinose	85.2	443.8	0.96 (0.96; 0.96)
Melezitose	84.7	498.8	1.00 (0.96; 1.01)
Inulin	83.2 \pm 0.49	2592	0.52 \pm 0.039 (4)*

The q-value of inulin from our earlier studies is lower than from the larger set of data given in Table 2 (0.698), which alone is presented in Figure 2.

TABLE II. The true equilibrium distribution coefficient or q-values or apparent equilibrium distribution coefficient or ρ -values of inulin and PEG-4000 in freshly killed Ehrlich carcinoma cells in the ascites form.

Solute	Mol. Vol. (cc.)	H ₂ O (%)	[S] _{ex} (%)	[S] _{in} (%)	q
inulin	2592	85.2	0.092	0.060	0.69 (+ 0.998)
		82.6	0.091	0.063	
		84.3	0.340	0.213	
		85.3	0.340	0.211	
		82.5	0.590	0.411	
		81.8	0.610	0.400	
		81.9	0.840	0.602	
		82.2	0.850	0.583	
		83.0	0.088	0.058	
		81.2	0.090	0.061	
		80.1	0.350	0.23	
		19.9	0.340	0.22	
		78.3	0.610	0.43	
		79.1	0.600	0.43	
82.5	0.860	0.59			
81.5	0.870	0.58			
PEG-4000	4717	80.7	0.95	0.31	0.35 (+ 0.946)
		80.0	1.10	0.37	
		75.8	2.71	1.11	
		77.4	4.87	2.24	
		78.0	5.48	2.02	
		76.7	5.67	1.86	

The respective q-values were determined from the slopes of the best fitting curves. The number in parentheses following are the linear correlation coefficients between the intra- and extra-cellular concentrations. The dahlia tuber inulin we used had a wide spread of molecular weights between 2000 and 5000. We obtained these figures from Sigma Company's 2004–2005 catalog on the item dahlia-tuber inulinF1TCA. To obtain the molecular volume we divided the average of the two limits (3500) by the solid density of inulin of 1.35 from Hodgman *et al*, 1961, p. 1051) to obtain the figure of 2592 cc.

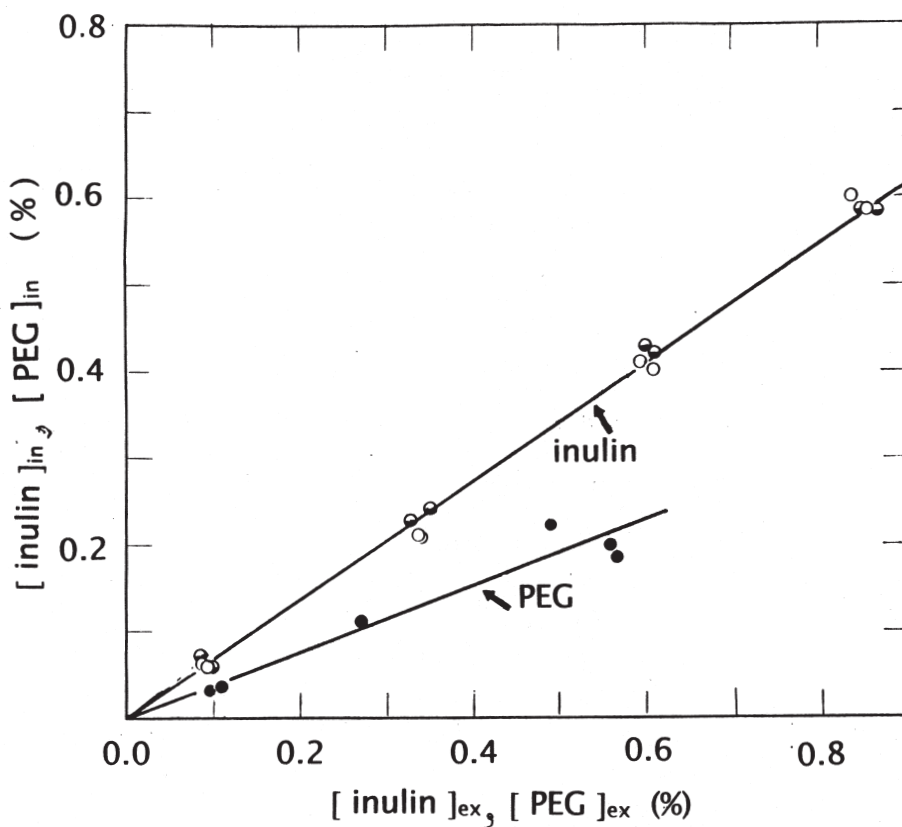


FIGURE 3. The equilibrium distribution of inulin and PEG-4000 in freshly killed Ehrlich carcinoma cells (25°C.) To kill the cells, freshly isolated cells were exposed to a Kreb's Ringer solution containing 1 mM NaCN and 5 mM iodoacetamide. As indicated in the graph, both the inulin concentration and that of PEG-4000 were in units of weight percentages. Numerical values are the same as those shown in Table II.

parameters chosen to fit best the solute distribution data points in water containing 36% native bovine hemoglobin. Ling's theoretical equation is given as Equation A1 in Endnote 1.

Conclusion and Discussion

The theoretical curve originally computed according to Equation A1 in Endnote that fits the set of the data from native hemoglobin and represented as solid triangles also fits the second set of data from dead Ehrlich carcinoma cells represented as empty circles. This agreement leads to two conclusions: (1) Water in dead Ehrlich ascites cells resembles water in the presence of suitable concentration of native protein, as predicted by the AI hypothesis. (2) Within the boundary of the experimental error, both sets of data behave in a way according to the PM theory of solute distribution expressed in Equation A1 in Endnote embodying the "size rule".

To give context to the observed similarity of water in the presence of native hemoglobin and in killed Ehrlich ascites cells we make three comparisons and one comment:

(1) Comparing water in dead Ehrlich carcinoma cells with water in a 36% solution of native hemoglobin

Up until 2003, no theory could explain the three sets of amazing observations on how special solid surfaces could alter profoundly the properties of truly deep layers of water molecules. They are Giguère and Harvey's unexpected demonstration of 10 micra thick layer of nonfreezing water held between polished AgCl prisms at the lowest temperature they could administer, -176°C (Giguère and Harvey 1956); Hori's demonstration of 300 Å thick layer of water film held between plates of polished glass, would not evaporate at 300°C (Hori 1956) and Tseng and Pollack's demonstration of exclusion of coated microspheres from water 100 micra or even further away from a solid polyvinyl alcohol gel (Tseng and Pollack 2003.) Each of these studies revealed respectively that water under the influence of suitable solid surfaces would not freeze, evaporate or exclude microspheres at distance far away from the solid surface. And then Ling offered his new theory of long range water polarization-orientation, which predicts each of these three unusual behaviors: non-freezing, non-evaporating at 300°C and exclusion from water 0.25 mm. away from the polarizing surface (Ling 2003.) For the theory predicts *ad infinitum* polarization-orientation of water under *ideal* conditions by an *idealized* NP surface with a water-to-water interaction energy stronger than that in ice and also strong enough to resist evaporation at 300°C .

However, of direct importance here is the fact that the suitable NP surface can make the water molecules assume an altered configuration and once this alteration has happened, the alteration would spread on by itself. In other words, except at the first and second layer of water molecules right next to the polarizing-orienting ideal or near-ideal NP surface, the high (negative) water-to-water interaction energy is uniform over a large volume of water involved.

As a matter of fact, this uniformity of water-to-water interaction energy was one of the fundamental assumptions in Ling's theory of size-dependent solute exclusion following the size rule (Ling 1993.) And it was discussed by Ling and Hu in an earlier paper on the exclusion of PEG-4000 from the 36% hemoglobin solution: that is, the q-value of 0.189 does not signify that 81% of the water in the 36% hemoglobin has zero solvency for PEG-4000 and the remaining 18.9% has normal 100% solvency. Rather, the entire amount of water in the 36% hemoglobin solution has uniformly reduced q-value of 0.81 for PEG-4000. The fact that the solute distribution data in dead Ehrlich cancer cells can be described by the same theoretical curve describing that of the 36% hemoglobin solution would suggest that the bulk-phase water has also a uniformly reduced solvency. In other words, all the water in the killed cancer cells are not normal liquid water plus a small amount of altered hydration water but polarized-oriented by a volume component of excess water-to-water interaction energy or ${}^{\circ}u_{vp}$ of some 4 cal/mole excess water-to-water interaction energy throughout (see Endnote 1 for a more detailed explanation of ${}^{\circ}u_{vp}$.)

(2) Comparing water in live and dead cells

To underscore the profound difference between water in living cells and water in dead cells, we have included in an inset of Figure 2, solute distribution data in living frog

muscles published earlier and the two sets of theoretical curves fitting what one may call ordinary solutes (lower curve) and solutes most of which are known cryoprotectants (lower curve.) According to the polarized-oriented multilayer theory or PM theory, which is a subsidiary of the AI Hypothesis, cryoprotectant molecules have surface attributes making them more closely interacting with, and thus making stronger the normal cell water's dynamic multilayer polarized-oriented dynamic structure. The outlines of these two sets of theoretical curves are also reproduced on the main graph of Figure 2. To underscore the profound change of the bulk-phase cell water upon death, we make the following quantitative comparison: While a solute with a molecular volume of 300 cc already has a q -value below 0.1 in the intracellular water of a living cell (frog muscle) (Ling *et al.* 1993); a solute with a molecular volume of more than three-times larger still has a q - (or p -value) in the realm of 0.9 in the intracellular water of a dead cell.

The cause for this change in the solute-distribution pattern seen on cell death is a pervasive and drastic loosening of the dynamic water structure. Thus, the theoretical curves which fit the living frog muscle data with a u_{vp} (the volume component of the excess water-to-water interaction energy) of 126 cal per mole. In contrast, the theoretical curve computed best to fit the native hemoglobin data (now shown to also fit the dead cell data), was computed on the basis of a corresponding u_{vp} of only 3.8 cal per mole, thus detecting a 32-fold decrease in the excess water-to-water interaction energy due to multilayer polarization and orientation.

Of course, it would be even more cogent to compare water in live Ehrlich ascites cells with water in dead Ehrlich ascites cells. As mentioned earlier, a study of solute distribution in living Ehrlich ascites cells have also been completed. In anticipation of what we will publish in the future, we mention that by and large, the data on living Ehrlich ascites cells are not too different from that in normal living frog muscle cells already in print and reproduced here in Figure 2.

It is remarkable that physiological phenomena like solute distribution are so exquisitely sensitive to such minute differences in the volume component of the water-to-water interaction energy, u_{vp} . A difference of 3.8 cal/mole of water, or 0.0038 Kcal./mole, is able to keep a molecule with a molecular volume of 4700 cc "off limit" from some 80% of the bulk-phase water. This sensitivity becomes even more striking if one recalls that the normal average water-to-water interaction described by the enthalpy of vaporization of liquid water is 9.7171 Kcal/mole (Rossini *et al* 1952), a figure more than 2500 times greater than the difference of 0.0038 Kcal/mole.

Perhaps this comparison offers some insight into just how extremely delicate and energy-efficient the living machines really are (Endnote 2.) After all, how else can a dung beetle fly almost as well as, or in some ways, even better than a gasoline-propelled airplane, when the dungbeetle's food is mostly grass, not ordinary grass, but grass from which the wildebeest and his stable of intestinal fauna and flora have extracted the most available nutrients?

(3) Comparing water in a solution of native protein with water in a solution of the same protein after its denaturation with NaOH.

In Figure 4 we reproduce a slightly modified version of a figure from Ling and Hu (1988.) In this figure, the size-dependent solute distribution profile of an 18% NaOH-denatured hemoglobin solution as well as the strikingly different profile of that of a 36% native

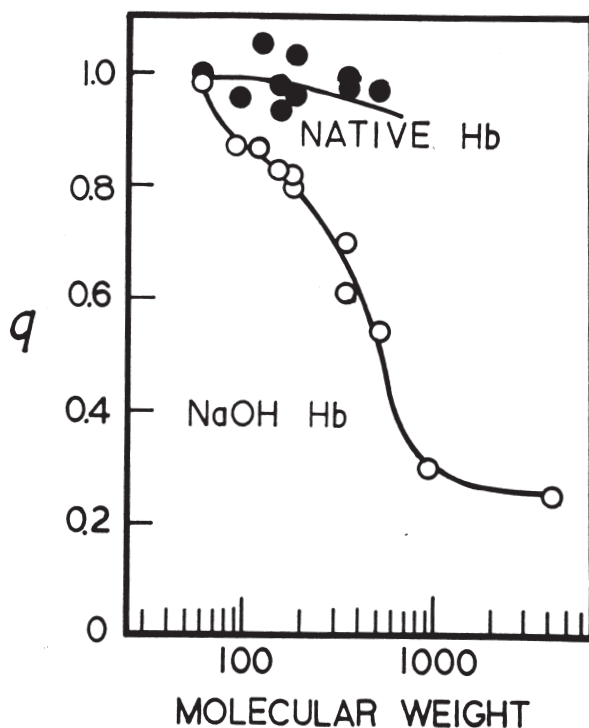


FIGURE 4. Plot of q -values of solutes of different molecular weights of solutes in the presence of NaOH-denatured hemoglobin (18%) (w/v) and an incomplete profile of q vs v from native hemoglobin. Data reproduced from an inset in an older publication to illustrate the different profiles of solute distribution in water under the influence of native protein and NaOH-denatured proteins. This graph is an older one made at the time when our q -value data shown in Figure 2 and 3 were still not available. (from Ling *et al.* 1993)

hemoglobin solution are given. We already know that the \mathcal{U}_{VP} of the water in the 36% native hemoglobin solution to be 3.8 cal/mole. At 18% concentration, the excess water-to-water interaction energy in the bulk phase water of the NaOH-denatured hemoglobin solution is only one half the strength of the native hemoglobin solution. Yet its \mathcal{U}_{VP} is 26.6 cal/mole and thus seven times higher than that in the *native* hemoglobin solution. The living frog muscle cell contains about the same concentration of proteins (20%) as the NaOH-denatured hemoglobin just mentioned, yet it has a \mathcal{U}_{VP} nearly five times higher still than water in the presence of NaOH-denatured hemoglobin. Ling *et al* had discussed the various causes that could have created this difference; the most important is probably the much higher degree of order of proteins in protoplasm than in a denatured protein solution (Ling *et al.* 1993.)

(4) The weak but nonetheless long-range polarization of water by native proteins

The weak but multilayer polarization of cell water in the presence of 36% native bovine hemoglobin was a subject already discussed in the companion paper by Ling and Hu (2004.) We only need to mention the essence of the tentative conclusion they reached: although a

large portion of the polypeptide NHCO groups of the native hemoglobin is engaged in the α -helical conformation, there is reason to suspect that the percentage of the polypeptide chains engaged in α -helical and other introvert conformation in a 36% native hemoglobin solution may not be quite as large as those derived from crystallographic studies and that a significant part of the polypeptide chains may actually adopt the fully-extended conformation leading to the weak but non-the-less multilayer polarization-orientation of the bulk-phase water as observed.

We thank Dr. Raymond Damadian and his Fonar Corporation and its many friendly and helpful members for their continued support. We also thank Margaret Ochsenfeld and Dr. Zhen-dong Chen for their dedicated and skillful cooperation, and librarian Anthony Colella and Michael Guarino, director of Media and Internet Services for their patience and tireless assistance.

References

- Bray, G. (1960) *Anal. Biochem.* 1: 279.
- Burton, R.M. (1957) In *Methods in Enzymology*, (Colowick, S.P. and Kaplan, N.O., eds.) Vol. 3, p. 246, Academic Press, NY.
- Ernst, E. (1963) *Biophysics of the Striated Muscle*, 2nd ed., Hungarian Academy of Science, Budapest, Hungary.
- Ernst, E. and Scheffer, L. (1928) *Pflugers Arch. Ges. Physiol.* 220: 655.
- Fischer, M.H. (1908) *Pflugers Arch. ges. Physiol.* 24: 69.
- Fischer, M.H. (1909) *Trans. College Physicians Philadelphia* 31: 457.
- Giguère, P.A. and Harvey, K.B. (1950) *Canad. J. Chemistry* 34: 798.
- Glasstone, S. (1946) *Textbook of Physical Chemistry*, 2nd ed., van Nostrand, New York.
- Gortner, R.A. (1930) *Trans. Faraday Soc.* 26: 678.
- Hodgman, C.D., Weast, R.C. and Selby, S.M. (1961) *Handbook of Chemistry and Physics*, The Chemical Rubber Co., Cleveland, Ohio.
- Hori, T. (1956) *Low Temperature Science A 15*: 34. English translation, Translation 62, US Army Snow Ice and Permafrost Research Establishment, Corps of Engineers, Wilmette, IL.
- Huxley, T. (1869) *Fortnightly Rev.* 5: 129.
- Karremans, G. (1980) In *Cooperative Phenomena in Biology* (Karremans, G., ed.), Pergamon Press, New York.
- Lepeschkin, W.W. (1928) *Science* 68: 45.
- Ling, G.N. (1962) *A Physical Theory of the Living State; the Association-Induction Hypothesis*, Blaisdell, Waltham, MA.
- Ling, G.N. (1964) *Biopolymers Symp. Suppl. No. 1*, p. 41.
- Ling, G.N. (1965) *Ann NY Acad Sci* 125: 401
- Ling, G.N. (1970) *Intern. J. Neurosci.* 1: 129.
- Ling, G.N. (1972) In *Water and Aqueous Solutions, Structure, Thermodynamics and Transport Processes* (A. Horne, ed.), Wiley Interscience, New York, p. 663.
- Ling, G.N. (1980) In *Cooperative Phenomena in Biology* (G. Karremans, ed.), Pergamon Press, New York, p. 39.
- Ling, G.N. (1984) *In Search of the Physical Basis of Life*, Plenum Press, New York
- Ling, G.N. (1987) *Physiol. Chem. Phys. & Med. NMR* 19: 193.
- Ling, G.N. (1992) *A Revolution in the Physiology of the Living Cell*, Krieger, Melbourne, FL.
- Ling, G.N. (1993) *Physiol. Chem. Phys. & Med. NMR* 25:145.
- Ling, G.N. (1994) *Physiol. Chem. Phys. & Med. NMR* 26: 121.
- Ling, G.N. (1997) *Physiol. Chem. Phys. & Med. NMR* 29: 123. http://www.physiologicalchemistryandphysics.com/pdf/PCP29-2_ling.pdf.

- Or open <<http://www.physiologicalchemistryandphysics.com>> and find link to same article now available online.
- Ling, G.N. (2001) *Life at the Cell and Below-Cell Level: the Hidden History of a Fundamental Revolution in Biology*, Pacific Press, New York.
- Ling, G.N. (2003) *Physiol. Chem. Phys. & Med. NMR* 35; 91. http://www.physiologicalchemistryandphysics.com/pdf/PCP35-2_ling.pdf
Or open <<http://www.physiologicalchemistryandphysics.com>> and find link to same article now available online.
- Ling, G.N. (2006) In *Water in Cell Biology* (Pollack, Cameron, and Wheatley, eds.), Springer Verlag, Berlin, New York, in press.
- Ling, G.N. and Hu, W. (1988) *Physiol. Chem. Phys. & Med. NMR* 20: 293.
- Ling, G.N. and Hu, W. (2004) *Physiol. Chem. Phys. & Med. NMR* 36: 143. http://www.physiologicalchemistryandphysics.com/pdf/PCP36-2_ling_hu.pdf
Or open <<http://www.physiologicalchemistryandphysics.com>> and find link to same article now available online.
- Ling, G.N., Niu, Z., Ochsenfeld, M. (1993) *Physiol. Chem. Phys. & Med. NMR* 25: 177. http://www.physiologicalchemistryandphysics.com/pdf/PCP25-2_ling.pdf
- Moore, B. and Roaf, H.E. (1908) *Biochem. J.* 3: 55.
- Moore, B., Roaf, H.E. and Webster, A. (1912) *Biochem. J.* 6: 110.
- Nasonov, D.N. (1930) *Zeitsch. f. Zellforsch. u. microscop. Anat.* 11: 179.
- Nasonov, D.N. (1962) *Local Reaction of Protoplasm and Gradual Excitation* (Transl. from Russian), Published for the National Science Foundation, Washington, D.C., (was available from Office of Technological Service, U.S. Department of Commerce, Washington, D.C.)
- Perutz, M. (1969) *Proc. Roy. Soc. B* 173: 113.
- Podolsky, R. and Morales, M.F. (1956) *J. Biol. Chem.* 218: 945.
- Roe, J.H. (1934) *J. Biol. Chem.* 107: 15.
- Roe, J.H. and Rice, E.W. (1948) *J. Biol. Chem.* 173: 507.
- Rossini, F.D., Wagman, D.D., Evans, W.H., Levine, S. and Jaffe, I. (1952) *Chemical Thermodynamic Properties*, National Bureau of Standards Circular 500.
- Somogyi, M. (1930) *J. Biol. Chem.* 86: 655.
- Troshin, A.S. (1966) *Problems of Cell Permeability*, Revised Ed., Pergamon Press, London.
- Tseng, J. and Pollack, G.H. (2003) *Physical Review E* 68: 031–408
- Weissbluth, M. (1974) *Hemoglobin: Cooperativity and Electronic Properties*, Springer Verlag, New York.

Received November 11, 2005;

accepted December 23, 2005.

Endnotes

(1) Theory of q-value

The theory of solute distribution in cell water and water in model systems was a subsidiary of the PM theory of cell water, which in turn is a subsidiary of the AI hypothesis. Using standard statistical mechanical method, a quantitative expression of the theory of solute distribution in an equation form was first presented in 1993 (Ling 1993) and is given below as Equation A1

$$q = \exp \left\{ \frac{1.23v\Delta E_s \left[1 - (1-b) \frac{(kv)^n}{1+(kv)^n} \right] - (\Delta E_v + 1.23\Delta e^*)v}{RT} \right\}, \quad (\text{A1})$$

Here the symbol v , represents the molecular volume of a solute under study; the symbol, ΔE_s represents the *specific surface (or solute) polarization energy per cm²* when the solute is transferred from normal liquid water to the polarized cell water or model water. ΔE_v is the *specific volume (or solvent) polarization energy per cm³*; it is equal to the difference in energy spent in excavating a hole 1 cm³ in size in the polarized water and the energy recovered in filling up a hole of the same size in the surrounding normal liquid water. Δe^* is the *increment of the activation energy* for overcoming the greater rotational restriction per unit surface area (cm²) of a solute when it is transferred from normal liquid water to the polarized water phase.) ΔE_{vp} , the *exclusion intensity* of water polarization is equal to the sum of the volume component, ΔE_v and the entropy component 1.23 Δe^* of the polarization energy. $^{\circ}u_{vp}$, called either “exclusion intensity” or the volume component of the excess energy is equal to ΔE_{vp} multiplied by the molecular volume of water, 18.02 (cm³). Similarly, $^{\circ}u_s$, the “surface polarization energy” is equal to ΔE_s multiplied by 18.02 (cm³.) R and T have the usual meaning. b, n and k are constants. b is a fractional number describing the low and steady probability of very large solute molecules in finding adsorbing sites on the water lattice. k and n are parameters describing the steepness of the declining probability of finding adsorbing sites in the water lattice with increasing molecular volume of the solute.

(2) Sensitivity of q-value to small changes in $^{\circ}u_{vp}$

Elsewhere Ling has commented on this extreme sensitivity and likened it to that of a two-pan analytical balance which can measure accurately a sample a fraction of a milligram in weight on pans weighing 200,000 times heavier (Ling 1993.)

Physiological Chemistry and Physics and Medical NMR INDEX

Volume 37, 2005

- Acatalasemic mouse liver damage
 low-dose X-ray irradiation effect on, 109
- AFONINOS, N.I., 127
- AIKOH, H., 65
- Albumin, egg and serum,
 binding of Na⁺ to, 1
- Aluminum ion *in vivo* absorption in mice
 amino acids effect on, 65
 link with calcium absorption, 65
- Amino acids effect on aluminum and calcium
 ion absorption in mice, 65
- Association-induction (AI) hypothesis, 1, 141
- ATP
 as electron-withdrawing cardinal adsorbent,
 1, 141
 in the control of K⁺ accumulation in living
 cells, 1, 141
- Auto-radiograph of ¹³⁴Cs loaded frog muscle
 cells, 1
- BERGMAN, D.J., 71
- Bioelectric Medicine
 book review, 85
- Calcium content in urine of mice administrated
 aluminum ion, 65
 amino acid effect on, 65
- Catalase, role in recovery of CCl₄-induced
 hepatopathy, 109
- Cardiac muscle of hypokinetic rats
 water, K⁺, Na⁺ levels in, 127
- Cardinal adsorbent
 ATP as a, 1, 141
 role in cooperative adsorption, 1, 141
- (β- and γ-) Carboxyl groups
 as seat of K⁺, Na⁺, Tl⁺, Cs⁺ adsorption, 1
- Cell water
 See Water, cell
- Chemical relaxation methods, simulation of,
 in study of telomerase binding, 89
- Close-contact association theory, experimental
 conformation of,
 in counter-ion association of long-chain
 electrolytes, 1
 in living frog muscle cells, 1
 in polystyrene sulfonate, 1
 in NaOH titrated hemoglobin, 1
 in “visible” Na⁺ in polyacrylate, 1
- Cooperative adsorption,
 control by cardinal adsorbent, 1, 141
- Current, electrical, of hornet silk cap
 temperature dependence, 71
- CZERLINSKI, G., 89
- Dielectric saturation, role on K⁺/Na⁺ ratio, 1
- Edelmann adsorption staining method, 1
- Electrical properties of hornet silk
 temperature dependence, 71
- Electrolyte changes due to hypokinesia
 in cardiac and skeletal muscle of rats, 127
- ERMAKOV, Y., 71
- FU, Y-Z., 141
- Hazelwood, C.F., 88
- Hemoglobin, NaOH-titrated
 K⁺, Na⁺ selectivity in, 1
- Hornet cuticle, electrical properties of, 71
 temperature dependence, 71
- Hornet silk
 See Hornet cuticle
- Hepatopathy induced by CCl₄
 effect of low-dose X-ray irradiation on, 109
- Hypokinesia, in rats
 effect on electrolyte and water levels in
 skeletal and cardiac muscle, 127

- Ion exchange resin, K^+ , Na^+ selectivity in, 1
- Ionic accumulation, selective
 in ion exchange resin, 1
 in living cells, 1
 in permutit, 1
 in soil, 1
 in NaOH-titrated hemoglobin, 1
- Ionic dissociation
 at infinite dilution, 1
 history of, 1
 misapplication, cause of, 1
- ISHAY, J.S., 71
- K^+ , Na^+ , Tl^+ , competition for same sites in cells
 or models, 1
- KAKURIS, K.K., 127
- KATAOKA, T., 109
- LING, G.N., 1, 141
- Ling's fixed charge hypothesis (LFCH), 1
 quantitative theory of selective K^+
 accumulation, 1
- Low-dose X-ray irradiation, effect of, 109
 on acatalasemic mouse liver damage, 109
 on antioxidant substances in acatalasemic
 mouse liver, 109
- Magnesium ion (Mg^{2+}),
 indifference of cell accumulation of K^+ to, 1
- NAKAMURA, K., 65
- NEOFITOS, E.A., 127
- NOMURA, T., 109
- Organic semiconductor, hornet cuticle as, 71
- Oubain
 as electron-donating cardinal adsorbent
 (EDC), 1
 effect on K^+ , Na^+ adsorption in frog muscle, 1
- Permutit, K^+ and Na^+ selectivity in, 1
- PLOTKIN, M., 71
- PM theory, 1, 141
- Polarized-oriented multilayer theory (PM) of
 cell water, 1, 141
- Polyethylene glycol (PEG)
 equilibrium distribution in dead Ehrlich
 ascites cells, 141
- Potassium ion levels in muscle of hypokinetic
 rats, 127
- Protective (blocking) agent, role in telomerase
 binding, 89
- q-value (true equilibrium distribution
 coefficient)
 of inulin in Ehrlich ascites cells, 141
 of PEG in Ehrlich ascites cells, 141
 of solutes in presence of NaOH-denatured
 hemoglobin, 141
- ρ -value (apparent equilibrium distribution
 coefficient), 141
 of solutes in Ehrlich ascites cells, 141
- Rapid mixing methods, simulation of,
 in study of telomerase binding, 141
- Resistance, electrical, level in hornet silk caps
 temperature dependence, 71
- Salt linkage hypothesis, in cells and models, 1
- Selective ionic accumulation
 See Ionic accumulation
- SHIBAHARA, T., 65
- Site fixation and aggregation on enhancement
 of ionic and molecular association
 history, 1
 kinetic theory of, 1
 theory of, 1
 thermodynamic theory of, 1
- Skeletal muscle of hypokinetic rats
 water, K^+ , Na^+ levels in, 127
- Sodium ion binding in
 egg and serum albumin, 1
 γ -globulin, 1
 hemoglobin, 1
 myoglobin, 1
- Sodium ion levels in muscle of hypokinetic
 rats, 127
- Soil, K^+ , and Na^+ selectivity in, 1
- TAGUCHI, T., 109
- Telomerase binding to telomeres
 mechanism of, 89
- Telomere-telomerase complex, 89
- Transmission electron micrographs of Cs^{+} ,
 Tl^+ -loaded muscle cells, 1
- Urinary metabolites in mice receiving
 aluminum ion, 65
- Voltage level in hornet silk caps
 temperature dependence, 71

WANG, D-H., 109

Water, cell

 long-range dynamic structure of, 141

 non-evaporating, 141

 non-freezing, 141

 polarized multiplayer theory of, 141

 polarized-oriented multiplayer theory of,
 141

Water excretion in hypokinetic rats, 127

X-ray irradiation, low-dose

 See Low-dose X-ray irradiation

YAMAOKA, K., 109

YAMATO, M., 65

YPMA, T., 89

ZORBAS, Y.G., 127